HELSINKI UNIVERSITY OF TECHNOLOGY
Department of Electrical and Communications Engineering
Laboratory of Acoustics and Audio Signal Processing

Sampo Vesa

Estimation of Reverberation Time from Binaural Signals Without Using Controlled Excitation

Master's Thesis submitted in partial fulfillment of the requirements for the degree of Master of Science in Technology.

Espoo, October 8, 2004

Supervisor:	Professor Matti Karjalainen
Instructors:	D.Sc. (Tech.) Aki Härmä

HELSINKI UNIVERSITY
OF TECHNOLOGY

ABSTRACT OF THE
MASTER'S THESIS

Author:	Sampo Vesa		
Name of the thesis:	Estimation of Reverberation Time from Binaural Signals Without Using Controlled Excitation		
Date:	October 8, 2004	**Number of pages:**	100
Department:	Electrical and Communications Engineering		
Professorship:	S-89		
Supervisor:	Prof. Matti Karjalainen		
Instructors:	D.Sc. (Tech) Aki Härmä		

This thesis concentrates on the task of estimating reverberation time from binaural audio signals. The reverberation time (RT) is one of the most important acoustic parameters describing the acoustic behavior of a space. An estimate of this parameter would be advantageous to many audio applications, such as augmented reality audio, mobile communications and intelligent hearing aids. Usually in these kind of applications no estimates of the room acoustic parameters are available and it is not possible to acquire the parameters online using standard measurement techniques.

An automatic algorithm for estimating the reverberation time was developed. This algorithm requires no a priori knowledge of the surrounding space and operates on an arbitrary binaural input signal, as opposed to standard acoustic measurement techniques. The basic idea of the algorithm is to first locate suitable signal segments for subsequent analysis and then calculate the reverberation time by applying the standard Schroeder integration method to each segment followed by some statistical analysis to derive a final RT estimate. The binaural nature of the input signals is also taken advantage of by using the inter-channel coherence in the analysis. Some new ideas for finding the integration and line fitting limits were also developed. A real-time version of the algorithm was implemented in C++. The algorithm performance was evaluated with both synthetic signals and real recordings. The results show that the algorithm can determine the reverberation quite accurately in most cases, even though there is some degree of variability between different rooms.

Keywords: reverberation time, automatic estimation, signal segmentation, coherence, real-time algorithm, Schroeder method

TEKNILLINEN KORKEAKOULU DIPLOMITYÖN TIIVISTELMÄ

Tekijä:	Sampo Vesa		
Työn nimi:	Jälkikaiunta-ajan estimointi binauraalisesta signaalista ilman tunnettua herätettä		
Päivämäärä:	8.10.2004	**Sivuja:**	100
Osasto:	Sähkö- ja tietoliikennetekniikka		
Professuuri:	S-89		
Työn valvoja:	Prof. Matti Karjalainen		
Työn ohjaajat:	TkT Aki Härmä		

Tässä työssä tutkittiin jälkikaiunta-ajan estimointia binauraalisesta äänisignaalista. Jälkikaiunta-aika (RT) on yksi tärkeimmistä akustisista parametreista, jonka tuntemisesta olisi hyötyä useissa sovelluksissa, kuten laajennetussa äänitodellisuudessa, matkaviestinnässä ja älykkäissä kuulolaitteissa. Tämän tyyppisissä sovelluksissa estimaattia jälkikaiunta-ajasta ei yleensä ole saatavilla eikä sitä ole mahdollista mitata standardimenetelmillä.

Jälkikaiunta-ajan estimointia varten kehitettiin automaattinen menetelmä, joka ei vaadi mitään etukäteistietoa ympäröivästä akustisesta tilasta ja toimii mielivaltaisella binauraalisella signaalilla, toisin kuin perinteiset mittausmenetelmät. Algoritmin perusideana on ensin paikantaa jälkikaiunta-analysiin sopivat signaalin osat ja sen jälkeen laskea jälkikaiunta perustuen Schröderin käänteiseen integrointimenetelmään. Jälkikaiunta-aikaestimaatti saadaan lopulta tilastollisen analyysin tuloksena. Binauraalisuutta hyödynnetään käyttämällä kanavien välistä koherenssifunktiota analyysissä. Käänteiseen integrointiin ja sitä seuraavaan suoran sovitukseen liittyvien rajojen etsintään keksittiin muutamia uusia metodeja. Algoritmista toteutettiin reaaliaikaversio C++ -kielellä ja algoritmin toimintaa arvioitiin sekä synteettisillä että todellisilla nauhoitetuilla signaaleilla. Tulokset osoittavat, että algoritmi kykenee estimoimaan jälkikaiunta-ajan melko tarkasti useimmissa tapauksissa, vaikka eri akustisten tilojen välillä onkin vaihtelua.

Avainsanat: jälkikaiunta-aika, automaattinen estimointi, signaalin segmentointi, koherenssi, reaaliaika-algoritmi, Schröderin menetelmä

Acknowledgments

This work was carried out in the Telecommunications Software and Multimedia Laboratory (TML) of the Helsinki University of Technology (HUT) as part of the KAMARA (Killer Applications for Mobile Augmented Reality Audio) project funded by Nokia.

First I want to thank my supervisor Matti Karjalainen and instructor Aki Härmä, who have provided me with valuable ideas and guidance during this work. Special thanks to Aki for the weekly meetings during the critical early part of writing this thesis. Miikka Tikander and Ville Pulkki have also been helpful during different parts of the work. Big thanks go to Juha Merimaa, who performed denoising of the binaural room impulse responses used in this work. The author is also grateful to Tapio Lokki for some interesting discussion on the subject and revealing the secrets of sweep measurements.

Finally, big thanks to my colleagues and roommates in A152, Heli, Iikka and Sami, for a great working environment and tolerating the constant hand claps and finger snaps.

Espoo, October 8, 2004

Sampo Vesa

Contents

List of symbols viii

Abbreviations x

List of Figures xiii

List of Tables xiv

1 Introduction 1

1.1 MARA technology 3

1.1.1 Overview of the MARA system 3

1.1.2 Application scenarios 6

1.1.3 Estimating the room acoustic parameters 6

2 Theory and methods 7

2.1 Signals and systems 7

2.1.1 Categorization of signals 7

2.1.2 Random signals 8

2.1.3 Impulse response of a system 8

2.1.4 Frequency response of a system 9

2.2 Room acoustic criteria 10

2.2.1 Reverberation time 10

2.2.2 Other criteria 13

2.3 Schroeder integration 13
2.4 Method of least squares 16
2.5 Coherence function 19
2.6 Spectral centroid 20
2.7 Signal detection, segmentation and classification 21
2.8 Sound event detection methods 23
2.8.1 Energy-based detection 23
2.8.2 Cross-correlation based detection 24
2.9 Signal classification and segmentation methods 25
2.9.1 Pattern recognition based approaches 25
2.9.2 Hidden Markov model based approaches 25
2.9.3 Machine learning based segmentation 26
2.9.4 Time-frequency representation based abrupt change detection . . . 26
2.9.5 Voice activity detection (VAD) 26
2.10 Reverberation time estimation methods 27
2.11 Estimation methods with controlled excitation 27
2.11.1 MLS 27
2.11.2 Sweep 27
2.12 Estimation methods without controlled excitation 28
2.12.1 Partially blind methods 28
2.12.2 Blind methods 30

3 The algorithm **31**

3.1 Segmentation 31
3.1.1 Coarse segmentation 32
3.1.2 Fine segmentation 35
3.1.3 Another algorithm for finding the upper limit of integration 38
3.2 Testing the segments 40
3.3 Estimation of RT 42

3.3.1 Finding the limits for line fitting 43
3.4 Deriving the final RT value based on statistics 44
3.5 Implementation of the algorithm 45

4 Evaluation 50
4.1 The signals and impulse responses used in evaluation 50
4.2 Tests with synthetic excitation signals 52
4.3 Tests with convolved real excitation signals 58
4.4 Tests with real-world recordings 65
4.5 Conclusions at this point 70

5 Conclusions 72

A Algorithm configurations used in evaluation 81

B Energy-time curves of signals used in evaluation 83

List of symbols

a	bias parameter in least squares method
b	slope parameter in least squares method
A	absorption area of a room
f_c	spectral centroid or cutoff frequency
f_s	sampling frequency
$D(t)$	integration curve calculated by the Schroeder method
$e_m(n)$	energy envelope of signal segment m
E_{marg}	a noise energy marginal used in the fine segmentation algorithm
E_{noise}	current mean value of noise power in decibels
E_{dB}	normalized energy of a signal subsegment in decibels
E_{down}	energy deviation threshold for detecting sound event offsets
E_{up}	energy deviation threshold for detecting sound event onsets
G_{lr}	one-sided cross-spectrum (between left and right channels)
G_{ll}	one-sided power spectrum (left channel)
G_{rr}	one-sided power spectrum (right channel)
$h(t)$	impulse response function
$H(\omega)$	frequency response function
n_{sub}	starting time index of a subsegment
$N_{seg}(m)$	length of signal segment i
N_{sub}	number of samples in a subsegment
r^2	correlation coefficient in least squares method
$s_m(n)$	signal segment m
S	total surface area of a room
T_d	the point in time where the diffuse sound starts
T_i	upper limit of Schroeder integration
T_s	sampling period

T_{10}	early decay time
T_{30}	reverberation time
T_{60}	reverberation time
$\hat{T}_{60}$	estimate for reverberation time
V	volume of a room
$x_l(t)$	input signal (left channel)
$x_r(t)$	input signal (right channel)
$X_l(f,T)$	Fourier transform of input signal (left channel)
$X_r(f,T)$	Fourier transform of input signal (right channel)
$\langle\cdot\rangle$	time average
$*$	convolution
α_h	forgetting factor for a fading histogram
$\bar{\alpha}$	average absorption coefficient
γ_{lr}^2	coherence function
$\kappa_{coh,dir}$	average coherence threshold for evaluating direct sound length
$\kappa_{coh,max}$	average coherence threshold for testing the segments
σ	standard deviation
τ_k	threshold in knee point location algorithm

List of abbreviations

ARA	augmented reality audio
ASR	automatic speech recognition
BRIR	binaural room impulse response
CDF	cumulative distribution function
DFT	discrete Fourier transform
EDT	early decay time
ETC	energy-time curve
FFT	fast Fourier transform
FHT	fast Hadamard transform
FIR	finite impulse response
GMM	Gaussian mixture model
GUI	graphical user interface
HMM	hidden Markov model
HRTF	head-related transfer function
IIR	infinite impulse response
IR	impulse response
KAMARA	Killer Applications for Mobile Augmented Reality Audio
LP-HMM	linear predictive hidden Markov model
LSF	least squares fit
MARA	mobile augmented reality audio
ML	maximum likelihood
MLP	multi-layer perceptron
MLS	maximum-length sequence
MSC	magnitude-squared coherence
MSE	mean squared error
OSF	order statistics filter

PDF	probability density function
PSD	power-spectral density
RMS	root mean square
RIR	room impulse response
RT	reverberation time
SNR	signal-to-noise ratio
STFT	short-time Fourier transform
SVM	support vector machine
TFR	time-frequency representation
VAD	voice activity detection
WARA	wearable augmented reality audio

List of Figures

1.1 A listener in a pseudo-acoustic environment. 4
1.2 A listener in an augmented environment. 4
1.3 One user experiences the sound environment heard by another user. 5
1.4 A generic diagram of an augmented reality audio system. 5

2.1 A linear system in time and frequency domains. 9
2.2 A simplified reflectogram presentation of a room impulse response. 10
2.3 Schroeder integration curves with different upper limits. 15
2.4 An example of the Schroeder method applied successfully. 15
2.5 A example of the Schroeder method applied less successfully. 16
2.6 An example of fitting an optimal line to a decay curve. 18
2.7 Another example of fitting an optimal line to a decay curve. 18
2.8 A general model for signal segmentation/detection/classification/recognition. 23
2.9 Hierarchy of signal content analysis methods. 23

3.1 Flowchart of the algorithm. 31
3.2 The coarse segmentation algorithm in action. 35
3.3 An example of Schroeder integration with the limits T_i and T_d. 39
3.4 The knee point location algorithm in action. 41
3.5 Finding the linear regression range when knee point algorithm was used. . . 44
3.6 Control window of the reverberation time estimation plugin. 46

4.1 Spectrograms of five synthetic pulses used in algorithm evaluation. 54

4.2 Short-time coherence of a synthetic convolved pulse ($f_c = \frac{7}{8}\frac{f_s}{2} \approx 19.3$ kHz). 55

4.3 Coherogram of a synthetic convolved pulse ($f_c = \frac{7}{8}\frac{f_s}{2} \approx 19.3$ kHz). 55

4.4 Short-time coherence of a synthetic convolved pulse ($f_c = \frac{1}{8}\frac{f_s}{2} \approx 2.8$ kHz). 56

4.5 Coherogram of a synthetic convolved pulse ($f_c = \frac{1}{8}\frac{f_s}{2} \approx 2.8$ kHz). 56

4.6 Short-time coherence of a synthetic convolved pulse with averaging ($f_c = \frac{7}{8}\frac{f_s}{2} \approx 19.3$ kHz, $\beta = 0.8$). 57

4.7 Coherogram of a synthetic convolved pulse with averaging ($f_c = \frac{7}{8}\frac{f_s}{2} \approx 19.3$ kHz, $\beta = 0.8$). 57

4.8 Estimates of T_{60} for room T3 with and without least squares limit lookup (Section 3.3.1), convolved signal. 60

4.9 Three different statistics calculated from T_{60} estimates for room T3, convolved signal. 61

4.10 Histogram of T_{60} estimates for room T3, convolved signal. 61

4.11 Estimates of T_{60} for room A152 with and without least squares limit lookup (Section 3.3.1), convolved signal. 62

4.12 Three different statistics calculated from T_{60} estimates for room A152, convolved signal. 62

4.13 Histogram of T_{60} estimates for room A152, convolved signal. 63

4.14 Estimates of T_{60} for room Pergola with and without least squares limit lookup (Section 3.3.1), convolved signal. 63

4.15 Three different statistics calculated from T_{60} estimates for room Pergola, convolved signal. 64

4.16 Histogram of T_{60} estimates for room Pergola, convolved signal. 64

4.17 Estimates of T_{60} for room A152 with and without least squares limit lookup (Section 3.3.1), real recording. 66

4.18 Three different statistics calculated from T_{60} estimates for room A152, real recording, line fitting range -5 to -25 dB. 67

4.19 Three different statistics calculated from T_{60} estimates for room A152, real recording, variable line fitting limits. 67

4.20 Histogram of T_{60} estimates for room A152, real recording, line fitting range -5 to -25 dB. 68

4.21 Histogram of T_{60} estimates for room A152, real recording, variable line fitting limits. 68

4.22 Three different statistics calculated from T_{60} estimates for room T3, real recording, variable line fitting limits. 69

4.23 Histogram of T_{60} estimates for room T3, real recording, variable line fitting limits. 69

A.1 Algorithm configuration for Sections 4.2 and 4.3. 81

A.2 Algorithm configuration for Section 4.4. 82

B.1 Snaps and claps convolved with BRIR of room A152. 83

B.2 Snaps and claps convolved with BRIR of room T3. 84

B.3 Snaps and claps convolved with BRIR of room T3 (pink noise added). . . . 84

B.4 Snaps and claps convolved with BRIR of room Pergola. 85

B.5 Snaps and claps convolved with BRIR of room Pergola (pink noise added). 85

List of Tables

4.1 Reverberation times of the three acoustic spaces used in evaluation. 52

4.2 Results of T_{60} estimation with synthetic stimuli. 54

4.3 Some statistics of T_{60} estimation in three different spaces using convolved recordings. 60

4.4 Some statistics of T_{60} estimation in room A152 using a real recording. . . . 66

Chapter 1

Introduction

An ongoing trend in mobile communications is the integration of multiple physical devices into a single portable one. The devices to be combined could be, e.g., a mobile phone, an MP3 player, an FM radio and a digital camera. At the same time, the possibilities for the applications are substantially increasing, also because of the increased data processing capabilities of the devices. This calls for new application ideas and completely new usage concepts.

One such concept is *augmented reality audio* (ARA), which becomes *wearable augmented reality audio* (WARA) when the devices are worn and *mobile augmented reality audio* (MARA) [20] when the devices used are portable and wireless. The basic idea of ARA/MARA technology is to add virtual sounds to the natural sound environment experienced by the user, while preserving the perception of the original environment as close to the original as possible. The added virtual sounds should have their acoustical properties adjusted to match those of the environment. The system and its applications are presented in Section 1.1 of this thesis and in [20], [19] and [36].

The augmented reality audio concept also includes continuously recording the binaural sound signal entering the ears of the user. Besides many other things, the obtained binaural signal could be used to analyze the acoustic environment around the user. One could think of localizing sound sources [35], recognizing the environment (e.g. home, car, restaurant) [15] and estimating the reverberation time [49] as examples of the kind of analysis that could be performed.

This thesis is concerned on analysis of the latter kind, namely the estimation of room reverberation time (T_{60}) from binaural signals. In a normal usage situation there is no a priori knowledge about the acoustical environment or a measurement setup available. The position of the microphones, i.e., the user, is unknown and the excitation signal can not be controlled. The acoustical parameters of the room have to be estimated from the live microphone signals containing arbitrary sounds from the environment. The goal is to develop an algorithm that could give a sufficiently reliable estimate of T_{60} by finding suitable sound segments from an arbitrary binaural signal and subjecting them to reverberation time analysis. The binaural nature of the input signal should be taken into account, i.e., there should be some inter-channel analysis steps. Different criteria for testing the suitability of the sound segments are used. Transient sounds, such as hand claps and snaps, have favorable properties related to reverberation time estimation. Some of the criteria are thus related to testing whether a certain sound event is a transient one.

The algorithm proposed in this work consists of several stages, the first of which is detection of interesting sound events. The obtained signal segments are then subjected to different analysis steps that try to decide whether the segment can be used for reverberation time analysis and to determine the exact part of the segment that is suitable for the analysis. The reverberation time is then calculated by using the well-known Schroeder method [52], followed by a standard line fitting procedure to obtain the estimate. Finally, some statistical methods are required to obtain the final estimate from an ensemble of estimates.

It is very challenging to develop an algorithm that can automatically detect the sound events and do all necessary decisions correctly. First of all, the signals used for estimation are completely arbitrary. Their frequency content might vary, which affects the reverberation time. The reverberation time is measured from free decay, during which all sound sources present should be silent. Therefore the areas of free decay should be somehow detected from the signal. The inherently statistical nature of room reverberation also causes some trouble, manifesting itself as variation in the reverberation time estimates. Most of these problems are tackled in the implemented algorithm somehow.

An estimate, even a rough one, of the reverberation time of the room around the user of an ARA system is useful for several purposes. First of all, the reverberation time can be used as one acoustic cue for recognizing the (type of) environment the user is in. Second, different signal processing strategies can be applied dependent on the amount of reverberation in the space that the user is in. One specific signal processing strategy is to modify the amount of reverberation added to augmented sound events (see Chapter 1.1), according to the estimated reverberation time of the environment, in order to make the artificially added sound more natural. The effect of adding reverberation to spatial audio displays has been studied previously in e.g. [54] and [13].

This work was carried out as a part of the KAMARA (Killer Applications for Mobile Augmented Reality Audio) project that was funded by Nokia[1]. An offline version of the algorithm was implemented in MATLAB[2] and the final real-time implementation was written

[1] http://www.nokia.com

[2] http://www.mathworks.com

in C++ using Mustajuuri[3] toolbox [21].

The structure of this thesis is as follows. Chapter 1 introduces the problem and the MARA system, part of which the algorithm was implemented. Chapter 2 reviews some relevant theory and methodology. The most important concepts are introduced and mathematical definitions given. Some methods for an important part of the algorithm, namely the segmentation/detection of the incoming sound signal, are also presented. The focus is on detection methods, even though the basic ideas of some segmentation/classification methods are also presented for the sake of completeness. Finally, methods for the measurement and estimation of reverberation time are presented. Some standard measurement techniques are described first, followed by methods that use more or less arbitrary sounds for the estimation of reverberation time. Chapter 3 gives a detailed description of the algorithm that was implemented in this work. The algorithm that was implemented in real-time in C++ is presented with pseudo code and flow charts. The actual implementation on Mustajuuri [21] framework and related issues are also discussed. Chapter 4 focuses on evaluation of the algorithm. The estimation algorithm is tested with both artificial and real signals. Chapter 5 gives the conclusions and describes some improvements and future work that could be done.

1.1 MARA technology

Since the results of the work presented in this thesis are to be used in the context of mobile augmented reality audio, the basic concepts related to the technology are reviewed here.

1.1.1 Overview of the MARA system

The basic idea in all augmented reality is to blend artificially generated and natural stimuli together as realistically as possible. In *augmented reality audio*, the idea is to simultaneously present *virtual sound environment* and *pseudo-acoustic environment* to the user as depicted in Figure 1.2 [20] [19]. The latter term refers to the presentation of the natural sound environment through a special headset that has microphone elements at the other side of the earphones. The microphones pick up the signals entering the ear canals of the user, preferably preserving the directional hearing cues, and a special device called *augmented reality audio mixer* (ARA mixer) combines the signals with the virtual sound environment signal. The latter signal could be generated with 3-D sound techniques (HRTF filtering), so that the user experiences virtual sounds superimposed to the sounds naturally present in the environment. A special application called *auditory telepresence* combines the pseudo-acoustic

[3] http://www.tml.hut.fi /˜tilmonen/mustajuuri/

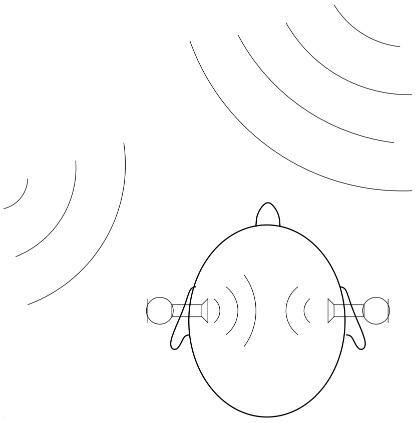

Figure 1.1: A listener in a pseudo-acoustic environment.

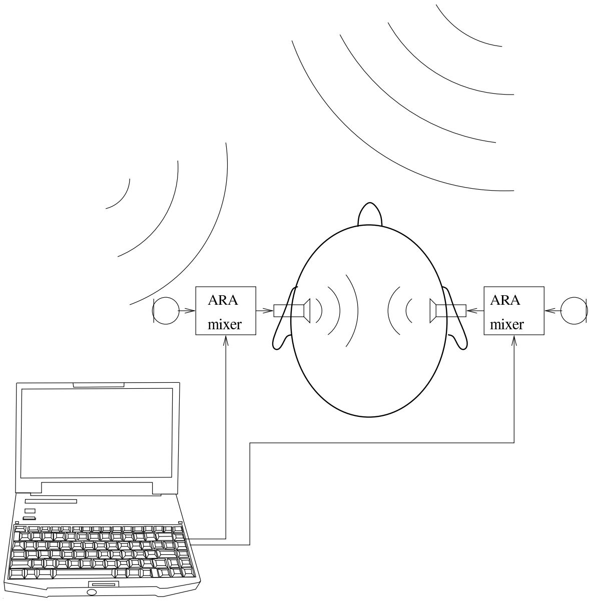

Figure 1.2: A listener in an augmented environment.

environment of the local user with that of a remote user (see Figure 1.3).

A more detailed schematic diagram of the MARA system is in Figure 1.4 [20] [19]. This thesis is concerned on estimating one important acoustic parameter based on the binaural environment signal. Knowledge of the reverberation time can be used, among other things, in adjusting a late reverberation unit that is hidden inside the auralization box of Figure 1.4. The early part of the impulse response (see Figure 2.2) could be generated based on some acoustic rendering technique, such as the image source method [51]. More details on the MARA system can be found in [20] and [19].

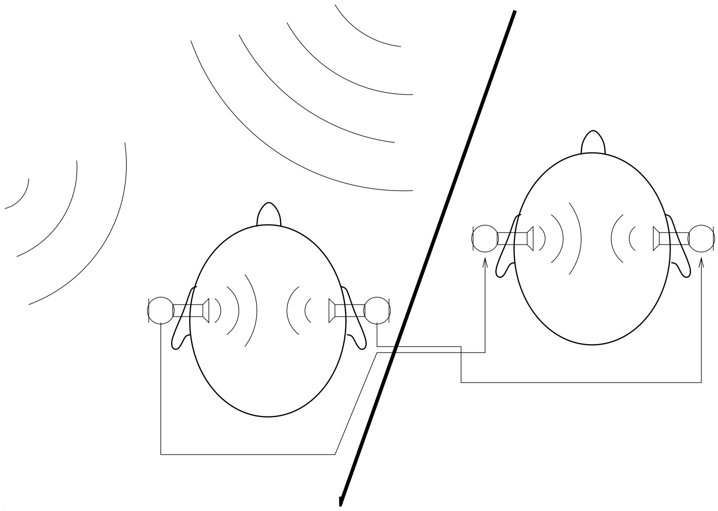

Figure 1.3: One user experiences the sound environment heard by another user.

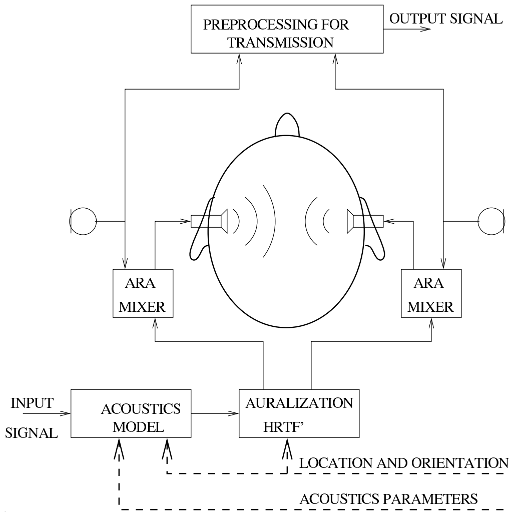

Figure 1.4: A generic diagram of an augmented reality audio system.

The instantaneous orientation and location of the user are necessary knowledge for a natural augmented audio experience. Knowledge on the orientation of the head of the user is especially important, because it allows the auralized sound events to stay stationary related to the user if he/she turns his/her head. Finding out the instantaneous orientation, sometimes also location, of the head of the user is called *head-tracking*. Many methods exist for head-tracking, most of which are unsuitable for a portable system. One alternative is to use acoustic signals as the basis for head-tracking. The acoustic signals could be played back by speakers present in the environment [58]. Alternatively, arbitrary sound signals present in the environment could be used. Cross-correlation between the left and right ear signals can be used as the primary cue in acoustic head-tracking [58].

1.1.2 Application scenarios

Some general application ideas were presented in the previous section. One can think of several application scenarios that an ARA system could be used in. The usefulness of the system increases substantially, when the system becomes mobile, adding an "M" to the abbreviation. A portable device could transmit and receive sound signals wirelessly, possibly leaving most of the signal processing to be done at a dedicated server. Some possible applications of MARA could be an automatic museum guide, an acoustic Post-It sticker and a 3-D calendar [36]. Different communications schemes, such as telepresence (see Figure 1.3) are naturally also important applications of MARA technology.

1.1.3 Estimating the room acoustic parameters

The topic of this thesis is the estimation of reverberation time from an arbitrary binaural signal. In the MARA context, this means using the binaural signals, recorded by the microphones of the headset, for estimating room acoustic parameters of the surrounding environment. It is assumed that the user is located somewhere in an acoustic space and that the sound environment around the user is composed of discrete *sound events* and *background noise*. This dichotomy calls for some procedure of locating the interesting sound events in time and performing some analysis on the obtained segments. Not all sounds present in the environment are suited for reverberation time estimation. This fact calls for some tests that have to be performed for each sound segment. Transient sounds, such as hand claps, snaps and pistol shots, are good for reverberation time estimation because of a high *signal-to-noise ratio* (SNR) and a relatively large bandwidth. The transient sounds are also closer to the ideal impulse than any other group of sounds, which motivates their use in this context.

In a larger context the estimation of room acoustic parameters could be seen as part of an auditory decomposition (see, e.g. [19]). Other parts of the decomposistion include localizing the sound events, calculating their distance and recognizing them. The decomposition could be divided to two major parts: the sound events in a space and the space itself. The decomposition aims at getting a description of the sound environment around the user at each time instant. Augmented reality applications could take advantage of the information given by the decomposition. The basic functionality of the MARA system also benefits from the decomposition.

Chapter 2

Theory and methods

This chapter reviews some of the theory behind the algorithm developed in this work. Relevant basic signals and systems theory is reviewed first, followed by theoretical background of reverberation time and the methods used in its measurement and estimation.

2.1 Signals and systems

The basis of all signal processing is the concept of *signals and systems*. A *signal* is a representation of the evolution of a (usually physical) quantity as a function of some independent variable, such as time or spatial location [40]. The properties of the signal change as it is passed through a *system*, which can be physical, such as a room, or non-physical, such as a digital filter implemented in a computer.

2.1.1 Categorization of signals

Signals can be categorized in many ways, most of which will not be discussed here. Real-world signals, such as sound pressure at a certain location, exist continuously in time and can have any amplitude value at a given instant. Such signals are usually referred to as *analog signals* and will be denoted as $x(t)$, where t represents continuous time. *Digital signals* are only defined at discrete time instants and have discrete amplitude values. They are denoted by $x(n)$, where n is the discrete time index. This thesis is mostly concerned with digital signals that are generated by sampling an analog sound signal at uniformly spaced time instants. This time interval is termed *sampling interval* and denoted by T_s. The inverse of the sampling interval is the *sampling frequency* or *sample rate*, denoted by $f_s = \frac{1}{T_s}$.

Another important categorization of signals is related to their statistical properties. A *deterministic signal* has each of its values fixed and the entire signal is determined by a mathematical expression, rule or a look-up table [40]. On the contrary, a *random signal* can not be predicted ahead in time with full confidence. Random signals are important in this thesis, because most acoustical measurements result in signals of random nature.

2.1.2 Random signals

Since this thesis is mainly concerned with discrete-time signals, the treatment of random signals will be limited to the discrete-time case. Thus a *discrete-time random signal* is a sequence of numbers that is generated as the outcome of some underlying *random process* [18]. The most important aspect relating to acoustical measurements is that the measured signals are usually different realizations of a certain physical phenomenon. For a complete description of the phenomenon, a complete set of possible realizations (an *ensemble*) would be needed [28]. Usually this kind of an ensemble is not available, so *time averages* have to be substituted for *ensemble averages* when calculating statistical measures. The former refers to averaging a single realization over time, while the latter refers to averaging the signal values at a fixed time over all realizations. This only applies to signals that are *wide sense stationary (WSS)*, meaning that the first order statistics of the signal do not change over time. The signal is said to be *ergodic* if time averages can be substituted for ensemble averages. When measuring stationary signals, it is often assumed that the phenomenon is ergodic [28]. The signals encountered in this work can hardly be regarded as stationary, making parameter estimation problems considerably more difficult.

2.1.3 Impulse response of a system

The *impulse response* of a linear system is the waveform that appears at the output of a system when a unit impulse (Dirac delta function) is presented at the input. The output $y(x)$ for arbitrary input $x(t)$ is obtained by convolving the input with the impulse response $h(t)$ (Figure 1) [28]

$$y(t) = x(t) * h(t) = \int_{-\infty}^{\infty} h(\tau)x(t-\tau)d\tau \tag{2.1}$$

The lower limit for integration is set to zero for physically realizable *causal systems*. The system is said to be *BIBO stable* (bounded-input, bounded-output) if the output is bounded for every bounded input. If the impulse response $h(t)$ does not change with time, the system is *time-invariant*. Finally, if the superposition principle holds, the system is *linear*. Systems that fulfill the two previous conditions are called *linear time-invariant (LTI)* systems.

When moving to the world of discrete-time systems, the convolution integral in Eq. 2.1

changes into a convolution sum,

$$y(n) = x(n) * h(n) = \sum_{k=-\infty}^{\infty} x(k)h(n-k) \tag{2.2}$$

where n is the discrete time index. The output sequence $y(n)$ is thus related to the input sequence $x(n)$ by a linear combination of the past and future values, the weights being given by the *unit sample response* $h(n)$. For causal systems the lower limit for the sum is zero.

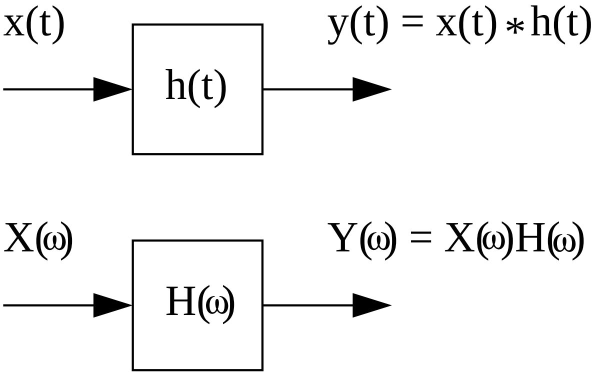

Figure 2.1: A linear system in time and frequency domains.

2.1.4 Frequency response of a system

The *frequency response function* of a system is defined as the Fourier transform of the impulse response [28]

$$H(\omega) = \int_0^{\infty} h(\tau)e^{-j\omega\tau}d\tau \tag{2.3}$$

The above equation can be interpreted as correlation between the impulse response function and a complex exponential of varying frequency. The resulting frequency response function is complex-valued. It is often divided into two components

$$\begin{aligned} H(\omega) &= |H(\omega)|e^{-j\phi(\omega)} \\ |H(\omega)| &= \sqrt{\Re\{H(\omega)\}^2 + \Im\{H(\omega)\}^2} \\ \phi(\omega) &= \tan^{-1}(\frac{\Re\{H(\omega)\}}{\Im\{H(\omega)\}}) \end{aligned} \tag{2.4}$$

where $|H(\omega)|$ is the *magnitude response* and $\phi(\omega)$ is the *phase response*. The frequency response function can also be defined as the ratio of the Fourier transforms of the output and input signals

$$H(\omega) = \frac{Y(\omega)}{X(\omega)} \tag{2.5}$$

2.2 Room acoustic criteria

The perception of an acoustic space can be characterized using different parameters. These perceptual parameters are called *room acoustic criteria*, following the terminology used in [45]. The core of this thesis is the estimation of the most important parameter, namely the reverberation time.

2.2.1 Reverberation time

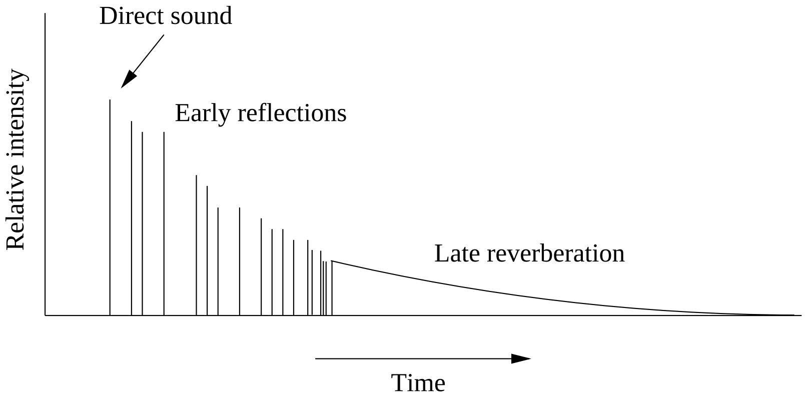

Figure 2.2: A simplified reflectogram presentation of a room impulse response.

The impulse response of a room can be divided into a few different stages (Figure 2.2). The direct sound arrives first, followed by some distinct *early reflections*. The early part of the impulse response is responsible for the perception of the reverberance of the room [45]. *Early decay time* (EDT, T_{10}) is the amount of time it takes for the sound energy level to decrease by 10 dB after the direct sound has ended.

When more reflections start to arrive, the sound field becomes increasingly diffuse and the decay process starts to exhibit exponential behavior. In an ideal case the sound energy level follows a pure exponential curve [45]

$$p^2(t) = p^2(0)e^{-kt} \tag{2.6}$$

where $p(0)$ is the initial sound pressure, $p(t)$ is the sound pressure at time t and k is a decay parameter. *Reverberation time* (RT, T_{60}) characterizes the slope of this curve with a single figure and is defined as the time for the sound energy level to decay 60 dB after the excitation has ended. If no further information is provided, T_{60} is assumed to be calculated on the octave band centered at 500 Hz [50]. Usually, T_{60} is calculated on several different octave bands to get some idea of the frequency behavior of the decay process of the room. Two kinds of reverberation times are commonly used, the other one being T_{30}, which is the time it takes for the sound energy level to decay 30 dB after the end of the excitation. In practice it is often not possible to measure T_{60} directly because the noise level is too high for that. To enable direct comparisons between different decay measures, T_{10} and T_{30} are scaled with factors 6 and 2, respectively, to match T_{60}. Actually, the subscripts 10, 30 and 60 simply refer to the length of the evaluation range. The different reverberation times are always scaled to match T_{60}. In this work no differences between different decay times are made, because the evaluation range may vary (see Section 3.3.1). Therefore all reverberation times, regardless of the evaluation range, will be denoted with T_{60} from now on.

The simplest way of calculating the reverberation time from a measured impulse response would be that of finding the time instant when the sound energy level falls below 60 dB from the peak level. However, usually the noise floor is too high for this. The effect of the direct sound and early reflections has also to be taken into account, because the early part might decay faster than the late part of the reverberation. There might also be two or more stages of decay with different time constants and the squared impulse response might exhibit warbling behavior [45]. To overcome the first two problems, only the portion of the decay curve[1] between -5 dB and -35 dB (or -5 dB and -25 dB) is normally used.

Simply measuring the time interval directly from the logarithmic decay curve is usually not accurate enough. The usual procedure is to use linear regression (described in Section 2.4) to fit a straight line to the data, possibly preceded by the *Schroeder method* (discussed in Section 2.3). It should also be noted that reverberation time on different frequency bands is often calculated and reported in addition to the average value.

The reverberation time of a room is mostly dependent on two properties of the room:

1. Volume of the room (V)

2. Absorption area of the room ($A = \bar{\alpha}S$, where $\bar{\alpha}$ is the average absorption coefficient of the room and S is the net area of the surfaces in the room)

[1] A few notes about the terminology should be made at this point. *Decay curve* may refer to either the idealized decay curve (Eq. 2.6), its noisy real-world manifestation (squared impulse response $h^2(t)$, also known as *energy-time curve* [45]) or the decay curve obtained by applying the Schroeder method presented in Section 2.3. When there is a need to distinguish between the squared impulse response and the decay curve obtained by the Schroeder method, the latter will be termed *integration curve* in this thesis. This term will be mostly used in Chapter 3.

A third property that is relevant only in large rooms is air absorption. The pioneering work by Sabine resulted in the discovery relating these properties to the decay process of a diffuse sound field in a room. The classical formula for reverberation time (T_{60}) will be derived here, starting from the definition of *energy density* [46]

$$\xi = \frac{p_r^2(t)}{\rho c^2} \tag{2.7}$$

where $p_r(t)$ is spatially averaged sound pressure of the diffuse sound field in the room, ρ is the density of the medium (air) and c is the sound velocity. There is a theorem stating that the rate at which energy is produced in the room (source power) has to be equal to the the rate at which it the energy increases throughout the room plus the rate at which it is absorbed by the surfaces. This can be expressed as a differential equation

$$\Pi = V\frac{d\xi}{dt} + \xi\frac{c\,\bar{\alpha}S}{4} \tag{2.8}$$

where Π is the power of the sound source, $V\frac{d\xi}{dt}$ is the rate at which the acoustical energy increases in the room and $\xi\frac{c\,\bar{\alpha}S}{4}$ is the rate at which the energy is absorbed by the surfaces of the room. By setting $\Pi = 0$ in Eq. 2.8 and integrating, the formula for sound energy decay is obtained as

$$p_r^2(t) = p_r^2(0)e^{-\frac{c\,\bar{\alpha}S}{4V}\,t} \tag{2.9}$$

where $p_r(0)$ is the sound pressure level at time $t = 0$ when the sound source is shut down. This equation, when converted to a difference in sound pressure levels, becomes

$$\begin{aligned}\Delta L_p &= 10\log_{10}\left(\frac{p_r^2(t)}{p_r^2(0)}\right) & (2.10)\\ &= 10\log_{10}\left(e^{\frac{-c\,\bar{\alpha}S}{4V}}t\right)\\ &= 10\left(\frac{-c\,\bar{\alpha}S}{4V}t\right)\log_{10}(e)\\ &= -4.35\left(\frac{c\bar{\alpha}S}{4V}\right)t\end{aligned}$$

$$\tag{2.11}$$

Since at $t = T_{60}$ the sound energy level should be -60 dB below the initial value, the reverberation time is obtained as

$$T_{60} = 13.8(\frac{4V}{c\,\bar{\alpha}S}) = \frac{55.2V}{c\,\bar{\alpha}S} \approx 0.16\frac{V}{A} \tag{2.12}$$

When taking air absorption into account, Eq. 2.12 can be re-written as

$$T_{60} = \frac{55.2V}{c\,\bar{\alpha}S + 4mV} \approx 0.16\frac{V}{A + mV} \tag{2.13}$$

where m is a constant related to air absorption, giving the percentage of absorption per cubic meter [50].

2.2.2 Other criteria

Reverberation time and early decay time are naturally not the only room acoustic criteria. Several other criteria exist as well [23], but most of them are irrelevant in this work. Perhaps the most important of them regarding this topic is the *interaural cross-correlation coefficient* (IACC). This criterion is a measure for diffusiveness of the sound field at the position of the listener [3]. Even though there are several IACC measures that differ in terms of the integration periods, they are all calculated from the *interaural cross-correlation function* $\mathrm{IACF}_t(t)$ [3]

$$\mathrm{IACF}_t(\tau) = \frac{\int_{t_1}^{t_2} p_{_L}(t)p_{_R}(t+\tau)dt}{\left[\int_{t_1}^{t_2} p_{_L}^2 dt \int_{t_1}^{t_2} p_{_R}^2 dt\right]^{1/2}} \tag{2.14}$$

where $p_{_L}$ and $p_{_R}$ are the sound pressure signals at the left and right ears, respectively. IACF can be seen as a normalized cross-correlation function calculated on a certain time interval $t_0 \leq t \leq t_1$. The IACC itself is defined as the maximum value of Eq. 2.14 on a realistic range of lags, calculated as [3]

$$\mathrm{IACC}_t = \max|\,\mathrm{IACF}_t(\tau)| \quad -1 < \tau < +1 \tag{2.15}$$

The commonly used IACC measures are IACC_A, IACC_E and IACC_L, with integration periods $[0,\ 1000]$, $[0,\ 80]$ and $[80,\ 1000]$ milliseconds, respectively. IACC_E is a measure for *apparent source width* (ASW), while IACC_L measures *listener envelopment* (LEV).

2.3 Schroeder integration

Calculating the reverberation time from a single measured impulse response is not very accurate. This is due to the random nature of the measured signal, especially when noise is used as the excitation. This is why methods derived from statistical signal processing come into the picture. A simple way of increasing accuracy of RT estimation is calculating an average value from several impulse response measurements. Since averaging over many realizations is quite laborous, a more elegant method would be preferred. The *Schroeder* *method* relates the ensemble average of all possible decay curves to the corresponding impulse response [52]

$$\langle y^2(t)\rangle_e = \int_t^{\infty} |h(\tau)|^2 d\tau = \int_0^{\infty} |h(\tau)|^2 d\tau - \int_0^{t} |h(\tau)|^2 d\tau \tag{2.16}$$

where $y(t)$ is the decaying response (the reverberant tail), $h(\tau)$ is the impulse response of the whole system (including the sound source, the measurement equipment and the room). The ensemble average is indicated by $\langle\cdot\rangle_e$. Equation 2.16 makes it possible to calculate the average decay curve from a single measured impulse response.

In practice the upper limit of integration in Eq. 2.16 is set to a time instant at which the decay curve is still a little bit above the noise floor. The practical formula for obtaining the ensemble average of the decay curve then becomes [7]

$$D(t) = N \int_t^{T_i} h^2(\tau) d\tau \tag{2.17}$$

where N is a constant proportional to the PSD of the noise on the frequency range measured and T_i is the upper limit of integration. According to [7] and [41], the choice of T_i should be made so that T_i is close to the point where the decaying signal “dives” into the noise floor, i.e., $T_i = 0.5s$ in Figure 2.3. It is generally better to choose T_i to be a little bit above the aforementioned point. ISO 3382 standard specifies that T_i should be set to a point where the impulse response is 5 dB above the noise floor [45].

A systematic procedure for determining T_i is presented in [7]. The idea is to first set T_i to a point that is much longer than the expected reverberation time and perform the Schroeder integration using Equation 2.17. The upper limit of integration, T_i, is then determined by inspecting the shape of the integration curve and locating the part where the curve turns linear the second time, corresponding to the constant noise level. This technique is quite inaccurate and can not be easily implemented automatically. Another idea from the same article is to subtract an estimate of the mean-square value of the background noise from the squared signal prior to integration. According to the authors, this should give best results and a large dynamic range of 30-40 dB for the decay curve.

Lundeby et al. [38] present a method for determination of the upper limit of integration. The algorithm is based on an interative simultaneous estimation of the background noise level and the decay slope. An averaged squared impulse response is used for the analysis. The averaging interval varies with the estimated slope at each iteration. After a few iterations, T_i is set to the point where the decay line crosses the background noise level.

A linear regression based method for locating the knee point is presented in [16]. Two optimal lines are fitted to the instantaneous squared signal. One is fitted to the decay part and another to the noise part. The upper limit of Schroeder integration is then set to the point where the two lines intersect. This method is not applicable for automatic reverberation time estimation since it involves the user manually choosing one of the limits of line fitting.

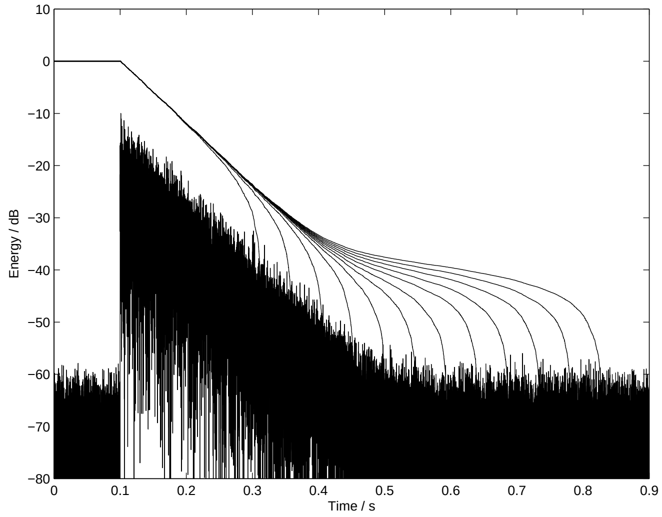

Figure 2.3: Schroeder integration curves with different upper limits.

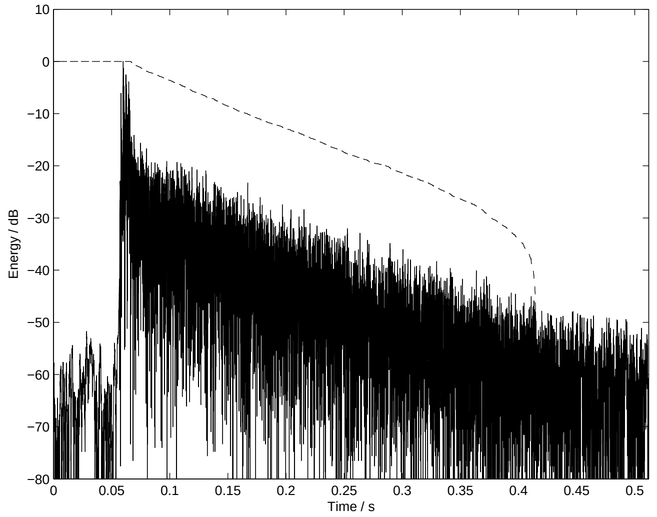

Figure 2.4: An example of the Schroeder method applied successfully.

Figure 2.4 shows the Schroeder integration curve calculated from the instantaneous energy plot of a handclap. The curve smoothes out the variations inherent in the instantaneous energy, giving an estimate for the true decay curve. The curve falls steeply near the upper limit of integration. The location of the upper limit of integration (the point where the curve falls down straight in Figure 2.4) is critical, because it affects the shape of the integration

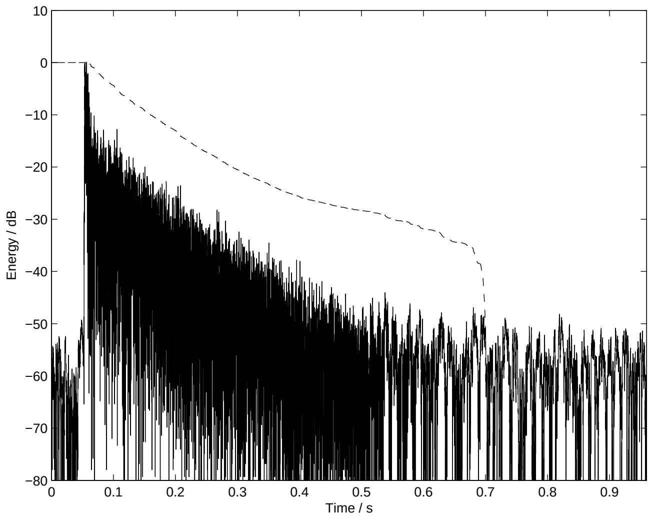

Figure 2.5: A example of the Schroeder method applied less successfully.

curve. Figure 2.3 shows the effect that the upper limit location has on the integration curves calculated from an artificially generated, exponentially decaying noise burst. If the upper limit is set too far in time into a part of the signal that does not correspond to the exponential free decay, the reverberation time might be overestimated. Figure 2.5 shows a less successful application of the Schroeder method into a different signal. The upper limit of the integration is set too far into the signal, radically affecting the end part of the integration curve. However, the entire integration curve does not need to be used for the reverberation time evaluation. These issues will be discussed in more detail later in this thesis. An example of fitting an optimal line into Figures 2.4 and 2.5 will be given in Section 2.4.

2.4 Method of least squares

It is quite common that a set of data obtained from measuring some property of a physical system is a linear function of some other variable (usually time). Sometimes this is the case only after a simple transformation of the data, such as taking a square or square root of each data element. The *method of least squares* is the most common method for fitting an optimal straight line to a data set. The idea is to fit a straight line $y = a + bx$ to given points $(x_1, y_1), \dots, (x_n, y_n)$ so that the vertical distance of these points from the straight line is minimized [26]. This is equivalent to finding the parameters a and b that minimize the sum of squares

$$q = \sum_{j=1}^{n} (y_j - a - bx_j)^2 \tag{2.18}$$

By taking partial derivatives with respect to the parameters a and b, we get the set of equations

$$\begin{aligned}
\frac{\partial q}{\partial a} &= -2\sum_{j=1}^{n}(y_j - a - bx_j) = 0 \\
\frac{\partial q}{\partial b} &= -2\sum_{j=1}^{n}x_j(y_j - a - bx_j) = 0
\end{aligned} \tag{2.19}$$

The two sums can be reordered and the normal equations are obtained as

$$\begin{aligned}
an + b\sum_{j=1}^{n} x_j &= \sum_{j=1}^{n} y_j \\
a\sum_{j=1}^{n} x_j + b\sum_{j=1}^{n} x_j^2 &= \sum_{j=1}^{n} x_j y_j
\end{aligned} \tag{2.20}$$

The parameters a and b can be solved from Eq. 2.20 as

$$\begin{aligned}
a &= \frac{\sum y \sum x^2 - \sum x \sum xy}{n\sum x^2 - (\sum x)^2} \\
b &= \frac{n\sum xy - \sum x \sum y}{n\sum x^2 - (\sum x)^2}
\end{aligned} \tag{2.21}$$

where $\sum$ stands for $\sum_{j=1}^{n} \ldots_j$. The goodness of the line fitting can be evaluated using the *correlation coefficient*

$$r^2 = \frac{\left(n\sum xy - \sum x \sum y\right)^2}{\left(n\sum x^2 - (\sum x)^2\right)\left(n\sum y^2 - (\sum y)^2\right)} \tag{2.22}$$

or the variance of the error between the actual data and the corresponding points on the line

$$s^2 = \sum_{j=1}^{n} \frac{e_j^2}{n-2} = \frac{n\sum y^2 - \frac{1}{n}\sum y - b(\sum xy - \frac{1}{n}\sum x \sum y)}{n-2} \tag{2.23}$$

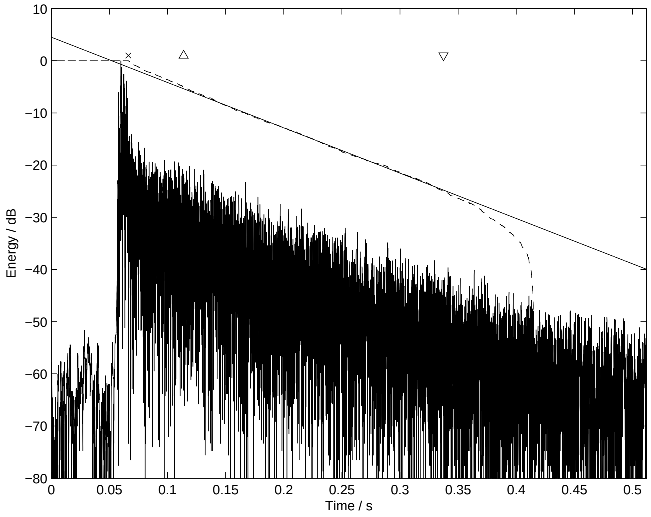

Figure 2.6: An example of fitting an optimal line to a decay curve.

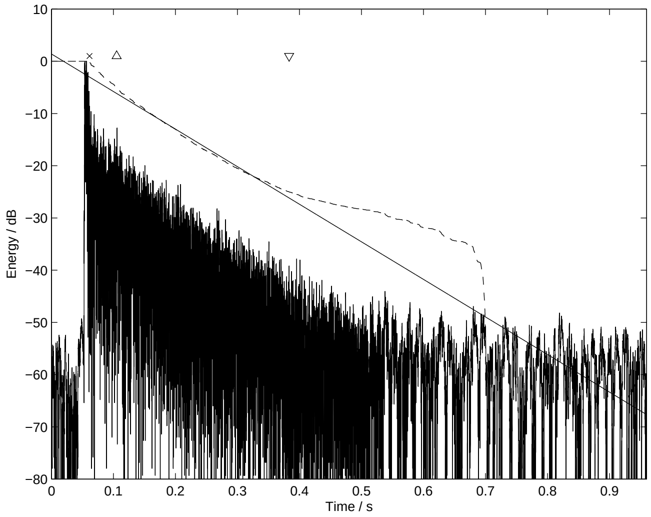

Figure 2.7: Another example of fitting an optimal line to a decay curve.

Figures 2.6 and 2.7 show an example of fitting an optimal line to integration curves obtained by the Schroeder method (see Section 2.3). The integration curves are normalized to have their maxima at 0 dB, which is also the case in Figures 2.4 and 2.5 in Section 2.3. The limits for line fitting are set to -5 dB and -25 dB on the normalized curves. The choice of the range of the decay curve used for line fitting is critical for the slope of the fitted line. A bias will be introduced to the estimated RT if the range of line fit includes a part of the downward bending slope characteristic of decay curves calculated with the Schroeder method. Naturally, all decay curves calculated from realistic signals more or less deviate from the ideal case (a straight line).

Simple least squares fit is not the only option for evaluating RT from the decay curve obtained by Schroeder method. A more sophisticated alternative method based on nonlinear regression is presented in [65]. The approach essentially fits two lines to the Schroeder integration curve to take into account the shape of the curve better than in the traditional approach. An improved version of the method is presented in [24].

2.5 Coherence function

The *coherence function* is a measure of linear correlation between two signals as a function of frequency. It is traditionally used e.g. in transfer function (input-output relationship) measurements to detect the frequencies of the signal that are contaminated by external noise. In this thesis, the coherence function is used for determining whether a certain part of a sound signal is suitable for reverberation time estimation.

Different coherence functions exist, but the most commonly used *magnitude-squared coherence*[2] (MSC) is defined as [5]

$$\gamma_{lr}^2(f) = \frac{|G_{lr}(f)|^2}{G_{ll}(f)G_{rr}(f)} \qquad 0 \le \gamma_{lr}^2(f) \le 1 \tag{2.24}$$

where G_{lr} is the one-sided cross-spectrum between x_l and x_r. G_{ll} and G_{rr} are the one-sided power spectra of x_l and x_r, respectively. One-sided spectra are used for convenience and computational efficiency, since there is no need to calculate the coherence value for negative frequencies. In this work, x_l and x_r are the signals entering the left and right ear, respectively. In real situations, the true spectra of Eq. 2.24 have to be replaced by estimates

$$\hat{\gamma}_{lr}^2(f) = \frac{|\hat{G}_{lr}(f)|^2}{\hat{G}_{ll}(f)\hat{G}_{rr}(f)} \tag{2.25}$$

The one-sided spectra in Eq. 2.25 are estimated using the formulas [2]

$$\hat{G}_{ll}(f) = \frac{2}{n_d T}\sum_{k=1}^{n_d} |X_{lk}(f,T)|^2 \tag{2.26}$$

$$\hat{G}_{rr}(f) = \frac{2}{n_d T}\sum_{k=1}^{n_d} |X_{rk}(f,T)|^2 \tag{2.27}$$

$$\hat{G}_{lr}(f) = \frac{2}{n_d T}\sum_{k=1}^{n_d} X_{lk}^*(f,T)X_{rk}(f,T) \tag{2.28}$$

[2] Also known simply as *coherence function* in some texts, e.g. [2]

where n_d is the number of signal segments of length T samples used in the estimation. $X_{lk}(f,T)$ and $X_{rk}(f,T)$ are the Fourier transforms of the kth signal segments of the left and right signals, respectively. There might be some overlap between the signal segments, but it is not necessary[3]. It is important to note that the spectra have to be estimated from more than one signal segment ($n_d > 1$), which are usually obtained by diving the signal into n_d sequences of equal length. If $n_d = 1$, the coherence estimate will be $\hat{\gamma}_{lr}^2(f) = 1$ for all f, which is a meaningless result.

In this work the number of signal segments will always be $n_d = 2$, since the focus is on the evolution of the coherence function over time, i.e., the short-time coherence. Averaging over two signal segments is the minimum amount of segments that will give meaningful results and $n_d = 2$ is therefore chosen.

It is also possible to approach the estimation of cross-spectrum and auto-spectra in a different way. Wittkopp [63] calculates the time averages of the spectra using a first order low-pass filter, which is defined for an arbitrary time series Q_k as [63]:

$$\langle Q_k \rangle = \beta \cdot \langle Q_{k-1} \rangle + (1-\beta) \cdot Q_k \tag{2.29}$$

where k is the time index and $\beta \in]0,1]$[4] is a forgetting factor that determines the amount of smoothing. The equations for estimating the spectra (Eqs. 2.27-2.29) will thus be:

$$\begin{aligned} \hat{G}_{ll,k}(f) &= \langle |X_{lk}(f,T)|^2 \rangle & (2.30) \\ \hat{G}_{rr,k}(f) &= \langle |X_{rk}(f,T)|^2 \rangle & (2.31) \\ \hat{G}_{lr,k}(f) &= \langle X_{lk}^*(f,T) X_{rk}(f,T) \rangle & (2.32) \end{aligned}$$

This way of calculating the short-time coherence results in a smoothing of the coherence function across time, which might be a favorable property for subsequent analysis, especially in terms of average of the short-time coherence across frequency.

2.6 Spectral centroid

One way to roughly describe the spectral content of a signal using a single figure is the *spectral centroid*, which can be thought as the center of the gravity of the spectrum. The definition used in this work is

$$f_c = \frac{\sum_{k=0}^{N/2-1} |X(k)| f(k)}{\sum_{k=0}^{N/2-1} |X(k)|} \tag{2.33}$$

[3] If there is overlap, the normalization terms $n_d T$ in Eqs. 2.27-2.29 should be adjusted accordingly .

[4] Note that setting $\beta = 0$ would results in coherence being identically one at all frequencies.

where N is the length of the DFT, $X(k)$ is the DFT of the signal to be analyzed and $f(k)$ is the frequency (in Hz) corresponding to the discrete frequency bin k.

The spectral centroid is usually attributed to the perceived brightness of the sound. A high value of the centroid indicates that there is considerable high frequency content in the signal, which is usually perceived as brightness in the sound.

2.7 Signal detection, segmentation and classification

Before the estimation of reverberation time can take place, it has to be decided which parts of the signal will be used for the estimation. That is, the relevant *sound events* have to be detected from the sound signals and the suitability of the obtained segments for reverberation time estimation has to be assessed (this will be considered in Section 3.2). Methods for signal detection, segmentation and classification will be presented in this section.

Audio signal segmentation and detection methods fall into two categories: general segmentation/detection methods and segmentation/detection methods for a specific class of sounds (e.g. speech). Methods from both categories will be presented in this chapter, even though the focus will be on methods with general applicability. Another way of categorizing the methods would be by features that are used in segmentation/detection. Some methods rely on a single feature, the most obvious one being the short-time energy of the signal. More advanced methods use either multi-dimensional features (such as *time-frequency representations* (TFRs), e.g. short-time Fourier transforms) or a combination of several different features calculated from short-time signal windows. The same set of features could also be used for signal classification. A general model that applies to signal segmentation, classification and detection alike, is presented in Figure 2.8.

The detection of speech, *voice activity detection* (VAD), is a very important and much researched sub-topic of general audio signal segmentation and detection. The importance of VAD is due to speech being the signal of interest that is to be transmitted in communications applications, most importantly cellular phone networks. The channel capacity has to be used as effectively as possible and thus transmitting useless information, i.e., noise, has to be avoided. This can be accomplished by detecting the time regions with voice activity in the signal picked up by the microphone. The VAD methods mostly fall outside of the scope of this work, because of their limited applicability to detecting sound events other than speech.

A few notes on the terminology should be made at this point. *Audio signal segmentation* usually refers to the process of identifying changes in signal content and is often followed by recognition or classification of the segments into discrete classes. The term is often used in the area of multimedia indexing and speech processing. *Signal segmentation* in general refers to locating the boundaries of change of a piecewise stationary signal, thus segmenting it into homogenous regions. *Sound event detection*[5] refers to locating interesting sound events that are then subjected to further processing, which could be classification or some other form of analysis. One important part of the work described in this thesis was to find a suitable way to *detect* important sound events from the continuous environmental sound signal and subject them to analysis of room reverberation time. Thus the word *detection* is more appropriate in this context, since *segmentation* is only concerned with finding any significant changes in signals, usually in statistical sense. However, the terms *detection* and *segmentation* will be used synonymously in this thesis, even though sound event detection can also be seen as a front-end to segmentation and classification, which is exactly the approach taken in this work. The idea is to first roughly pick the possibly interesting sound events and then do further processing, i.e., classification and segmentation on them. Sections 3.1.1 and 3.1.2 describe the sound event detection and segmentation algorithms used in this work. It should be noted that the former will be termed *coarse segmentation* and the latter *fine segmentation* starting from Chapter 3.

It is important to realize that all methods, whether termed detection, segmentation, classification or recognition, all have the basic structure presented in Figure 2.8. Different short-time features are calculated from an input signal, followed by a decision block that gives the result of the analysis as a function of time. One hierarchy of the four classes of methods can be found in Figure 2.9. Detection is the crudest form of signal content analysis, being only concerned with roughly locating possibly interesting events in the signal. Segmentation is more detailed analysis aiming at dividing the signal into homogenous regions, with respect to some feature(s), e.g. the short-time frequency content. Classification puts each segment, or a combination of segments, into discrete categories. Example categories could be “speech”, “music”, “environmental sounds” and “silence”. Recognition is a more accurate form of classification attempting to recognize the sound more or less exactly. For example, the category of environmental sounds might include “dog bark”, “car wheel noise”, “crickets”, “bird song” and “unknown environmental sound”. Even though the relationships between the different hierarchy levels in Figure 2.9 are unidirectional, there could be interaction from a higher to a lower level as well.

The area of signal segmentation and detection is so broad that only a small part of the available methods will be reviewed here. The emphasis will be on methods that are relevant in this work.

[5] The term “detection” usually refers to detecting a *known* signal buried in noise in the area of telecommunications signal processing.

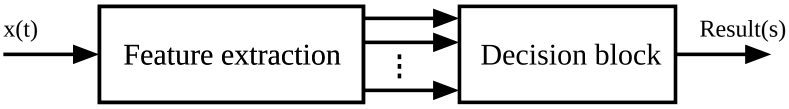

Figure 2.8: A general model for signal segmentation/detection/classification/recognition.

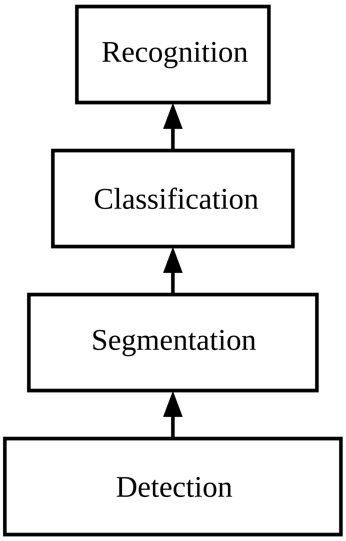

Figure 2.9: Hierarchy of signal content analysis methods.

2.8 Sound event detection methods

Sound event detection is a coarse form of sound signal segmentation. It is concerned with roughly locating the boundaries of interesting events in the sound signal. The simplest audio event detection algorithms rely on a single feature calculated from windowed segments of the signal. Actually, detection algorithms are just a subset of segmentation algorithms. The crudest and simplest forms of segmentation will be in this category.

2.8.1 Energy-based detection

The most obvious and most simple basis for signal detection would be the assumption that interesting sound events have higher signal energy than the background noise. In all energy-based detection schemes the signal energy is continuously calculated from consecutive signal windows. The signal windows are usually non-overlapping and of fixed length.

If the noise level is known to be time-invariant, a fixed threshold could be set and when the signal energy exceeds the threshold by some amount, an event onset is detected. This kind of a trivial approach is naturally not suitable for real situations where the background noise level might by varying.

The varying background noise level should be taken into account somehow when detecting audio events based on the signal energy level only. The most straightforward idea is to calculate the signal energy on a fixed-length signal window. The mean short-term signal energy computed in the previous signal frames is used as the reference. If the signal energy in the current frame exceeds the reference by a certain amount, a new event is detected. The mean of the signal energy can also be replaced by the median over the previous signal frames.

For more reliable detection of events, the time variations of the noise level can be taken into account [60]. The *energy prediction* method uses calculated energy values from a number of previous windows to predict the energy value for the current window. If the estimate differs from the true value by certain amount, an event is detected. The prediction is done using the *spline interpolation method* [26] to extrapolate the next energy value from the past measurements. The details on how exactly this is done are not given in [60]. Naturally, any other interpolation (or prediction) method could be used besides splines. The abovementioned detection method based on the average of short-time energy could also be thought as a predictive interpolation method (or more precisely, extrapolation method), even if a simple one. In that case the next short-time energy value is predicted to stay close to the average across a few frames.

2.8.2 Cross-correlation based detection

The similarity between two signals can be measured by evaluating the cross-correlation function between the signals. By thresholding the maximum value of the cross-correlation function calculated between two consecutive signal windows, abrupt changes in the signal statistics can be detected as minima in the sequence of maximum cross-correlation values [60] [59]. If the energies of the signal windows are normalized to have a maximum value of one before calculating the correlations, the method will be suitable for detecting transients, because the short onset will cause the rest of the energy values of the window to be scaled down to very small values. This will cause the sequences of correlation maxima to have a steep local minimum at the transient location.

This method can also be seen from the perspective of prediction. It is predicted that the correlation properties of the signal stay the same until something interesting, i.e., an event, happens. Yet another point of view would be that of signals and systems (see Section 2.1). The reverberation time is a property of the system and thus it can not be estimated when the output signal of the system is stationary. When there is a change in the output, a property of the system (RT in this case) can be estimated if some conditions (such as a high enough SNR) are met.

2.9 Signal classification and segmentation methods

When the interest in the signal content is not confined to its overall energy or some other simple measure, more advanced methods are needed. This section reviews some common methods that are used for signal segmentation and classification. These two tasks are often interconnected by the fact that the same or partially same set of features is used by both. Segmentation can also appear as a "byproduct" of classification, because the segment boundaries are at the time instants at which the classification result changes. The categorization presented here is not very strict, many methods might actually fall into several categories.

Since recognition is just a more accurate form of classification, it will not be treated separately in this thesis. Many of the methods presented here can also be used in recognition, even though recognition usually requires more features than classification to discriminate between the larger number of categories. *Speech recognition* is not treated here at all, even though some of the methods presented here are used in that area as well.

2.9.1 Pattern recognition based approaches

Since audio segmentation and classification can be seen as a pattern recognition problem, methods from that field have been applied to the problem by many authors, including [64] [34], [6], [33] and [44]. The usual procedure common to all approaches of this kind is to calculate some features from short-time signal windows and then pass the obtained feature vector to a classifier. The segmentation then follows from changes in the classification result. The actual classification of the segments into discrete categories might follow as the next separate stage. It is also common that a thin line exists between segmentation and classification. For example, the classification module might first discriminate between speech and non-speech signal (which is actually voice activity detection, see Section 2.9.5), followed by classification of the non-speech category into environmental sounds, music and silence [37]. The actual segmentation then follows from combining the results of the classified shorter segments.

2.9.2 Hidden Markov model based approaches

The time evolution of the statistics of a signal can be taken into account as an additional "feature" to increase recognition performance. A popular way to do this is to use *hidden Markov models* (HMMs) [47] as classifiers. The basic idea is that the statistics of the signal are modeled as states, to which initial state probabilities and state transition probabilities are assigned. The word "hidden" comes from the fact that the current state is not observable. Instead, an output is observed with a certain probability. The output can be e.g. a feature vector calculated from the signal. When using hidden Markov models as classifiers, the model has to be trained first, a procedure to which several algorithms have been developed. One model is trained for each class. A given observation sequence is assigned to the class for which the model score (likelihood) calculated from the sequence is greatest. Some examples of using HMMs for audio signal classification can be found in e.g. [15] [14] [44].

2.9.3 Machine learning based segmentation

One subset of pattern recognition based approaches are machine learning based methods [11] [12]. In practice this means applying *support vector machines* (SVM) to the segmentation process. The idea is to continuously teach a support vector machine classifier with features calculated from a number of previous signal windows and test the current signal frame features on the SVM classifier. If the SVM decides that the current signal segment does not belong to the class defined by the data set used for teaching, a signal segment boundary is detected. The features are usually based on time-frequency representations of the signals, e.g. spectrograms or other time-frequency distributions.

Other machine learning methods, such as *multi-layer perceptrons* (MLPs), could possibly be used instead of SVMs, even though not reported in literature.

2.9.4 Time-frequency representation based abrupt change detection

There exists several papers on non-parametric statistical abrupt change detection based on different measures calculated from time-frequency representations of the signals [29] [30] [31] [55]. The idea is to calculate a *stationarity index* at a certain time instant. The stationarity index compares slices of two time-frequency representations around the current time instant using some distance measure. A high value indicates that there is a sudden change in the spectral content of the signal at the current time instant. Yet again, this could be seen as one form of prediction.

2.9.5 Voice activity detection (VAD)

Voice activity detection (VAD) is a category for methods for deciding whether or not there is speech present in a given signal frame. A multitude of methods are mentioned in the literature [56]. However, the common idea in most methods is to choose features that are found to discriminate well between speech and non-speech waveforms and use them in a classifier. Most most VAD methods are thus based on pattern recognition (see Section 2.9.1).

2.10 Reverberation time estimation methods

The main task of this work is to estimate the room reverberation time (T_{60}) using arbitrary binaural signals. This section reviews some methods related to reverberation time estimation, starting from standard measurement techniques, in which the excitation signal can be controlled. Some methods that use more or less arbitrary environment signals as the excitation are described next.

2.11 Estimation methods with controlled excitation

All standard room acoustic measurements methods involve the possibility to send a controlled excitation signal to the acoustic space and the possibility to measure the response signal. The impulse response is then derived mathematically based on the excitation signal and the measured signals. Sometimes the excitation signal is not completely in control, but can be measured simultaneously with the response signal (two-channel measurement). The reverberation time is obtained from the measured room impulse response (RIR) by methods such as the method of least squares and/or Schroeder method (see Sections 2.3 and 2.4). The most common types of excitation signals are an impulse (pistol shot), a swept sine wave [42] and the *maximum length sequence* (MLS) [53]. A presentation of some typical excitation signals can be found in [45].

2.11.1 MLS

The MLS method uses a pseudo-random deterministic binary sequence as the excitation signal. The sequence has special properties that allow an efficient calculation of the impulse response by calculating a circular cross-correlation between the excitation and the response signals. The *fast Hadamard transform* (FHT) can be used for efficient calculation of the cross-correlation. The MLS method has some properties that make it attractive for impulse response measurements, such as a high signal-to-noise ratio, the possibility to calculate very long impulse responses and computational efficiency. However, much of the former hype around MLS has vanished with the increase of computational power and memory capacity of computers [42].

2.11.2 Sweep

The *sweep method* uses swept sine waves as the excitation signals. As with all excitation signals used in measurements, the excitation should include all frequencies of interest. The swept sine waves typically move from low to high frequencies, either in linear or logarithmic fashion. The advantages of the sweep method over MLS are higher immunity against time variance and distortion. The immunity against harmonic distortion makes it possible to attain a significantly higher signal-to-noise ratio than with the MLS method, without introducing distortion artifacts to the impulse response [42]. Thus the sweep method is especially suitable for measuring (binaural) impulse responses for high-quality auralization purposes, where an SNR higher than 90 dB is required [42]. Non-idealities in the measurement chain can also be easily compensated in the sweep measurements.

2.12 Estimation methods without controlled excitation

Often it is desirable to get an idea of what the reverberation time of a concert hall is at the situation where it is used, i.e., with audience and musicians playing. Measurement methods based on controlled excitation signals (Section 2.11) cannot be used in most cases. MLS could be used because the excitation signal could be played back at an inaudible level. However, very long measurement periods would be required [17]. With applications such as hearing aids it would be totally unfeasible to actively generate an artificial test signal into the environment. Methods that use sounds that are already present in the environment, e.g. speech and music, for estimation of the reverberation time are therefore needed. Not very many such methods have been proposed in the literature and it seems that this area of room acoustical analysis is constantly evolving.

Using passively received sounds as the basis for room acoustics analysis causes extra difficulties that are not present when using an impulse response measured with dedicated equipment. It is unrealistic to set a goal of estimating the room acoustic parameters to the same precision. With the focus on reverberation time, in applications such as intelligent hearing aids it is enough to know only roughly how reverberant the current environment is [48].

The methods presented in this section are divided into two categories according to a taxonomy presented in [49]. *Partially blind methods* do require some a priori knowledge about the room or the signal or some form of segmentation procedure to find the interesting sounds in the environment. The algorithm developed in this work (see Chapter 3) belongs to this category. *Blind methods* require minimal amount (if none) of a priori knowledge. The *maximum likelihood* (ML) estimation based method in [49] belongs to this category, as well as all blind deconvolution techniques, which give the room impulse response as a byproduct.

2.12.1 Partially blind methods

A method of using musical signals for the estimation of reverberation was presented in [17]. The method is based on the autocorrelation function of the reverberated musical signal. The idea is that the envelope of the autocorrelation function can not decay faster than the room impulse response. Thus the reverberation time can be calculated from the envelope of the autocorrelation function of the reverberated signal. Averaging over many estimates is naturally needed and unsuitable signal sections have to be discarded in advance.

An interesting approach for RT estimation is to use artificial neural networks for the estimation procedure [10]. The idea is to train a multilayer feedforward network with a large number of artificially created test signals that have known reverberation times. The test signals used in [10] are short speech utterances convolved with artificially generated room impulse responses of varying reverberation times. Short time RMS values are used as the features. The trained network should be able to estimate the reverberation time when the same speech utterances are spoken in an acoustic space. The method does not currently work with unrestricted speech or arbitrary signal, which limits the applicability of the method.

A dereverberation method that includes estimation of the reverberation time is presented in [32]. The algorithm presented consists of locating the parts of the signal with exponential decay and the estimating reverberation time from the obtained segments. A smoothed energy envelope is used for the calculations. The details of the detection of decaying signal parts are not given in [32].

Baskind and Warusfel mention a method for reverberation time estimation in [1]. The method is based on the idea of locating the areas of decay from an RMS plot of the signal and then calculating the Schroeder integral from each segment. The RT estimates are derived from the decay curves by linear regression. The final RT estimate is derived by discarding values that are too far from the mean and then choosing the minimum from the remaining values. It is notable that this method is the only one (of the methods presented here) which uses binaural signals for the analysis. However, the binaural nature is exploited only so that two estimates are calculated for each segment and the mean of the estimations is taken. The use of the interaural correlation function is also postulated in [1] to discriminate between free decay and the resonance of a sound source.

A quite similar automatic reverberation time estimation method based on Schroeder integration was presented in [61]. The idea is to calculate the decay curve by the Schroeder method using overlapping windows. The decay curve is calculated only when the energy of the current window is smaller than that of the previous window, indicating that the sound energy is decaying. This reduces the number of false estimates. An optimal line is fitted to each decay curve using the least squares method and the final RT estimate is derived as the maximum of a histogram of estimates. The method is quite simple and seems to depend on the window length, because a too long or short window will cause bias in the decay curves and the fitted lines.

2.12.2 Blind methods

All blind deconvolution methods, whether or not related to room acoustics, give the impulse response of the system as a byproduct. By deconvolving the impulse response out of a signal recorded in an acoustic space, reverberation time can be calculated from the response by standard methods such as the Schroeder method. Different approaches for blind deconvolution exist, some being related to blind dereverberation. Blind deconvolution only works when the impulse response is minimum-phase, a condition that is not fulfilled in most real rooms [49]. This limits the applicability of the method.

A novel approach for a completely blind maximum likelihood (ML) estimation of room reverberation time was proposed in [49]. A computationally efficient version of the algorithm has also been developed by the same authors [48]. The method is based on an exponential decay model for the diffuse reverberant tail of the room impulse response. As the response is convolved with arbitrary sound radiated into the acoustic space, the exponential decay will be present in the resulting signal. The idea is to formulate a likelihood function for the observed sample sequence and find the maximum. The sample values are taken from a sliding window, resulting in continuously updated estimates of the decay parameter, which is directly related to the reverberation time.

There are certain difficulties in implementing the method though. First, the equation that gives the value of the decay parameter that maximizes the likelihood function is transcendental, i.e., it can not be solved directly. Numerical methods have to be used instead, the authors proposing a combined use of the Newton-Raphson and bisection methods. Second, the estimates have some variance, due to the fact that not all of them are calculated from a free decay part in the signal. The main idea is that the measured signal can not decay faster than the rate specified by the reverberation time. Thus, the output of an *order statistics filter* is used to pick the decay parameter value corresponding to the peak value of a certain part of the histogram of estimates.

Another ML based approach is presented in [8] and [9]. The method somehow resembles the one presented in [49]. However, the models used are quite different. The method proposed by Couvreur is based on an AR model of reverberation and a two-state *linear predictive hidden Markov model* (LP-HMM) of the underlying clean speech, the two states being called “silence” and “speech”. The errors in reverberation time estimation of the system are in the order of 80 ms for speech convolved with real measured impulse responses and in the order of 50 ms for artificial impulse responses. This estimation method is applied for model selection in *automatic speech recognition* (ASR) systems. The idea is to train the system with artificially reverberated speech, the impulse responses having varied, known reverberation times. The model with RT most closely matching the one estimated from the environment is chosen. An increase in the ASR performance is reported in [9].

Chapter 3

The algorithm

The implemented algorithm will be presented in this chapter. The algorithm can be divided into four stages, to each of which a separate section will be devoted. Figure 3.1 presents the general structure of the algorithm.

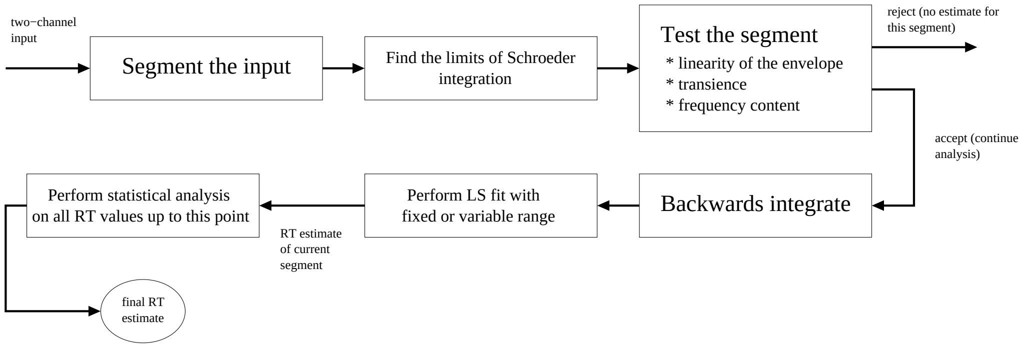
two−channel input
Segment the input
Find the limits of Schroeder integration
Test the segment
* linearity of the envelope
* transience
* frequency content
reject (no estimate for this segment)
accept (continue analysis)
Backwards integrate
Perform LS fit with fixed or variable range
RT estimate of current segment
Perform statistical analysis on all RT values up to this point
final RT estimate

Figure 3.1: Flowchart of the algorithm.

3.1 Segmentation

An important part of the algorithm is segmentation of the continuous audio stream into discrete sound events. Since reverberation time is calculated from an energy decay curve, it motivates the use of short-time signal energy as the basis of the segmentation procedure. In traditional acoustic measurements the signal-to-noise ratio is an important parameter used in evaluating the quality of measurement results. It is desirable to have a large SNR in measurements. Thus the approach in this work is also mainly based on short-time signal energy and the concept of signal-to-noise ratio.

The segmentation procedure consists of two parts. Coarse segmentation[1] is performed first. The basic idea of the coarse segmentation algorithm is to calculate an estimate for the mean background noise level and to detect sound event onsets whenever there is a large enough sudden increase in signal energy. The size of required deviation from the mean can be adjusted too meet the desired SNR requirements, since the maximum upward deviation of short-time signal energy from the noise level can be thought as an estimate for the SNR of a sound segment. Too low SNR will result in an unreliable estimate of the reverberation time.

Fine segmentation follows the coarse one, giving the exact limits that will be used for Schroeder integration (described in Section 2.3) and thus RT estimation. Each signal segment obtained as the result of coarse segmentation will be subjected to this fine-scale analysis. This part of the algorithm is the only part where the binaural nature of the signals, i.e. the fact that two different input signals exist, is used. The interaural coherence function, described in Section 2.5, is used for estimating the length of direct sound. The idea is that the average of short-time coherence over frequency tells something about the diffusiveness of an acoustical situation [63]. One could think that areas of low coherence correspond to free decay and those of high coherence to direct sound. However, the situation is more complicated than that, because the average coherence seems to depend on the frequency content of the signal and the way the different frequencies are spread across time, acting as an indicator of how transient-like a sound is (a fact that will be exploited in the estimation algorithm). More discussion on using the coherence follows in Section 4.2.

3.1.1 Coarse segmentation

The first part of the segmentation algorithm detects interesting sound events based on short-time energy values calculated from *subsegments* of length N_{sub}, i.e., short windowed sequences of the signal. The length of a subsegment is typically around 50 ms. Each subsegment sample $x(n)$ is calculated as an average of the two channels, i.e., $x(n) = 0.5(x_l(n) + x_r(n))$. The start sample index of each subsegment is denoted by n_{sub}. The energy E_{dB} of each subsegment is calculated and compared against an estimate for background noise energy level, which is the average of N_{noise} latest subsegment energy values E_{dB}. Calculation of the noise level is implemented as a circular buffer of length N_{noise}.

If the energy level of the current segment exceeds the background noise energy level by amount E_{up}, a sound event is detected. When the algorithm is started, it is assumed that the signal is background noise. It takes a few subsegments time before the algorithm gets a good estimate for the background noise level. The background noise level estimation is

[1] "Sound event detection" could be also used, but it is more clear to call the entire algorithm "segmentation", which is divided into two parts, coarse and fine segmentation.

naturally turned off during a sound event. It is also possible to clear the circular buffer at this point. The end of an event is detected when the subsegment energy level falls to $E_{noise} + E_{down}$ or when the sound event buffer is filled completely. It is usually a good idea to set E_{down} to 0 dB, because the sound event might otherwise be cut too short. The algorithm can be presented in pseudo-code as follows:

```
Algorithm Segment (coarse)
Input: Sequence of signal subsegments
Output: A contiguous signal segment
(* Initialize the "inside a sound event" flag ISE = 0 (0 - false, 1 - true). *)
(* Set subsegment counter to zero. *)
for each subsegment $x(n) = 0.5(x_l(n) + x_r(n)) \quad , n_{sub} \geq n \geq n_{sub} + N_{sub} - 1$
    do calculate the normalized energy $E = \frac{1}{N_{sub}} \sum_{n=n_{sub}}^{n_{sub}+N_{sub}-1} x^2(n)$
       convert to decibels $E_{dB} = 10 \log_{10}(E)$
       if the current frame is the first frame
         then set $E_{noise} = E_{dB}$
       if $E_{dB} > E_{noise} + E_{up}$ and ISE = 0 (noise, outside of a sound event)
         then set ISE = 1
              advance subsegment counter by one
         else if $E_{dB} > E_{noise} + E_{up}$ and ISE = 1 (inside a sound event)
                then advance subsegment counter by one
                else if $E_{dB} < E_{noise} + E_{down}$ and ISE = 1 (inside a sound event)
                       then clear the "inside a sound event" flag
                            calculate the segment length (if necessary)
                            reset the subsegment counter
       if ISE = 0 (not inside a sound event)
         then store the noise energy value into an circular buffer of size $N_{noise}$
              calculate the mean value of the buffer and convert to decibels
              store the mean as the latest noise level estimate $E_{noise}$
         else clear the circular buffer of noise level estimates (optional)
              store the subsegment sample values (both channels) into a larger buffer
              that will contain the entire sound event
       if a sound event has just ended or if sound event buffer is full
         then copy the sound event buffer to another buffer for analysis
              store the latest noise energy level estimate for analysis
              tell the low-priority (non-realtime) thread to start analyzing the latest
              segment
```

The pseudo-code in Algorithm *Segment (coarse)* describes the real-time C++ implementation. However, the only actual real-time specific part is the last conditional statement related to starting the analysis part which is performed by a separate low-priority thread. An off-line version of the algorithm could just simply perform reverberation time analysis on each segment after the entire signal has been segmented.

Figure 3.2 contains an example of the coarse segmentation algorithm operating on a sound sample consisting of three hand claps recorded in an office environment. The upper plot contains the short time energy values and the estimated noise energy level as a function of time. The noise energy level curve tracks the average of the short-time values quite accurately. The noise level estimate is not updated during a sound event, which is also evident in the figure. The lower plot shows the instantaneous energy of the sound sample with the coarse segment boundaries indicated by vertical lines. In this case the segmentation works very well. The parameters used were: $N_{sub} = 2048$, $N_{noise} = 50$, $E_{up} = 10$ dB and $E_{down} = 0$ dB. The sample rate was $f_s = 32000$ Hz.

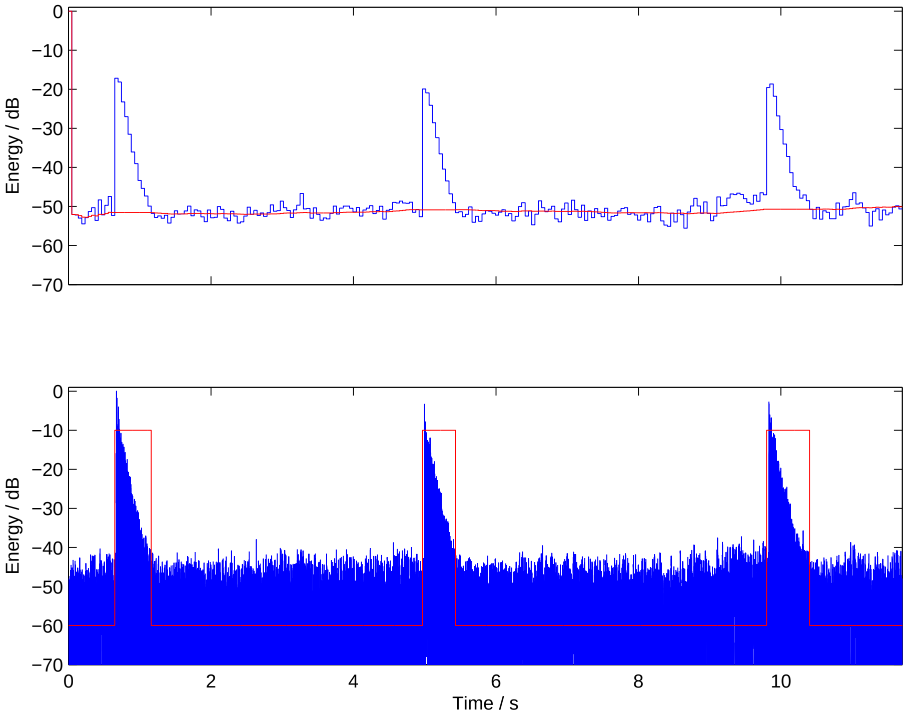

Figure 3.2: The coarse segmentation algorithm in action.

3.1.2 Fine segmentation

The purpose of the fine segmentation algorithm is to find the limits of Schroeder integration for each segment obtained as the result of Algorithm *Segment (coarse)* described in Section 3.1.1. As discussed in Section 2.3, an upper limit of integration T_i (see Equation 2.17) has to be decided prior to using the Schroeder method. A combination of two different algorithms is used here. The simplest of the two algorithms is based on the fact that a noise energy level estimate is available for each segment as a result of the coarse segmentation algorithm. The approach used here is to find the location of T_i based on the noise energy level and energy envelope of the signal. The latter is calculated from logarithmic instantaneous energy sequence of the signal using a standard envelope follower with different rise and fall times, adjusted properly for this application. The resulting envelope will follow the peaks of the instantaneous energy and can thus be used for finding T_i. The idea is to count how many samples of the envelope are under the latest estimate for noise energy level E_{noise} plus an extra marginal value E_{marg}, and then subtract this value from the buffer length[2]. This procedure is only done from the maximum value location to the end of the buffer, because there might be low enough energy values before the maximum, causing T_i to be set too early. It is also to be noted that in some cases T_i will be set to the end of the buffer if there are no samples in the envelope filling the above-mentioned criterion. A pseudo code description of the algorithm is presented in Algorithm *Segment (fine)*.

A more complicated algorithm for location T_i is described in Section 3.1.3. This algorithm requires that a part of each segment contains background noise only, i.e., the part of the signal after the decaying sound has dived below the noise floor having almost constant energy level. If there is too little samples of "background noise only" in the segment, the more complicated *knee point location* algorithm will fail to correctly determine the integration end point (see Section 3.1.3 for more discussion). This typically happens when the coarse segmentation algorithm sets the end of the segment to some point during the free decay part (before diving below the noise floor). In this case T_i should be set to the very end of the segment so that a maximal portion of the decay part is used for calculating the integration curve. The simple algorithm for T_i usually sets T_i to the last sample of the segment in these cases, even though the extra marginal E_{marg} should be properly set for this to happen. A combination of the two algorithms is therefore used for deciding the location of T_i. If the simple algorithm gives $T_i = N_{seg}(m)$, i.e., the end of the current segment, T_i is set at the end. Otherwise the the knee point location algorithm is ran and the resulting T_i is used. In this case there is need to truncate the segment from the end.

There is still one part of the overall algorithm belonging to the fine estimation procedure: locating T_d, the point up to which the decay curve is calculated using the Schroeder method. According to [16], the direct sound and first reflections have to be excluded from the reverberation time calculation. T_d should thus be set to a location where the diffuse sound field starts. One way of locating T_d would be simply by finding the point in time where the sound energy level falls below -5 dB from maximum. This approach is not very accurate though, so a more sophisticated approach is taken. The coherence function, described in Section 2.5, is used to find the length of the part of the signal containing the direct

[2] It is assumed that the energy envelope decays "almost monotonically" until the end of the envelope. This is one condition that should be fulfilled if the segment contains a transient-like sound. The other conditions will be described in Section 3.2.

sound and possibly some early reflections (see Section 4.2 for more discussion). The use of the coherence function is motivated by the hypothesis that the average of the short-time coherence function (across frequency) between left and right ear signals can be used as a measure for diffusiveness of a particular acoustic situation [63]. The interaural coherence should thus be high during the direct sound and low during the decay. However, the short time coherence depends on some other things as well. It can be used as an indicator of how transient-like the direct sound is, because transient sounds have a lot of energy across a wide range of frequencies, which in turn are concentrated around a small area in time. Thus the short-time average coherence rises to a value close to one during a transient direct sound. This fact will be exploited in Section 3.2 to discard unsuitable sound segments before the actual RT analysis.

The short-time coherence function is evaluated in the fine segmentation part of the algorithm, using it to find the point in time where the diffuse field starts by counting the number of envelope samples during which the average of the short-time coherence is above a certain threshold. The start of the diffuse sound, T_d, is calculated as follows: $T_d = T_{max} + n_c$, where T_{max} is the location of the maximum value of the envelope and n_c is the number of samples that are over the coherence threshold $\kappa_{coh,dir}$. This way of calculating T_d should give a crude estimate for the point in time at which the diffuse sound starts. It should be noted that T_{max} might be at any location during the direct sound, not just at the beginning, and thus T_d might be overestimated. This is not a big issue because the system is designed for transient sounds, which are usually not very lengthy. Overestimation is better than underestimation also because underestimation will bias the integration curve upwards whereas slight overestimation merely lowers the signal-to-noise ratio a bit.

The short-time coherence function is evaluated from overlapping windows of the entire segment. Two N_{FFT} point fast Fourier transforms (FFT) are calculated from each window of length $2N_{FFT}$, one from the first N_{FFT} samples and another from the last N_{FFT} samples. Thus there are no overlapping samples used when calculating the two transforms from a single window. The reason for calculating two transforms for each short-time coherence function is that time averages have to be used when calculating coherence (see Section 2.5 and Eq. 2.25). This part is done for both channels, resulting in a total of four FFTs per window.

The short-time coherence can alternatively be calculated using first order low-pass smoothing of the spectra, as discussed in Section 2.5. The user can change the amount of smoothing by adjusting the forgetting factor β. Setting $\beta = 0$ will revert into using the way of calculating the coherence that was described before.

The algorithm can be summarized as follows:

Algorithm *Segment (fine)*

```
Input: Signal segment of size $N_{seg}(m)$, where $m$ is the segment index
Output: A contiguous signal segment
for segment $s_m(n)$ $,0 \geq n \geq N_{seg}(m) - 1$
    do calculate the energy envelope $e_m(n)$ of segment $s_m(n)$
        find the number of samples $N_s$ that fulfill $e_m(n) < E_{noise} + E_{marg}$
        set the upper limit of Schroeder integration to $T_i = N_{seg}(m) - N_s$ (in samples)
        if knee-point location algorithm is to be used
          then if $N_s = 0$ (i.e. $T_i = N_{seg}(m)$, at the end of the segment)
                  then $T_i$ is kept at the value calculated before
                  else determine $T_i$ location using the algorithm described in Section
                       3.1.3
        calculate the short-time coherence function from overlapping windows
        find the amount $n_{coh}$ of short-time average coherence functions that fulfill the
        condition $\frac{1}{k}\sum_{k=0}^{N_{FFT}/2-1} G_{lr}(k,n) > \kappa_{coh,dir}$, $n$ is the start sample index for
        the coherence window
        length of the direct sound is then obtained as $n_c = (2N_{FFT} - O_{verlap})n_{coh}$,
        where $O_{verlap}$ is amount of overlap between two consecutive windows (in samples)
        estimate for the start of the diffuse sound is $T_d = T_{max} + n_c$
return $T_i$ and $T_d$
```

Figure 3.3 shows an example of using the short-time average coherence to locate the start of the diffuse sound T_d. The line fitting limits (-5 dB to -35 dB in this case) are denoted by ▽ and △ in Figure 3.3 (and also in all other plots in this thesis). By inspecting the figure it is clear that the method gives a somewhat better estimate for T_d than merely locating the point where the envelope (thick line in upper plot) falls -5 dB below its maximum value. However, by visual inspection it is also clear that T_d should be set a little bit further in time. Size of the coherence calculation window and the overlap naturally have an effect on the estimated value of T_d, since T_d will be a multiple of the difference between those parameters (see Algorithm *Segment (fine)*).

3.1.3 Another algorithm for finding the upper limit of integration

This algorithm is used in conjunction with the simpler algorithm described in Section 3.1.2 for locating, T_i, the upper limit of Schroeder integration. The simpler algorithm is likely to fail in some cases, depending on how the coarse segmentation algorithm has cut the segment (see Section 3.1.2 for discussion). If there is enough "noise only" in the end of the segment, a more complicated algorithm should be used.

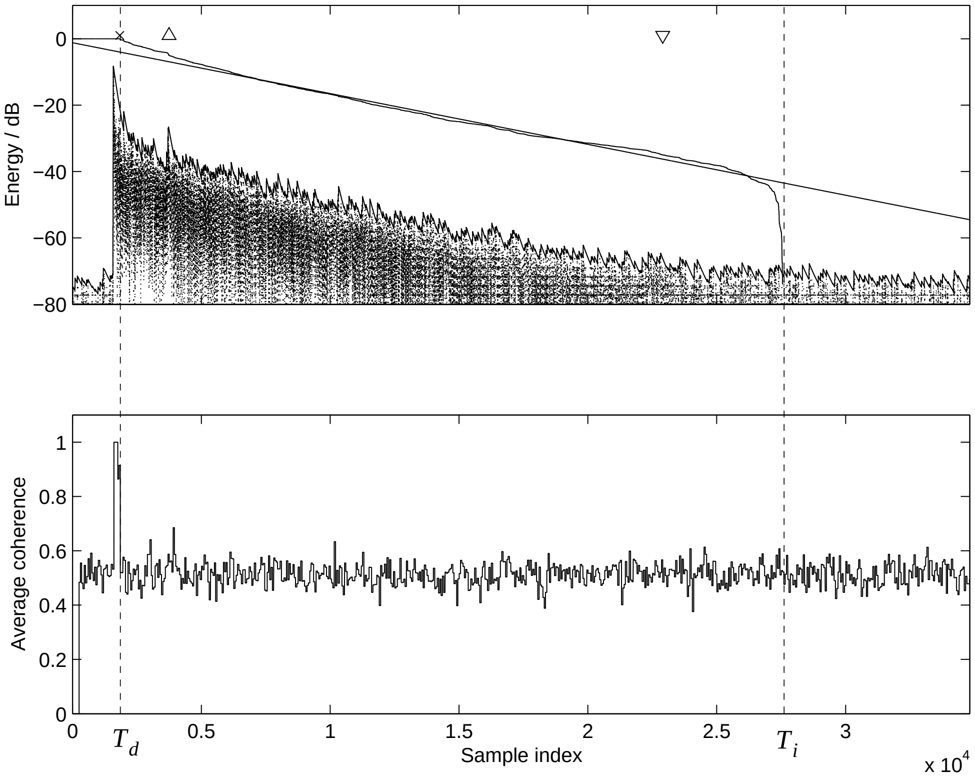

Figure 3.3: An example of Schroeder integration with the limits T_i and T_d.

As was discussed in [7], [41] and in Section 2.3, T_i should be set to the "knee point" on the squared impulse response, i.e., the point where the decay hits the noise floor. This point is an ideal choice for T_i, because at the knee point the contribution of noise to the shape of the curve is minimal and a maximal portion of the decay curve is used for evaluating the Schroeder integral.

This algorithm locates the knee point by first calculating a *cumulative distribution function* (CDF) of the envelope samples. This is done by counting the number of samples that are below certain threshold values that increase in equal sized steps. Because the *probability density function* (PDF) is the derivative of the cumulative distribution function [39], it is easy to get an estimate for the PDF by approximating the derivative of the CDF at each point. This is done simply by calculating the difference between two successive elements[3] of the CDF. The maximum location of the PDF is then taken as an estimate for the noise level on the envelope, $E_{noise,env}$. This is justified by the fact that if the noise level stays constant enough, there will be lots of noise samples around a certain area in the envelope. These samples are located after the knee point of the envelope curve. The number of enve-

[3] The `diff` function of MATLAB does this by default.

lope samples that are over the level $E_{noise,env}$ plus a marginal value, gives T_i when summed together with T_d.

The approach presented here performs best when the noise level is constant and does not have much fluctuations. Figure 3.4 illustrates the performance of the algorithm. The upper panel shows the instantaneous energy and its envelope. T_i is marked by a vertical line. The curve obtained by Schroeder integration is also shown. In this case the algorithm performs very well. The cumulative distribution function is plotted in the middle panel. A rapid rise around 50-60 dB is visible in the curve. The lower panel presents the difference function (derivative) of the CDF. There is a clear peak around 55 dB, which seems a plausible estimate for the noise level of the energy envelope in the upper panel.

As was discussed in Section 3.1.2, the knee point location algorithm fails if there are too few or no samples of “background noise only” in the segment. In these cases the PDF will contain multiple peaks corresponding to slight variations of the decaying envelope. The energy envelope level of the noise will be most likely overestimated, resulting in T_i to be set too early in time. In these cases T_i should be set to the end of the segment.

Algorithm *Find knee point*
Input: Energy envelope of length $N_{seg}(m)$, where m is the segment index
Output: Upper limit of Schroeder integration T_i

```
1.  for envelope $e_m(n)$ , $T_d \geq n \geq N_{seg}(m) - 1$
2.      do for threshold $\tau_k = -100$ , $\tau_k < 0$
3.          do find the number of envelope samples that fulfill $e_m(n) < \tau_k$
4.             store the number in array $CDF(p)$
5.             update the threshold $\tau_k = \tau_k + 0.5$ (dB)
6.      calculate the difference for each element of the array $PDF(p) = CDF(p+1) - CDF(p)$ (excluding the last element)
7.      find the decibel value corresponding to the maximum peak of the PDF
8.      count the number of samples over the threshold and add together with $T_d$ to obtain $T_i$
9.      return $T_i$
```

3.2 Testing the segments

Each segment will be subjected to a few tests that try to determine whether the sound segment is suitable for reverberation time estimation. Transient sounds, such as hand claps, snaps and pistol shots, are usually clearly localized in time and have a broad frequency content, thus being the best class of sounds to be used for calculating the reverberation

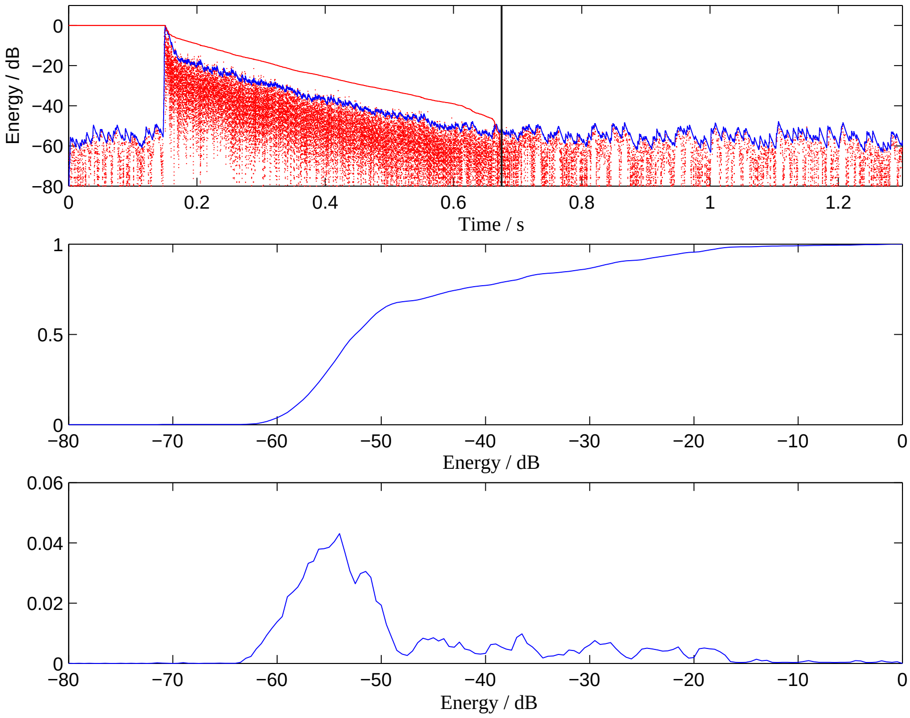

Figure 3.4: The knee point location algorithm in action.

time.

There are basically three tests that are performed on each segment. The order of the three tests is not important, even though they are presented here as an ordered list. Each test involves calculating a certain figure from the segment data and checking whether the value is within limits specified by the user. The three tests are:

1. Testing the linearity of the energy envelope[4]

2. Checking that the sound is transient enough

3. Roughly calculating the frequency content and rejecting sounds with frequency content concentrated too low or too high

The first one of the tests is done by fitting an optimal line to the energy envelope. The line fit range is from the maximum value to the end of the buffer. The end point of Schroeder integration (denoted by T_i, see Section 3.1.2) could also be used as the other limit of the range. However, the idea of the line fit at this point is to check that the sound segment decays linearly enough to be used in subsequent analysis. Therefore it is better to also include the

[4] Exponential decay is linear on decibel scale.

end of the buffer for this check, since something might happen after T_i, indicating that the current segment is not very suitable for reverberation time analysis. This is intended to be a very coarse check to make sure that there is nothing strange happening in the current segment. A value for correlation coefficient of line fitting as low as 0.8 could be used.

The motivation behind the second test is the fact that transient sounds, such as hand claps, have desirable properties for reverberation time estimation. Transient sounds usually have their frequency content concentrated around a small time window, which in turn raises the short-time average coherence. The test involves further inspection of the short-time average coherence that was calculated in Algorithm *Segment (fine)* (Section 3.1.2). The maximum value of the short-time coherence is compared against a user-definable threshold value $\kappa_{coh,max}$[5]. If the maximum value is below the threshold, the segment is discarded.

The reverberation time varies as a function of frequency and since arbitrary sounds may have arbitrary frequency content, the frequency content of each sound segment has to be taken into account. If a single figure, the reverberation time T_{60}, is given, it is usually assumed to be calculated on the octave band centered at 500 Hz (see Section 2.2.1). Sound segments that have considerable frequency content at lower and higher frequencies should thus be excluded from the reverberation time analysis. This is done by first calculating the spectral centroid defined in Section 2.6. The spectral centroid is calculated from a single window starting from the maximum value of the energy envelope. If the centroid value is outside a frequency band specified by the user, the sound event is discarded. The spectral centroid is a very rough measure of the frequency content of a signal, but quite adequate for this application, since the idea is to simply rule out extreme cases, especially sounds that have substantial low frequency content. Another way of getting rid of low-frequency segments could be high-pass filtering of the signal prior to analysis. The cut-off frequency could be somewhere around 100 Hz.

3.3 Estimation of RT

This part of the overall algorithm is quite straightforward and relies on the well-known Schroeder method (see Section 2.3) and the least squares method for line fitting (see Section 2.4). The Schroeder integral is calculated from the instantaneous squared signal for a range of T_d to T_i. The integration curve is normalized to have its maximum value at 0 dB. This is done by subtracting the maximum value from the curve. Line fitting is then performed on the normalized integration curve. There is just one important decision related to the least squares fit, namely the range of the integration curve that the line is fitted to. A simple choice would be a fixed range, -5 to -25 dB or alternatively -5 to -35 dB. There is a

[5] This is not the same threshold that was used in locating the end of direct sound in Section 3.1.2.

problem with the fixed range approach though. A bias might be introduced to the slope of the fitted line at either end of the integration curve. This is a big problem especially with uncontrolled excitation signals, when nothing can be done to improve the signal-to-noise ratio. An algorithm (or rule) for finding the range of line fitting was developed as part of this work (see Section 3.3.1).

The reverberation time T_{60} itself is calculated from the slope of the fitted line by a very simple formula:

$$T_{60} = -\frac{60}{b}\frac{1}{f_s} \quad , b < 0 \tag{3.1}$$

where b is the slope of the fitted line and f_s is the sampling frequency.

3.3.1 Finding the limits for line fitting

The limits of the least squares fit are important for accurateness of the RT estimates. Even a small bending of the integration curve may strongly affect the slope of the fitted line and the RT calculated based on the slope. The lower limit for line fit[6] is especially important, since the Schroeder integration curve always bends down at the end. If the integration is started too far in time, i.e., during the background noise, the integration curve will be bent upwards at the end, making RT to be overestimated. It would be advantageous to do the line fitting to a part of the integration curve that is as linear as possible, yet having a maximal portion of the curve to be included in the fitting.

One possible solution is based on doing the line fitting multiple times, moving the lower limit from the end (or -25 / -35 dB) towards the -5 dB point, at which the other limit of line fit is kept fixed. A small marginal is left near the -5 dB point, since the least squares fit becomes very noisy in this application when the data record is too short. Obviously there is no point in doing the line fitting for just a couple of integration curve samples. The end point is moved after each least squares fit calculation and T_{60} is calculated from the slope of the line b (using Equation 3.1). Finally the correlation coefficient r^2 is stored in an array. It is hypothesized that the best reverberation time estimate could be found by locating the maximum of the r^2 curve and picking the T_{60} from the same location in time.

Figure 3.5 shows the RT (middle panel) and correlation coefficient (lower panel) plotted as a function of the location of the rightmost line fitting limit. The rightmost limit of line fitting starts from -35 dB and moves with hops of 40 samples towards the -5 dB point, leaving a 100 sample marginal. It seems that a good choice for the rightmost limit of line fitting would be at the point where the correlation coefficient reaches its maximum value (marked by ’x’ in the figures). The effect of downward bending of the integration curve is

[6] The one that is further in time.

clearly visible in the lower panel of Figure 3.5. It seems that picking T_{60} from the location corresponding to the maximum of r^2 is advantageous compared to simply taking the -35 dB value, which is somewhat under the true value in this case[7]. The hypothesized advantage of the method will be tested at the evaluation section of this thesis (Chapter 4).

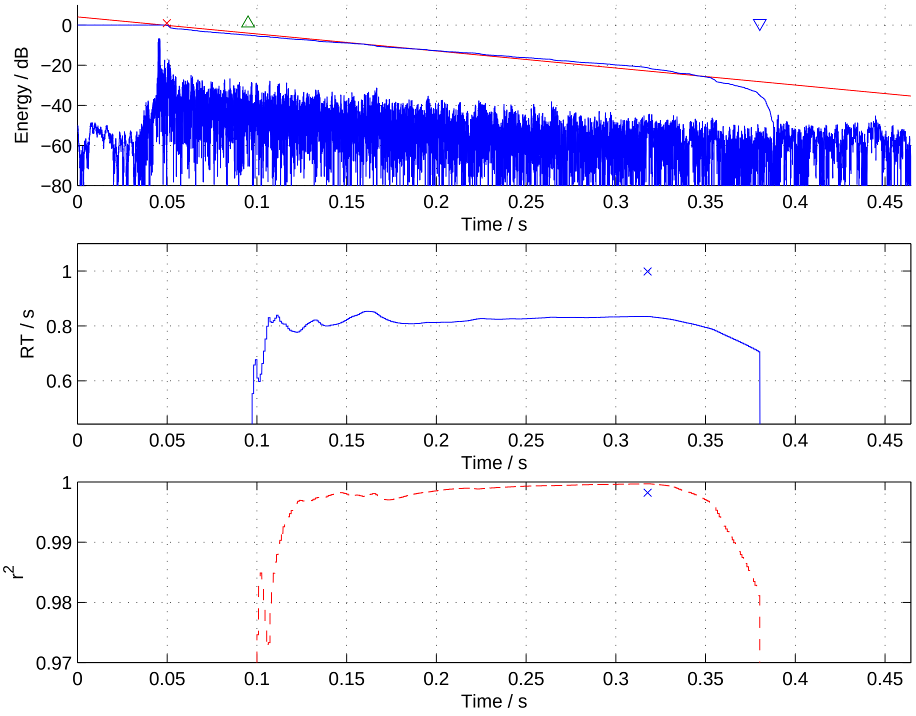

Figure 3.5: Finding the linear regression range when knee point algorithm was used.

3.4 Deriving the final RT value based on statistics

Since reverberation is a random process (see Section 2.1.2), it is impossible to get an accurate estimate of the reverberation time based on just one realization of the process, i.e., one decaying segment, especially with uncontrolled excitations. Several estimates are needed as well as a method for calculating T_{60} based on the ensemble of estimates. The most obvious idea would be calculation of a running mean from a number of latest estimations. This approach has some flaws though, because if the distribution of RT estimates is not symmetric, the mean will not give the location of the peak in the distribution. The mean will also be biased by outlier values, causing the resulting estimate to be very noisy. The next idea would be to calculate a running median instead of the mean. The median is the middle

[7] $T_{60} \approx 0.8$ s, the sound sample is a reverberant hand clap.

value after ordering a number of samples, i.e, 50 % of the distribution will be below the median. For perfectly Gaussian distributions the median will be equal to the mean, giving the peak location in the distribution (or probability density function).

The running median and the running mean are actually special cases of an *order statistics filter*[8] (OSF) [4]. The mean is a purely linear operation while the median is non-linear, moving to the area of *non-linear filtering* [27]. A general order statistics filter gives out a linear combination of ordered sample values. If only the middle value is given out, the resulting filter is the median filter. Ratnam et al. [49] [48] use an order statistics filter to derive the final RT estimate from a histogram of estimates using an order statistics filter. They propose two different strategies to be used in different situations. One idea is to output a value that limits 10 % of the histogram (distribution) values below itself. The other idea is also motivated by the histogram of estimates and is not actually an order statistics filter. The idea is to choose the RT value corresponding to the lowest peak in the histogram. This is also very suitable for the current algorithm, because unlike in the algorithm proposed by Ratnam et al., the estimates are only calculated from the parts of the signal with free decay, provided that the checks in Section 3.2 do not fail. No estimate is calculated from other parts and the histogram should thus have a clear peak close to the true RT value. Due to the statistical nature of reverberation and the fact that the incoming signal is arbitrary, it will take a few estimates before a prominent peak will appear in the histogram.

It is also possible to set a forgetting factor $\alpha_h \in]0, 1]$ to create a "fading" histogram. After a new estimate is calculated and the corresponding histogram bin value is accumulated by one, each histogram bin is multiplied by α_h. The motivation behind the fading histogram is that when the user moves into another room, the new RT will be picked up by the algorithm sooner, thanks to the decreasing RT peak of the previous room. The value of α_h is typically a little bit below one. If $\alpha_h = 1$, the histogram remains untouched after each new estimate is added.

3.5 Implementation of the algorithm

An initial version of the algorithm was first written for MATLAB. The MATLAB implementation was then translated to a real-time implementation in C++ using the Mustajuuri [21] framework. The real-time algorithm uses *threads* [57] to divide the computational burden over time. A real-time DSP thread is responsible for collecting samples to buffers and locating sound events based on short-time energy calculations (more detailed discussion in Section 3.1). The latter process will be termed "segmentation" (see Section 2.7 for more discussion). After the end point of a sound segment is decided, the corresponding segment

[8] Also known as *L-filter* [27]

is handed over to another thread with lower priority. This makes it possible to do intensive calculations without overloading the processor.

The algorithm has several parameters that the user can adjust using the GUI of the algorithm as shown in Figure 3.6. The plug-in running the algorithm also connects itself into plugins that create the late reverberant part into the signal that is to be auralized. This makes it possible to automatically adjust the amount of late reverberation to match the reverberation of the surrounding environment. Even if there are lots of user-adjustable parameters, most of them need not to be touched. The default values will work fine for most situations.

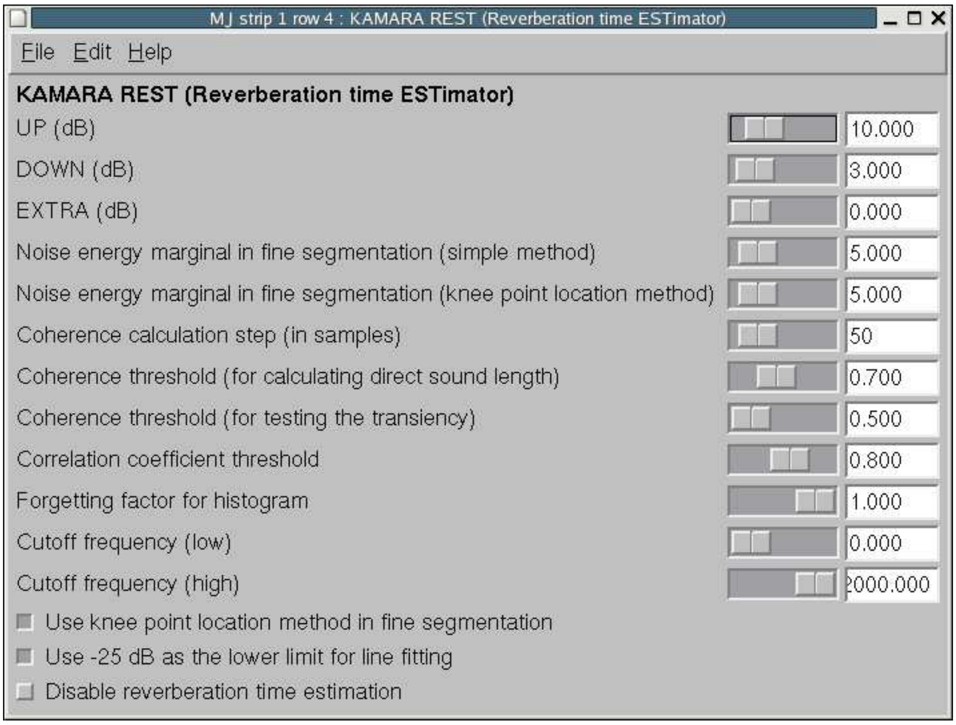
MJ strip 1 row 4 : KAMARA REST (Reverberation time ESTimator)
File Edit Help

KAMARA REST (Reverberation time ESTimator)

UP (dB)	10.000
DOWN (dB)	3.000
EXTRA (dB)	0.000
Noise energy marginal in fine segmentation (simple method)	5.000
Noise energy marginal in fine segmentation (knee point location method)	5.000
Coherence calculation step (in samples)	50
Coherence threshold (for calculating direct sound length)	0.700
Coherence threshold (for testing the transiency)	0.500
Correlation coefficient threshold	0.800
Forgetting factor for histogram	1.000
Cutoff frequency (low)	0.000
Cutoff frequency (high)	2000.000

■ Use knee point location method in fine segmentation
■ Use -25 dB as the lower limit for line fitting
□ Disable reverberation time estimation

Figure 3.6: Control window of the reverberation time estimation plugin.

The adjustable parameters of the control window are presented next.

UP (dB) This is the energy deviation threshold (E_{up}) used in the coarse segmentation algorithm (see Section 3.1.1). It determines the sensitivity of the system for detecting sound events. A typical value would be 10 dB or more, depending on how good quality RT estimates are required. If E_{up} is set too low, the system will be clogged with false detections.

DOWN (dB) It is often necessary to set the end of a sound segment a little bit over the current noise level E_{noise}. The energy deviation threshold E_{down} determines how far into the decay the coarse segmentation algorithm sets the end of the segment. A too low value will cause too much noise to be left into the segments, while a too high value will cut the segment too early. A good choice for E_{down} would be around 2-5 decibels.

EXTRA (dB) If a high SNR and good quality estimates are desired, it might be advantageous to analyze only those sound segments that have a large upward deviation from the noise mean, yet excluding segments with lower SNR from calculating the noise level. By adjusting this parameter to a value greater than zero, only segments that have an onset of more than $E_{up} + E_{extra}$ decibels will be included in reverberation time analysis. Segments with onset greater than E_{up} will be excluded from the noise level calculation but not included in RT analysis, i.e., the low-priority thread is not started.

Noise energy marginal in fine segmentation (simple method) When the simple fine segmentation method, described in Section 3.1.2, is used for determining the truncation point T_i, an energy threshold little bit greater than the noise mean is needed. In practice, this marginal (E_{marg}) determines how far into the decay T_i is set. A typical value for this parameter would be around 1-5 dB.

Noise energy marginal in fine segmentation (knee point location method) This is the same parameter as the previous one with the exception that this one is used in the more advanced knee point location method described in Section 3.1.3. It is thus possible to adjust the marginals of the two algorithms separately. This parameter is also usually set around 1-5 dB.

Coherence calculation step (in samples) This is the window “hop” size for calculating the short-time coherence of each signal segment. A too high value will cause the average coherence to be too coarse over time, whereas a too low value will most likely clog the system, as the calculation will take too much time. A typical value for this parameter is around 50 (samples).

Coherence threshold (for locating the start of diffuse sound) In Section 3.1.2 it was hypothesized that the average of short-time coherence could be used to find the start point of the diffuse sound and thus the point onwards from which the reverberation time would be evaluated. This parameter controls $\kappa_{coh,dir}$, a threshold value for the average short-time coherence. The start of diffuse sound is located based on the average coherence being higher during the direct sound and reflections. A typical value for this threshold would be around 0.7 - 0.9. It is generally better to set this threshold into a high enough value.

Coherence threshold (for testing transience) There is a clear peak in the average short-time coherence for transient sounds. By thresholding the maximum value of the average short-time coherence for a given sound segment, the sounds that are "transient enough" can be detected. A typical value for this parameter would be around 0.8 - 0.9. Setting this parameter to 0.5 effectively turns the transiency check off, since for diffuse, non-correlating sound segments the average coherence over frequency will fluctuate around 0.5, so there is always one value that is equal or greater than 0.5.

Correlation coefficient threshold Each segment is tested for anomalities in the energy envelope shape, as described in Section 3.2. The idea is to rule out very nonlinearly shaped envelopes, indicating that there is not well-behaving linear decay in the current sound segment. A sound segment is totally useless for RT evaluation if there is no exponential decay[9] present in the energy envelope. This parameter would be typically set to a value around 0.8, effectively ruling out the most pathological cases.

Forgetting factor for histogram It is possible to get a fading histogram by setting this value to less than one. The histogram values are multiplied by the forgetting factor after each new estimate has arrived, i.e., the corresponding histogram bin value is accumulated by one. A typical value for the forgetting factor would be greater than 0.9. Setting the forgetting factor to one effectively results in a normal, non-fading histogram.

Lower limit for spectral centroid (in Hz) The frequency content of the binaural signals should somehow be taken into account, since reverberation time of an acoustic space is more or less frequency dependent. This algorithm approaches the problem by discarding segments that have their energy concentrated too high or too low (see Section 3.2). The spectral centroid, described in Section 2.6, is calculated from a signal window starting at the maximum value of the buffer (which is roughly close to the start

[9] Exponential decay is linear on a logarithmic scale.

of the direct sound). This parameter gives the lower limit for acceptable value of the spectral centroid in Hz. If the spectral centroid of a given segment is below this lower limit, the segment is excluded from subsequent analysis. A typical value for this parameter could be around 300-500 Hz.

Upper limit for spectral centroid (in Hz) This is the upper limit for spectral centroid (see discussion above), typically set around 5 kHz.

Use knee point location method in fine segmentation If checked, the more complicated algorithm for locating the upper limit of Schroeder integration (T_i) will be used (see Section 3.1.3).

Use -25 dB as the lower limit for line fitting If checked, -25 decibels will be used as the lower limit in the least squares calculations (see Section 2.4). Otherwise -35 dB will be used. It should be noted that the algorithm that searches for the optimal linear regression range (see Section 3.3.1) will use the same lower limit as a starting point, if activated.

Disable reverberation time estimation Checking this box will disable the RT estimation, i.e., the low-priority thread is not started. The coarse segmentation and noise level estimation will keep on running.

Chapter 4

Evaluation

This chapter is devoted to the evaluation of the implemented algorithm. Some basic properties of the algorithm are tested first using synthetic excitation signals. The algorithm is also tested with more realistic signals by convolving an anechoic recording with binaural room impulse responses measured from a few different spaces.

It is important to verify the basic functionality of the algorithm. The first part of evaluation uses simple artificial signals to check that the algorithm estimates the decay correctly. Test signals of systematically varied frequency content are fed into the system to get an idea of how the frequency content affects the estimation results. Short time coherence plots are also investigated to see how the frequency content of the input signal affects the average of the coherence and whether the coherence actually can be helpful in discriminating between the direct sound/reflections and the diffuse tail.

Moving towards more realistic usage of the algorithm, the next part of evaluation consists of convolving anechoic source signals with *binaural room impulse responses* (BRIRs) measured from different rooms. This part of evaluation is quite similar to the part with synthetic signals. The purpose is to verify that the algorithm also works with non-synthetic signals.

The true performance of the algorithm is what really counts. That is why the algorithm is also evaluated by using realistic signals, simulating a real usage situation. The binaural signals from microphones worn by the user are recorded using a portable hard-disk recorder.

4.1 The signals and impulse responses used in evaluation

In order to test the algorithm, some monophonic anechoic source signals and binaural room impulse responses are needed to compose the test signals. The author made a few recordings in the small anechoic chamber of the HUT Laboratory of Acoustics and Audio Signal

Processing[1]. The recordings consisted of hand claps, finger snaps and some miscellaneous utterances, all performed by the author.

Binaural room impulse responses were obtained by various methods. The author measured one of the responses from an office space (A152). Another impulse response of a small lecture hall (T3) was provided courtesy of a colleague of the author and yet another one (Pergola) was obtained from the Ramsete web site[2]. Thus a total of three different binaural room impulse responses were used for the evaluation. All responses have reverberation times differing by more than approximately 200 milliseconds. All BRIRs were processed by a method proposed in [22] in order to extend the reverberant decay below the original noise floor. This is necessary for good quality auralization.

The true reverberation times were measured from each response by the standard Schroeder method with the integration limits chosen by manual inspection. The objective was not to get a very high quality estimate for the RT, but a "close enough" value. A high quality RT estimate would have required several impulse response measurements. Results of the manual reverberation time evaluation can be found from the in Table 4.1. The evaluation ranges were also given. The range of T3 is five decibels shorter, because the poor SNR did not allow evaluation up to -35 dB. The response measured from A152 has the best SNR, thanks to the sweep measurement method (see Section 2.11.2).

The BRIR of the author's office room was calculated as follows. A Genelec[3] monitor speaker was fed with a logarithmic sine sweep of length 3 seconds plus 2 seconds of silence. The same amount of data was simultaneously recorded by using a custom-made headset (see Section 1.1) worn by a user located approximately two meters from the speaker. Using the acquired data, the BRIR was obtained by frequency domain division $H(z) = Y(z)/X(z)$, which is also the frequency-domain definition of transfer function. The method used for measuring the BRIR did not include compensating for non-idealities in the measurement chain, as described in a tutorial paper on sweep measurements by Müller and Massarani [42]. Sweep method was chosen, because it gives a better signal-to-noise ratio than MLS and is also easier to implement [42]. An estimate for the true reverberation time was calculated by Schroeder integration and line fitting. The integration limits T_d and T_i (see Section 3.1.2) were chosen by hand. The procedure was performed for both channels and the final T_{60} value was derived as the mean between the two channels. The same method was used for determining the approximate true RTs of the two other responses (see Table 4.1).

[1] `http://www.acoustics.hut.fi`

[2] `http://www.ramsete.com/Public/Aurora_CD/RoomIR/`

[3] `http://www.genelec.com`

Table 4.1: Reverberation times of the three acoustic spaces used in evaluation.

Room	RT (s)	Evaluation range (dB)
T3 (a small lecture hall)	≈ 0.6	-5 to -20
A152 (office room)	≈ 0.8	-5 to -25
Pergola (unknown space)	≈ 1.2	-5 to -25

4.2 Tests with synthetic excitation signals

The system was first tested with synthetic signals. The test signals were generated by convolving short 30 ms low-pass filtered bursts of white noise with a binaural room impulse response calculated from the office room of the author (A152, see Section 4.1), with reverberation time of approximately 0.8 seconds. Each test signal had eight similarly filtered pulses with seven seconds of silence in between the pulses. The long silence was required to avoid segmentation errors. The pulses were filtered with cut-off frequencies $\frac{7}{8}\frac{f_s}{2}$, $\frac{5}{8}\frac{f_s}{2}$, $\frac{3}{8}\frac{f_s}{2}$ and $\frac{1}{8}\frac{f_s}{2}$ (see Table 4.2). The sample rate used was $f_s = 44100$ Hz. Spectrograms of the pulses can be found in Figure 4.1. The uppermost pulse in Figure 4.1 is an unfiltered pulse that was not used in the evaluation. The four filtered pulses are then presented in the order of decreasing cut-off frequencies.

Table 4.2 presents the estimation results. It should be noted that the results in Table 4.2 are simply calculated as the mean values of all estimates, excluding estimates that are over 1.5 seconds long (there were none in this case). All other estimates are included in the mean calculation, i.e., the tests described in Section 3.2 are not used here. The time evolution of the estimates was not a concern here, so all of the results presented later in this section are the mean values after the input signal has ended. The knee point location algorithm (see Section 3.1.3) was used for locating T_i, whenever applicable (see Algorithm *Segment (fine)*). The algorithm for locating the line fitting limits is also not used. Instead, a fixed range of -5 to -25 dB was used.

By inspecting Table 4.2 it is clear that there is some variation in the estimation results. It seems that the frequency content of the signal does not have a big influence on the estimation results in this case. Nevertheless, if the signal has much low frequency content (the cases where $f_c = \frac{1}{8}\frac{f_s}{2}$, the lowest row), the reverberation time is somewhat larger. The frequency-dependency of T_{60} also depends on the particular room. Even though the system was not tested with high-pass signals, signals with frequencies concentrated at high frequencies usually result in shorter RT estimates.

Obviously it is a good thing that the frequency content does not have more influence on the RT estimations. By discarding the bad segments with frequencies concentrated too low or too high, the RT estimation will be more accurate. Natural signals have more complicated spectra, so the influence of the frequency content on the estimated RT values is more complicated.

The energy threshold E_{down} does not have much influence on the estimation results. However, the standard deviation (presented in brackets in Table 4.2) seems to be higher when $E_{down} = 2$ dB. The effect of E_{down} is basically to adjust the energy level where the coarse segmentation algorithm cuts the segment off, relative to the estimated noise level. A higher value will basically result in the segment ending sooner than with a lower value.

Figures 4.2 and 4.4 present the average of the short-time coherence for two pulses with different frequency content. The upper panel contains the instantaneous energy, its envelope, and the fitted line (similar to the plots in Chapter 3). The lower panel contains average of the short-time coherence as a function of time. Length of the original pulse (30 ms) can be clearly seen in the lower panel of Figure 4.2. There is also a short peak at the starting point of the pulse, after which the coherence decreases. This is possibly due to the early echoes and diffuse decay that start to appear in the coherence calculation window. In the case of Figure 4.2 the signal has a broad bandwidth close to white noise. When the bandwidth is reduced (Figure 4.4), it becomes difficult to see anything useful in the short-time average coherence.

The short-time coherence as a function of time, a coherogram, is presented in Figures 4.3 and 4.5, for the $f_c = \frac{7}{8}\frac{f_s}{2}$ and $f_c = \frac{1}{8}\frac{f_s}{2}$ cases, respectively. The short-time coherence is calculated as is presented in Section 3.1.2. The effect of signal frequency content on the coherence is evident in both plots. The broadband pulse has a clear rise in coherence over a wide range of frequencies, whereas the narrowband pulse does only raises the coherence on low frequencies and not very much. A basic property of the coherence can be seen from the figures: the coherence is always quite high on the lowest frequencies (for frequencies below about 500 Hz).

It is clear that several improvements could be made to the coherence calculation. First of all, some time averaging could be introduced into the evaluation of the cross-spectra and auto-spectra needed in calculation of the coherence, as is done in [63] (see Section 2.5). This would smoothen the short-time average coherence and the coherence. Figures 4.6 and 4.7 present an example of smoothing with the forgetting factor set to $\beta = 0.8$. It is evident that the average coherence and the coherogram are much smoother now, compared to Figures 4.2 and 4.3. However, the value of the average coherence is lower during the decay. In fact, the average coherence is dependent on the forgetting factor β and both coherence thresholds, $\kappa_{coh,dir}$ and $\kappa_{coh,max}$, should be re-adjusted when the β is changed. How exactly this should be done remains unclear at the moment.

Table 4.2: Results of T_{60} estimation with synthetic stimuli.

f_c (kHz)	$\hat{T}_{60}$ (s), E_{down} = 2 dB	$\hat{T}_{60}$ (s), E_{down} = 3 dB	$\hat{T}_{60}$ (s), E_{down} = 5 dB
$\frac{7}{8}\frac{f_s}{2} \approx 19.3$	0.80 ($\sigma = 0.073$)	0.81 ($\sigma = 0.015$)	0.77 ($\sigma = 0.014$)
$\frac{5}{8}\frac{f_s}{2} \approx 13.8$	0.81 ($\sigma = 0.044$)	0.79 ($\sigma = 0.0051$)	0.76 ($\sigma = 0.011$)
$\frac{3}{8}\frac{f_s}{2} \approx 8.3$	0.81 ($\sigma = 0.025$)	0.81 ($\sigma = 0.0093$)	0.80 ($\sigma = 0.0081$)
$\frac{1}{8}\frac{f_s}{2} \approx 2.8$	0.84 ($\sigma = 0.082$)	0.87 ($\sigma = 0.10$)	0.85 ($\sigma = 0.031$)

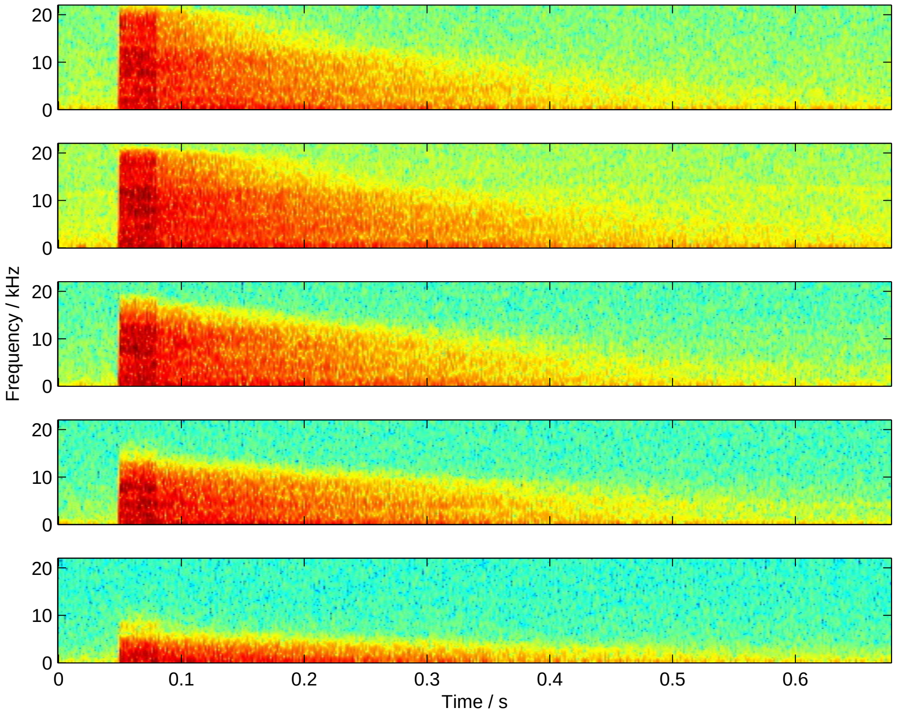

Figure 4.1: Spectrograms of five synthetic pulses used in algorithm evaluation.

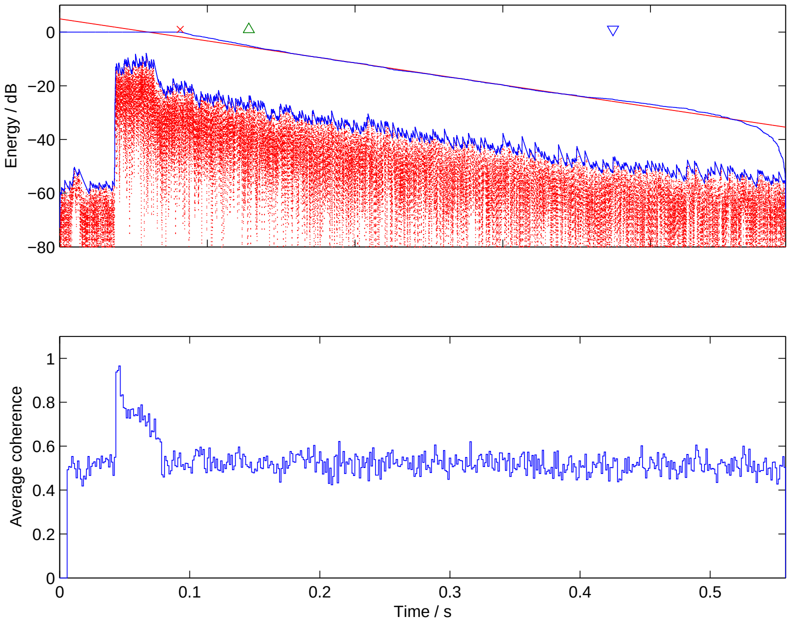

Figure 4.2: Short-time coherence of a synthetic convolved pulse ($f_c = \frac{7}{8}\frac{f_s}{2} \approx 19.3$ kHz).

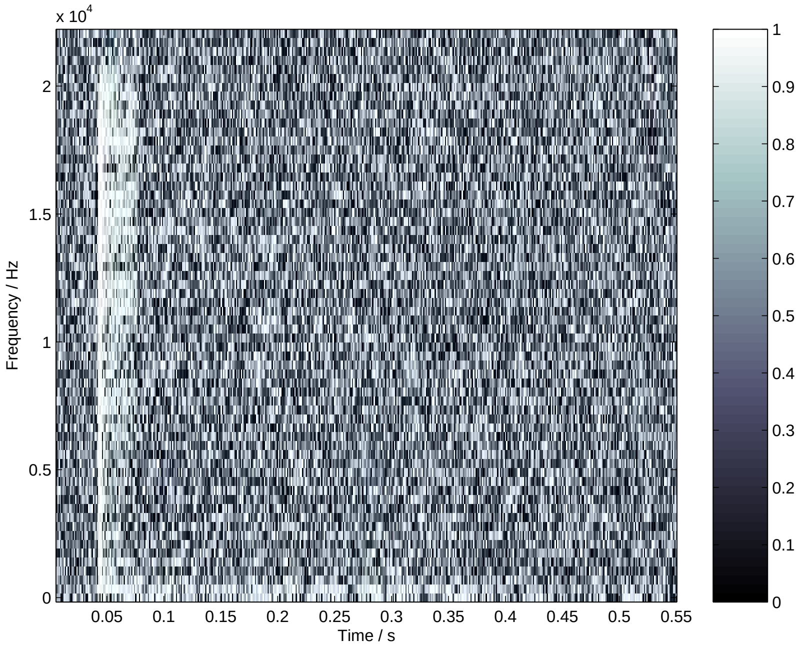

Figure 4.3: Coherogram of a synthetic convolved pulse ($f_c = \frac{7}{8}\frac{f_s}{2} \approx 19.3$ kHz).

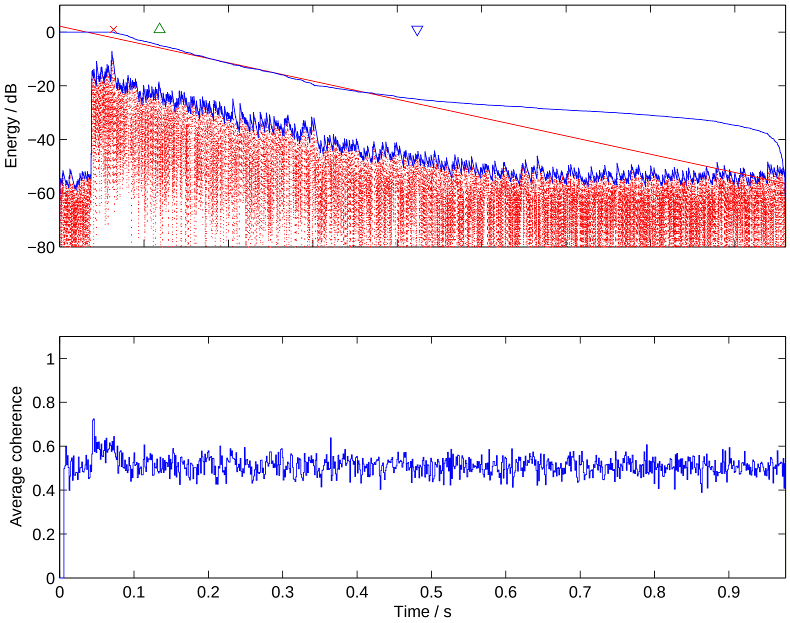

Figure 4.4: Short-time coherence of a synthetic convolved pulse ($f_c = \frac{1}{8}\frac{f_s}{2} \approx 2.8$ kHz).

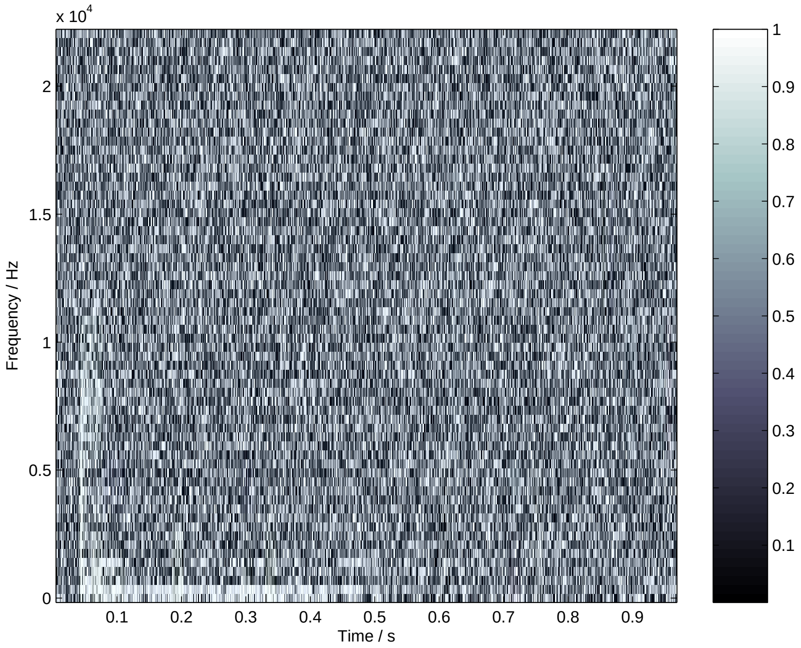

Figure 4.5: Coherogram of a synthetic convolved pulse ($f_c = \frac{1}{8}\frac{f_s}{2} \approx 2.8$ kHz).

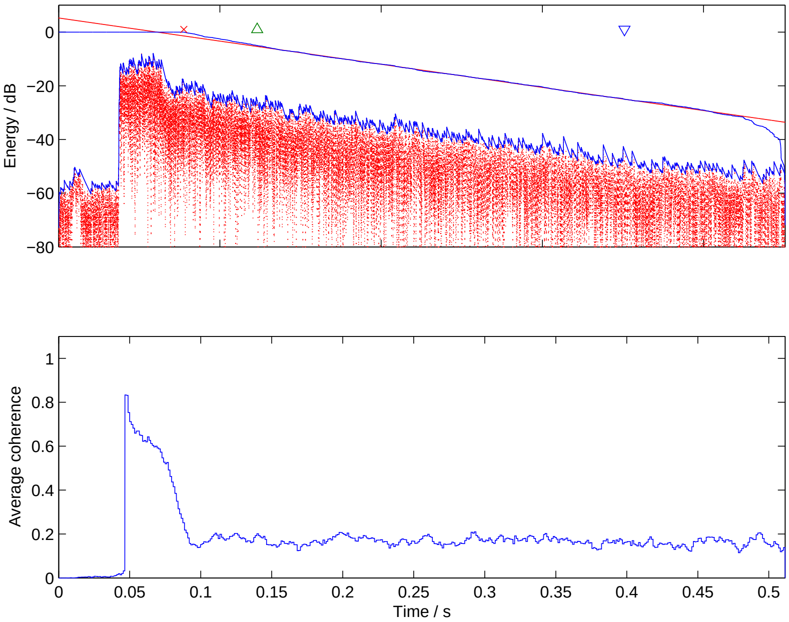

Figure 4.6: Short-time coherence of a synthetic convolved pulse with averaging ($f_c = \frac{7}{8}\frac{f_s}{2} \approx 19.3$ kHz, $\beta = 0.8$).

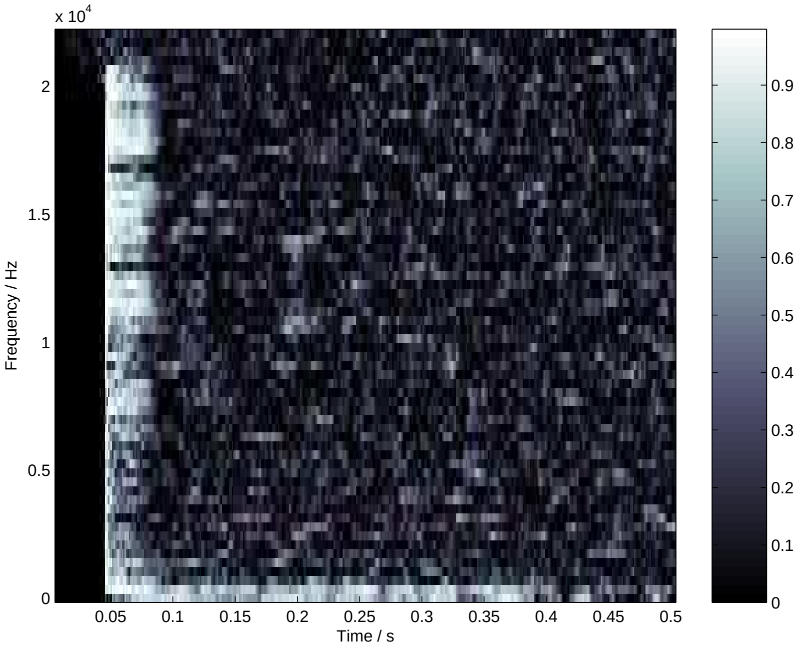

Figure 4.7: Coherogram of a synthetic convolved pulse with averaging ($f_c = \frac{7}{8}\frac{f_s}{2} \approx 19.3$ kHz, $\beta = 0.8$).

4.3 Tests with convolved real excitation signals

The algorithm was tested with binaural signals that were created by convolving an anechoic mono recording with different BRIRs. An anechoic recording of 20 hand claps and finger snaps was used as the source recording. Some pink noise was added to the signals convolved with BRIRs of rooms T3 and Pergola (see Figures B.3 and B.5 in Appendix B), because a sufficiently constant noise level was not achieved with these two responses, probably due to low SNR of the original responses prior to denoising. An independent pink noise signal was added to both channels in order to achieve diffuseness, i.e., decorrelation between channels. Figures B.1-B.5 show energy-time curves of the convolved signals. Notice the considerably higher SNR of the signal convolved with BRIR of room A152. This is most likely due to the fact that the BRIR of that particular room was measured with the sweep method while the others most likely were not. The artificial SNR extension, i.e., denoising (see [22]), does not seem to remove the effect of noise completely. Because of the need to add artifical background noise to two of the recordings, the results are not completely comparable and realistic.

Figures 4.8-4.16 are groups of three different types of plots. Three plots are made of each of the three spaces (T3, A152 and Pergola, see Section 4.1). Figures 4.8, 4.11 and 4.14 show the calculated T_{60} values for each accepted segment of the signal in question. The left panels show the T_{60} values calculated by fitting a line to the -5 to -25 dB range while the right panels show the T_{60} values calculated by fitting a line to a range found by the line fitting limit location algorithm (see Section 3.3.1). Figures 4.9, 4.12 and 4.15 present the evolution of three different statistics calculated as each new T_{60} value arrives. The three statistics are mean, median and the maximum locations of the histogram. All these statistics were calculated from the fixed line fitting limits case. The true value of T_{60}, as measured from the impulse responses, is denoted with a horizontal dashed line in all figures. Figures 4.10, 4.13 and 4.16 contain the histograms of all calculated T_{60} values for each room. The histogram bins are all of width 0.058 seconds (25 adjacent bins between 0.05 to 1.5 seconds).

Table 4.3 lists some statistics calculated from the three test signals. The p-value of T-test[4] indicates the probability that the T_{60} samples, assumed to be taken from a Gaussian (normal) distribution, have the true value (see Table 4.1) as mean. The p-values might give some insight into the performance of the algorithm and to the question of whether or not the mean should be used as the T_{60} estimate. The number of estimates is indicated in the n column. The mean values and absolute errors (compared to the measured true value) after all observations are also listed in Table 4.3 for both fixed and non-fixed line fitting limits.

[4] Performed using the `ttest` function of MATLAB.

The individual T_{60} values, calculated from line fit to -5 to -25 dB range, seem to be somehow centered around the true value in rooms T3 and A152 (see left panels of Figures 4.8 and 4.11). There are a few clear outlier values though. The case where the algorithm for finding the line fit limits (see Section 3.3.1) was used does not seem significantly different by visual inspection of Figures 4.8 and 4.11. The same cannot be said about room Pergola with the longest RT (Figure 4.14), in which the T_{60} values obtained by both methods are far from the true values and there is also a clear difference between the two methods.

Turning the attention to Table 4.3, it is clear that the T test gives very different scores for the three rooms. T3 seems to get much better score than A152 even though there is not a big (visual) difference in the performance of the means (see Figures 4.9 and 4.12 and Table 4.3), both seem to be very close to the true value at the end of the algorithm run. Pergola gets a very low score of $p = 0.00$, which indicates that the algorithm fails miserably in this case. However, when the line fitting limits are searched by the special algorithm of Section 3.3.1, the p value is around 0.5, giving the best performance for that algorithm in all of the three cases. Since in two cases out of three, the fixed line fitting limits give the best performance, it seems that the idea of choosing the lower line fitting limit by maximum correlation coefficient is not entirely justified. Possibly a more advanced algorithm to analyze the fitted lines could be developed. It is perhaps also not a good thing that the evaluation ranges change from estimate to estimate, since that adds an extra random factor affecting the results that are generated by observing an inherently random process.

The standard deviations listed in Table 4.3 are quite close to each other in the case of fixed LSF limits. However, the standard deviation alone cannot be used to judge the algorithm behaviour. It is clear also from visual inspection that there is more variance in the case of using the special algorithm for LSF limits and this is also objectively verified by the larger standard deviation values.

All three cases seem to be different in terms of the behaviour of the different statistics. The mean and median of room T3 (Figure 4.9) seem to be consistent estimators in this case, since the mean and median approach the true value as the number of observations increases. The same applies to room A152 (Figure 4.12). The opposite seems to apply to the room Pergola (Figure 4.15), where the statistics seem to diverge from the true value (the first T_{60} value is at the true value by chance). In all cases except Pergola, the histogram maximum behaves quite smoothly, avoiding large sudden changes of T_{60} between two estimates. Therefore the histogram maximum could be a good candidate for the value to be used in adjusting a late reverberation unit. Informal subjetive tests by the author also verify this, even though in some cases the histogram peak location may change suddenly at the beginning of the algorithm run when there are very few estimates and the peak location may move quickly between competing maxima.

Table 4.3: Some statistics of T_{60} estimation in three different spaces using convolved recordings.

Room	n	p value of T-test (fixed)	p value of T-test (alg)	σ (fixed)	σ (alg)
T3	14	0.93	0.27	0.30 s	0.36 s
A152	17	0.42	0.17	0.22 s	1.09 s
Pergola	13	0.00	0.51	0.40 s	1.34 s
Room		Mean of all estimates (fixed)	Mean of all estimates (alg)		
T3		0.59 s	0.71 s		
A152		0.84 s	1.19 s		
Pergola		0.68 s	1.45 s		
Room		Abs. error of mean (fixed)	Abs. error of mean (alg)		
T3		0.01 s	0.11 s		
A152		0.04 s	0.39 s		
Pergola		0.52 s	0.25 s		

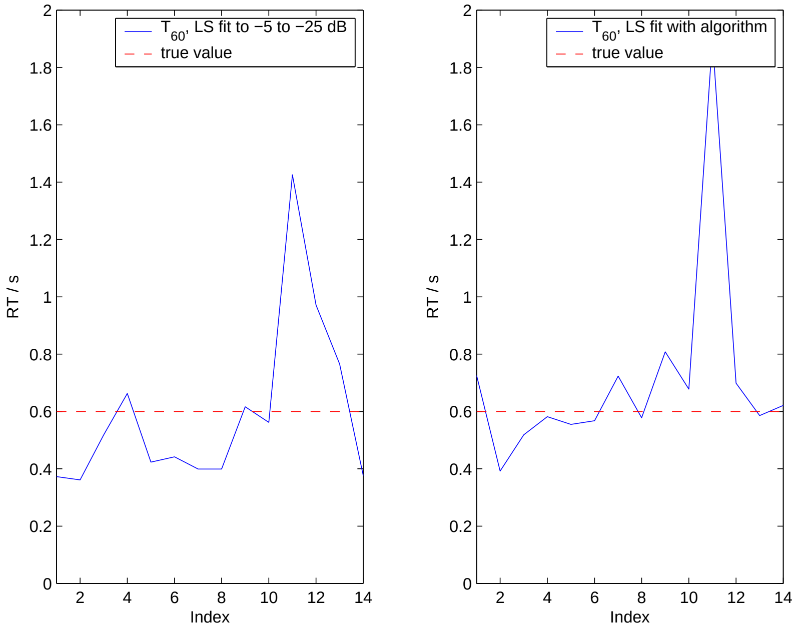

Figure 4.8: Estimates of T_{60} for room T3 with and without least squares limit lookup (Section 3.3.1), convolved signal.

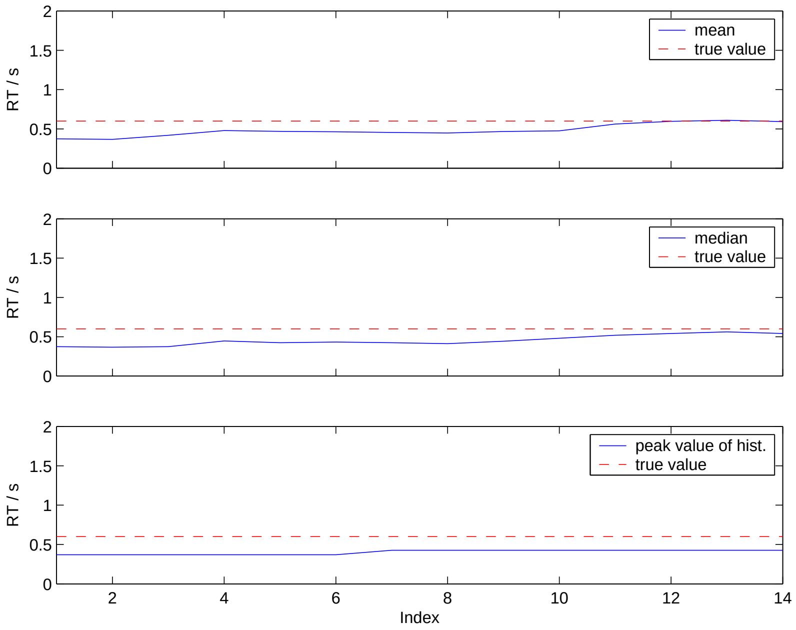

Figure 4.9: Three different statistics calculated from T_{60} estimates for room T3, convolved signal.

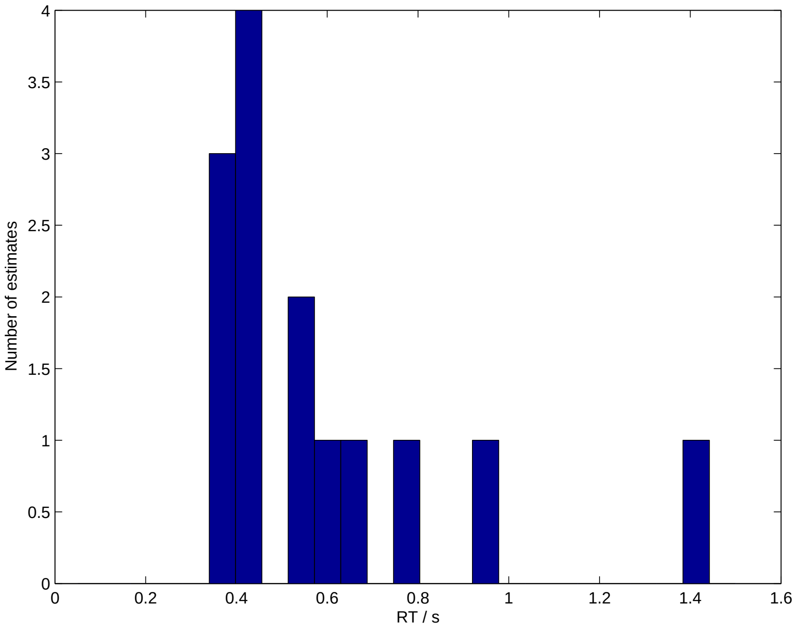

Figure 4.10: Histogram of T_{60} estimates for room T3, convolved signal.

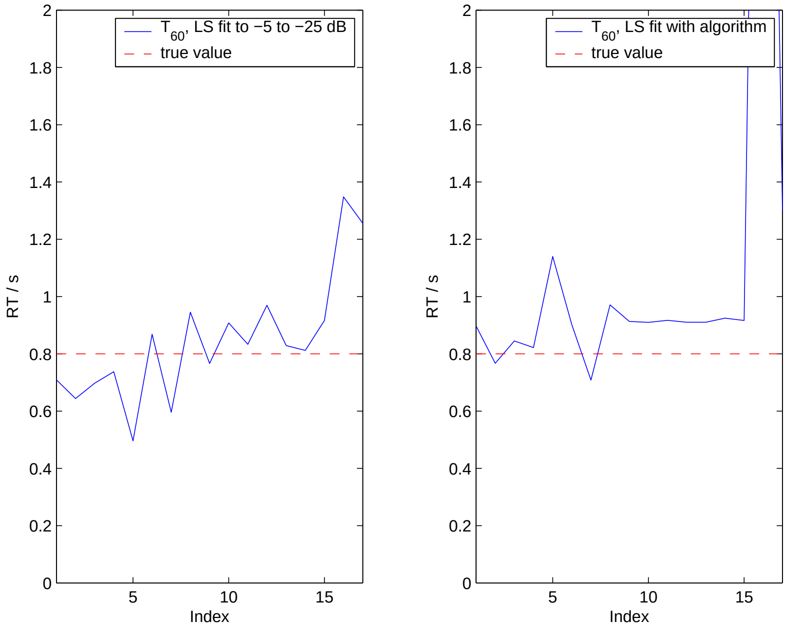

Figure 4.11: Estimates of T_{60} for room A152 with and without least squares limit lookup (Section 3.3.1), convolved signal.

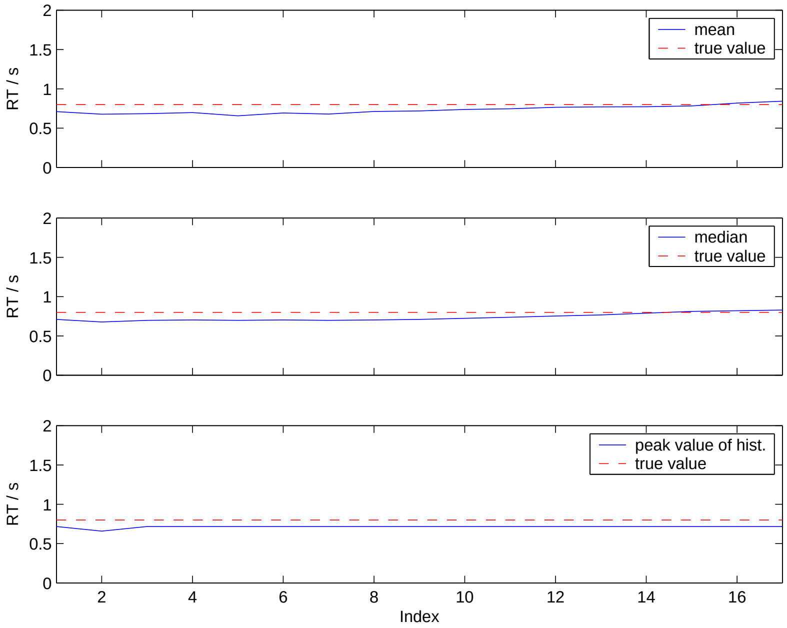

Figure 4.12: Three different statistics calculated from T_{60} estimates for room A152, convolved signal.

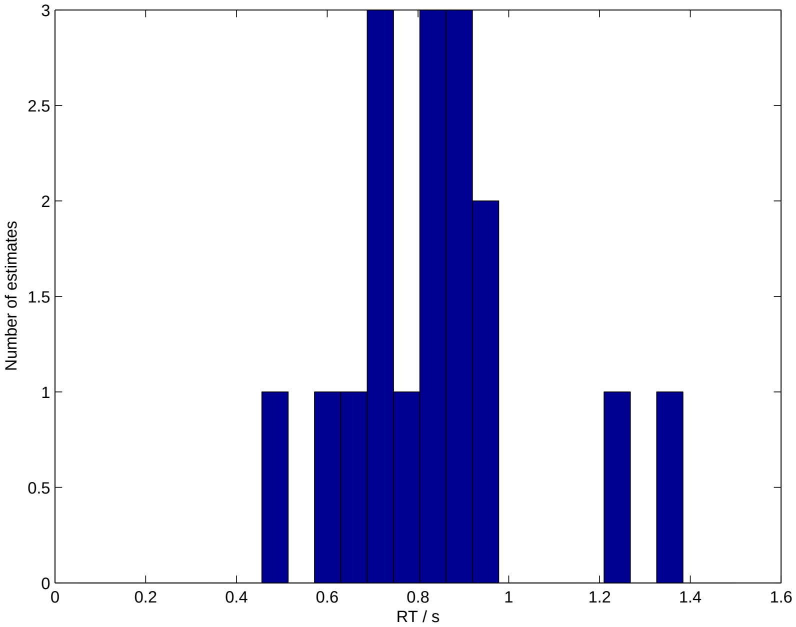

Figure 4.13: Histogram of T_{60} estimates for room A152, convolved signal.

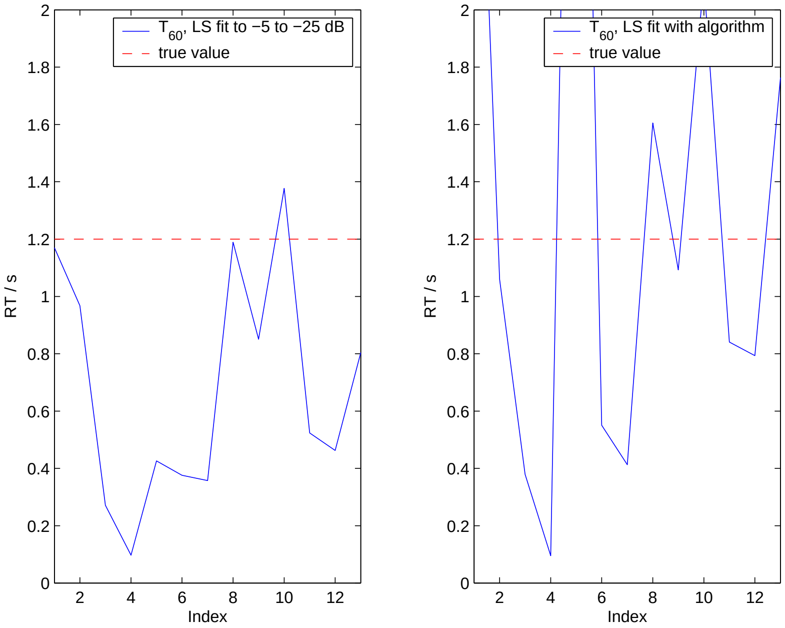

Figure 4.14: Estimates of T_{60} for room Pergola with and without least squares limit lookup (Section 3.3.1), convolved signal.

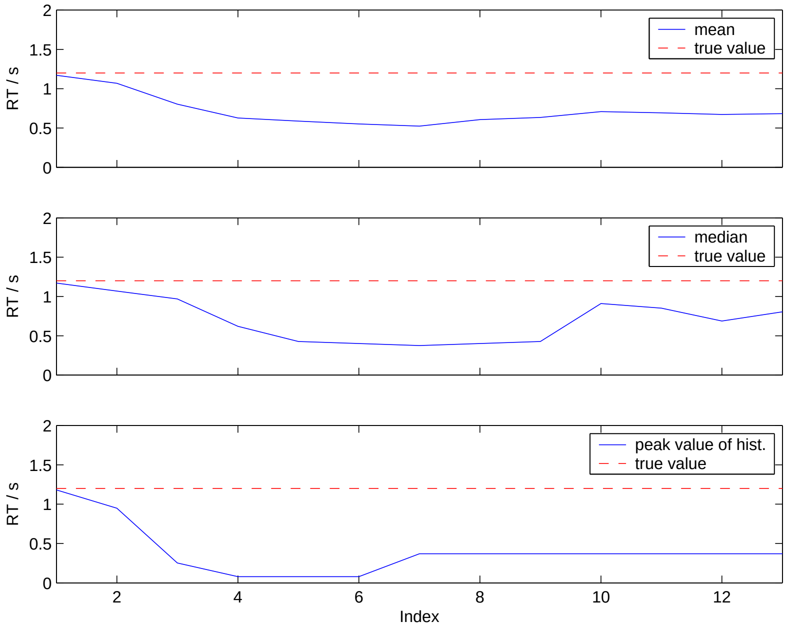

Figure 4.15: Three different statistics calculated from T_{60} estimates for room Pergola, convolved signal.

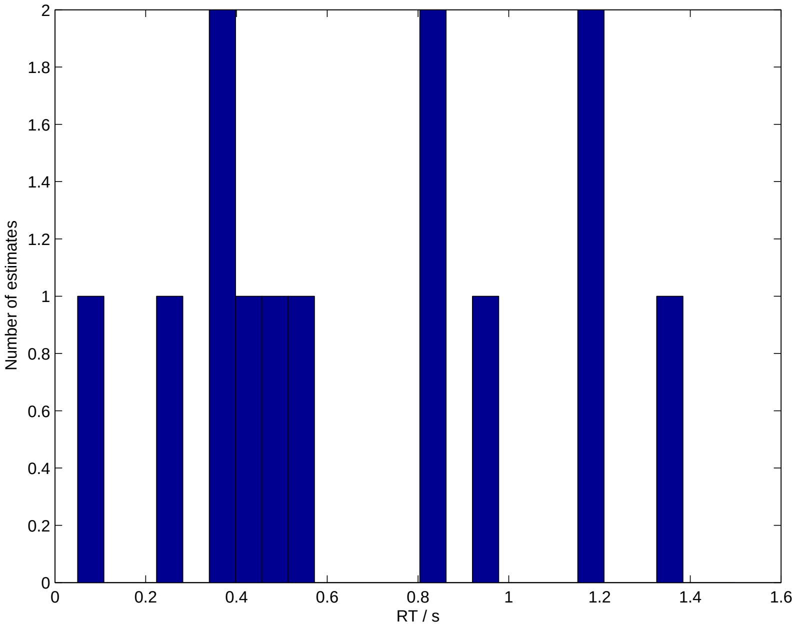

Figure 4.16: Histogram of T_{60} estimates for room Pergola, convolved signal.

4.4 Tests with real-world recordings

This section presents some results of running the algorithm with a real-world binaural recording made in the office room of the author (A152). The recording consisted of several short impulsive sounds, such as hand claps, finger snaps and taps on the table. The length of the recording was 100 seconds. Figures 4.17, 4.18 and 4.20 present the observations, three different statistics and the final histogram, respectively (see previous section for details). Figure 4.18 has ±100 millisecond bounds around the true value denoted by dotted horizontal lines. Table 4.4 presents some statistics, similar to Table 4.3. In addition to the plots familiar from the previous section, Figures 4.19 and 4.21 present the three statistics and the histogram for the case when the variable line fitting limits algorithm (Section 3.3.1) was used. The used algorithm setup is depicted in Figure A.2.

The algorithm seems to perform quite well in both cases, i.e., fixed or non-fixed line fitting limits, even though the latter seems to give a more accurate final estimate in this case (if the mean is used, as can be seen from Table 4.4). Figure 4.18 shows that the algorithm underestimates T_{60} by an amount little bit greater than 100 ms for most of the time when the line fitting limits are fixed at 0 to -25 dB. However, when the lower line fitting limit is set at the maximum of correlation coefficient (Section 3.3.1), the algorithm seems to perform substantially better, as is evident in the running mean and median in Figure 4.18. The mean and median both stay within the ±100 ms bounds from the true value. On the other hand, the running peak value seems to perform similarly as in the fixed line fitting limits case. The T-test gives quite bad results in both cases. Naturally, the T-test cannot be used as the only criterion when evaluating the algorithm performance. The standard deviation is lower than was the case with convolved signals in previous section.

To ensure that the variable line fitting limits method did not perform well in the case of room A152 by accident, the algorithm was also run on a 2 minute binaural recording of impulsive sounds made in room T3 ($T_{60} \approx 0.6$ s). Figures 4.22 and 4.23 show the three statistics and the histogram when the line fitting limits algorithm was used. It is clear that the algorithm performs even better in this case. This time there is a clear peak in the histogram of Figure 4.23 and the center of that histogram bin seems to be very close to the true RT of the room, as is evident in the lower panel of Figure 4.22. The fact that the distribution of estimates has a bigger tail towards the lower RT values seems to cause the mean and the median to slighthly underestimate the RT. The number of estimates was $n = 55$ and the standard deviation was $\sigma \approx 0.18$ s.

Overall it seems that the algorithm perfoms better in real conditions than with synthetic convolved signals[5], at least in these two particular spaces. However, the results presented

[5] The synthetic signals had quite bad SNRs because of the necessary artificially added noise

here should not be generalized to all typical signals and acoustic spaces.

Table 4.4: Some statistics of T_{60} estimation in room A152 using a real recording.

Room	n	p value of T-test (fixed)	p value of T-test (alg)	σ (fixed)	σ (alg)
A152	38	0.00	0.31	0.15 s	0.20 s
Room		Mean of all estimates (fixed)	Mean of all estimates (alg)		
A152		0.66 s	0.83 s		
Room		Abs. error of mean (fixed)	Abs. error of mean (alg)		
A152		0.14 s	0.03 s		

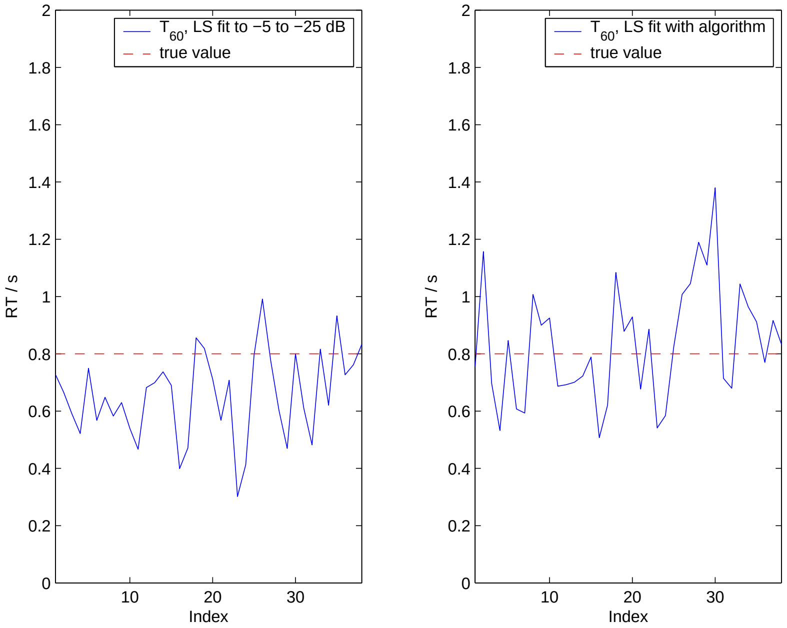

Figure 4.17: Estimates of T_{60} for room A152 with and without least squares limit lookup (Section 3.3.1), real recording.

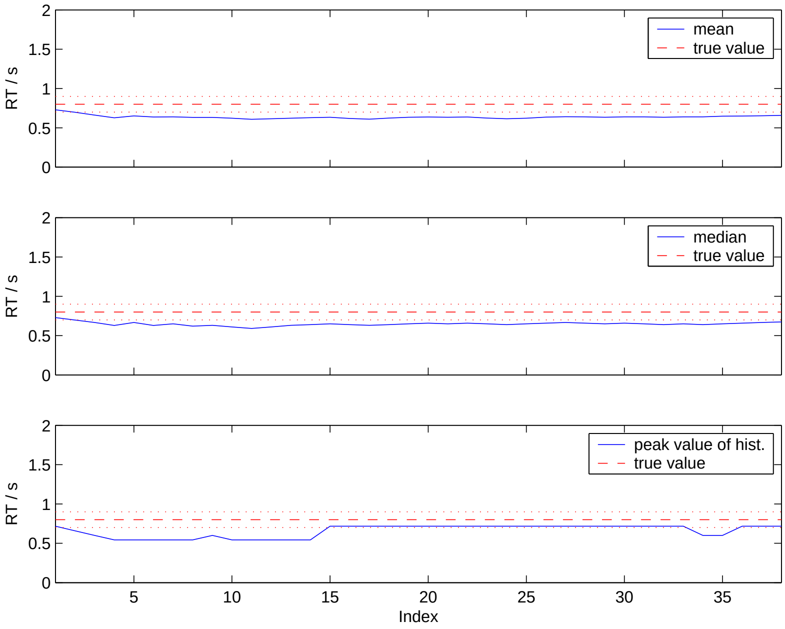

Figure 4.18: Three different statistics calculated from T_{60} estimates for room A152, real recording, line fitting range -5 to -25 dB.

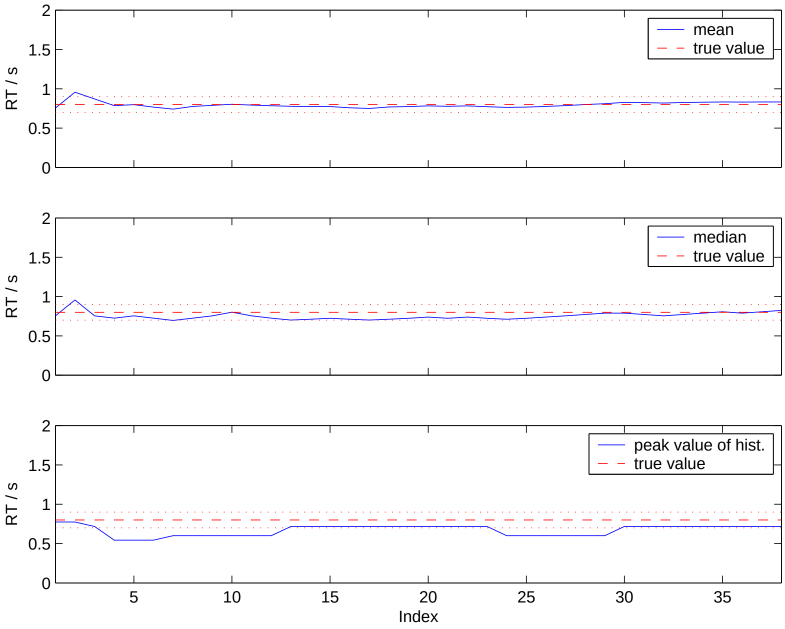

Figure 4.19: Three different statistics calculated from T_{60} estimates for room A152, real recording, variable line fitting limits.

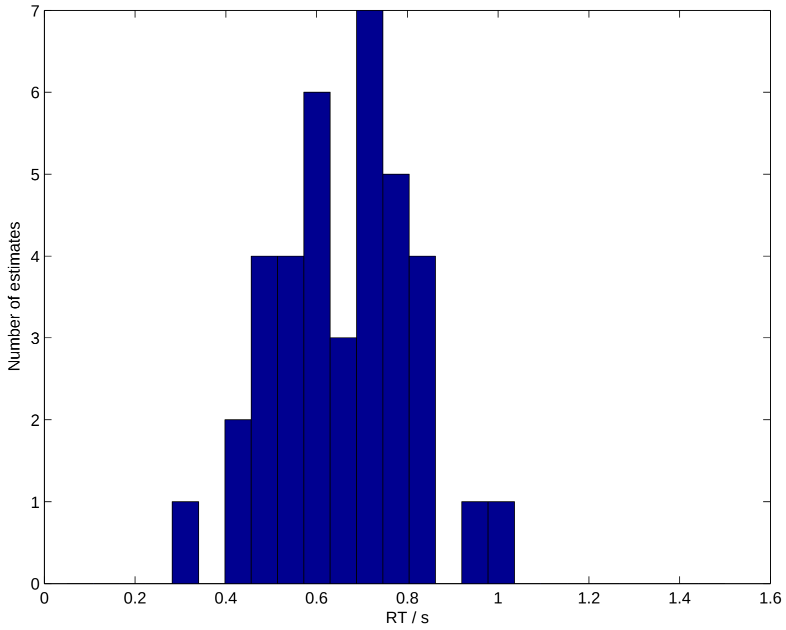

Figure 4.20: Histogram of T_{60} estimates for room A152, real recording, line fitting range -5 to -25 dB.

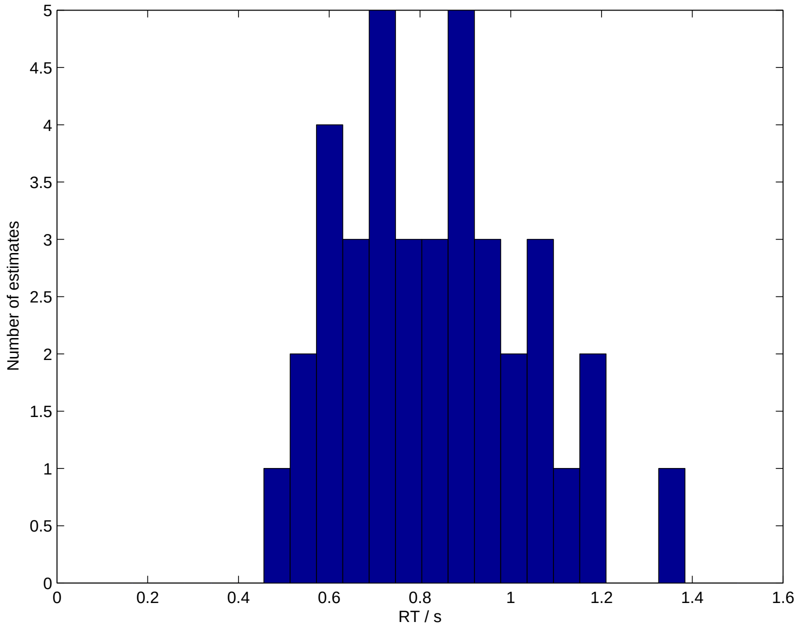

Figure 4.21: Histogram of T_{60} estimates for room A152, real recording, variable line fitting limits.

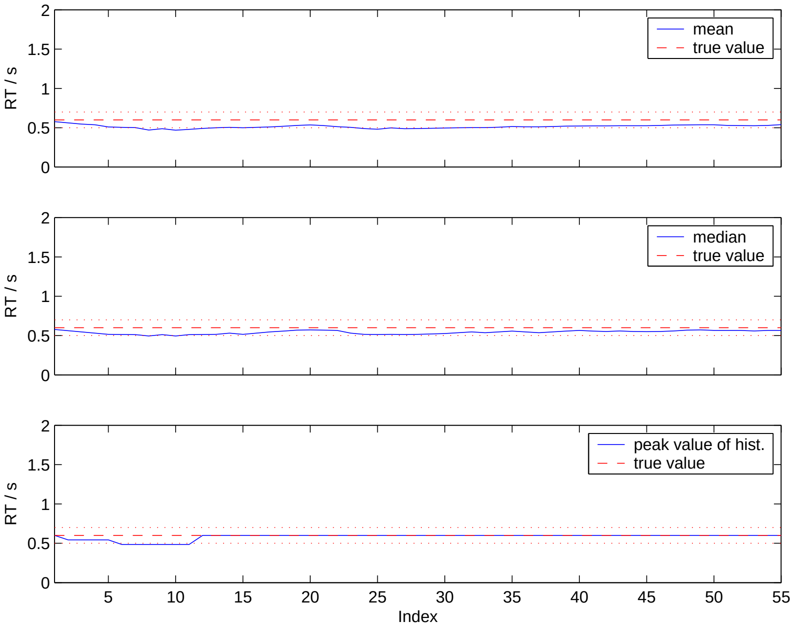

Figure 4.22: Three different statistics calculated from T_{60} estimates for room T3, real recording, variable line fitting limits.

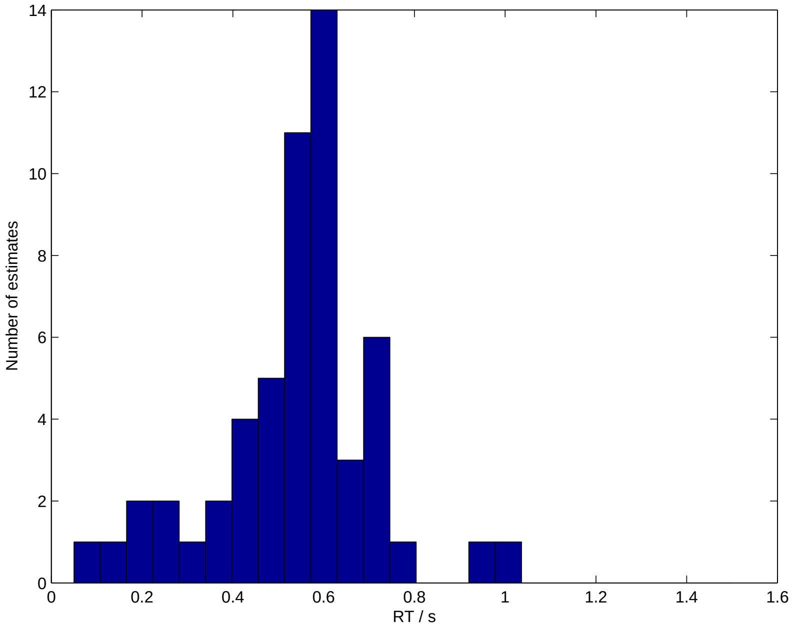

Figure 4.23: Histogram of T_{60} estimates for room T3, real recording, variable line fitting limits.

4.5 Conclusions at this point

It is clear that the algorithm needs further improvements. The algorithm is quite complicated and there are many parts affecting the final estimation results. The segmentation part of the algorithm is especially critical, since a failed segmentation results in badly shaped Schroeder integration curves. The lower limit of integration, T_i, is perhaps the most important parameter affecting the estimation results. The current algorithm for determining T_i is not very advanced and should possibly be replaced by the Lundeby method (see [38] and Sections 2.3 and 3.1.2), which was successfully used in the IRMA measurement system described in [45].

The other limit of integration, T_d, is located based on the average of the short-time coherence between channels. While the idea of locating the start of the diffuse sound based on average coherence seems to be a good idea in theory, in practice it is not that simple. The evaluation results verify that the frequency content of the signal affects the average of the coherence. Broadband signals have a higher average coherence when the average is taken over the whole frequency range. Wittkopp [63] proposes a frequency-dependent weighting to be applied to the calculation of average coherence: frequency bands are weighted according to the amount of energy present in each band. This kind of an approach might be incorporated also into this algorithm.

A special algorithm was developed for finding the limits of line fitting. The evaluation results suggest that while the algorithm succeeds very well in some cases, there is some room for improvement. In [45] it is noted that a higher correlation coefficient of line fit does not necessary result in more reliable results. Perhaps the curve that plots RT as a function of line fitting end limit (solid line in lower panel of Figure 3.5) could be somehow used together with the correlation coefficient to decide the end limit for line fitting. Also, the start point of line fitting should maybe also be adjusted. Nevertheless, it is a good news that the algorithm was found to perform very well with line limits lookup when a real recorded signal was fed to the algorithm. Using variable lower limit of line fitting seems to remove the systematic error in RT values caused by bending of the decay curves.

Effect of the three tests for discarding some segments by their frequency content and shape of the energy-time curve has not been investigated yet, even though all the tests were included in the evalution (in the tests presented in Sections 4.3 and 4.4). It is thus unclear, whether those tests significantly benefit the results by discarding outliers.

One thing that was completely left unexplored is the computational efficiency of the algorithm. Since the algorithm is very complicated, it is not easy to describe its complexity by the standard “Big-Oh” notation [62]. Subjective experience with the algorithm suggests that the algorithm is computationally quite heavy, as threading is required to divide the computational burden over a longer time[6]. A few buffer underflows also occurred during the evaluation runs, i.e., the real-time algorithm did not have time to process all incoming data. Because of this, two algorithm runs on a same audio file might give slightly different results.

[6] The algorithm was ran real-time on a 1.6 GHz Linux PC.

Chapter 5

Conclusions

The main goal of this work was to develop a method for estimating the reverberation time from a binaural signal when the excitation signal cannot be controlled, i.e., the input signal to the algorithm is arbitrary. It was hypothesized that the binaural nature of the signals could be exploited to distinguish the diffuse decay from the direct sound and early reflections. This would make it possible to accurately locate the starting point for reverberation time analysis, which was decided to be based on the well-known Schroeder method. The whole approach for reverberation time estimation was based on the idea of locating interesting sound events from the input signal and then subjecting the obtained signal segments to subsequent analysis. This approach is related to the auditory decomposition (see Section 1.1.3), part of which is the detection and localization of interesting sound events in the environment around a listener, solely based on the binaural signals.

It is clear that the approach chosen in this work has some inherent problems. The most important of them is that the algorithm requires transient excitation sounds for RT estimation. This leaves many usable longer sounds with a sudden offset, which is followed by a reverberant tail, out of the analysis. Because of this, the algorithm cannot determine RT from speech, which is a very important and common signal class in everyday environments. A natural future improvement to the algorithm would be rewriting the coarse segmentation part. The most similar RT estimation algorithm reported in literature [61] performs the analysis on signal segments that have decreasing energy. The criterion of decreasing energy could also be included in the coarse segmentation algorithm of this work, so that instead of looking for transient sounds, the algorithm would find the parts of the signal that have a sound event onset with large enough SNR, which is later followed by a decrease in energy with a steep enough slope. Only the part of the segment with decreasing energy would be included in subsequent analysis. This way the algorithm would get a lot more estimates in a normal environment, which normally does not have very many transient sounds.

Nevertheless, the algorithm performs quite fine in a real environment, as was found out in Chapter 4. The method for finding the line fitting limits (Section 3.3.1) works quite well for real signals and significantly improves the accuracy of the RT estimations. It would be interesting to compare the algorithm performance to the RT discrimination abilities of humans. Naturally, humans can rarely give an absolute RT value for a room, but they can discriminate changes in the environment. According to [43], the difference limen for reverberation time is on the order of 40 ms in rooms with mid-frequency $T_{60} < 600$ ms. Another study reported the mean upper and lower just noticeable differences for reverberated speech to be in the range of $3.3 - 9.6$ % of the corresponding RT [25]. Since one of the main applications of this algorithm was to use the estimated RT to adjust a late reverberation unit of an augmented reality application (see Section 1.1), it would be advantageous to match the RT as closely to the surrounding space as possible. The algorithm estimated the RT to an accuracy ranging from 10 to 500 ms, depending on the room and the statistics used. The algorithm therefore matches the difference limen of humans at its best. But it is unclear how big changes between the true RT of a room and the RT of the artificially added sound sources is allowed for the listener to perceive the augmented sources as not belonging to the environment around the listener.

Automatic estimation of reverberation time is a relatively unexplored topic in the area of audio signal processing. There are not very many different algorithms mentioned in the literature at the moment. The work described in this thesis provides some new contributions to the field of automatic RT estimation. While the algorithm is quite choosy about the sounds that it accepts, the quality of the estimates is relatively high. A downside of the algorithm is its complexity, in both computational and algorithmic sense. There are more than 10 adjustable parameters, which is quite a lot. However, once a good combination of parameter values is found, there is no need for re-adjusting them.

Bibliography

[1] Alexis Baskind and Olivier Warusfel. Methods for Blind Computational Estimation of Perceptual Attributes of Room Acoustics. In *Proceedings of the AES 22nd International Conference on Virtual, Synthetic and Entertainment Audio (AES22)*, Espoo, Finland, June 2002.

[2] Julius S. Bendat and Allan G. Piersol. *Engineering Applications of Correlation and Spectral Analysis*. John Wiley & Sons Ltd, 1980.

[3] Leo Beranek. *Concert and Opera Halls - How They Sound*. The Acoustical Society of America, New York, 1984.

[4] Alan C. Bovik, Thomas S. Huang, and Jr. David C. Munson. A Generalization of Median Filtering Using Linear Combinations of Order Statistics. *IEEE Transactions on Acoustics, Speech, and Signal Processing*, ASSP-31(6):1342–1350, December 1972.

[5] G. Clifford Carter, Charles H. Knapp, and Albert H. Nuttall. Estimation of the Magnitude-Squared Coherence Function Via Overlapped Fast Fourier Transform Processing. *IEEE Transactions on Audio and Electroacoustics*, AU-21(4):337–344, 1972.

[6] Michael A. Casey. MPEG-7 Sound-Recognition Tools. *IEEE Transactions on Circuits and Systems for Video Technology*, 11(6):737–747, 2001.

[7] W. T. Chu. Comparison of Reverberation Measurements Using Schroeder's Impulse Method and Decay-Curve Averaging Method. *Journal of The Acoustical Society of America*, 63(5):1444–1450, 1978.

[8] Laurent Couvreur and Christophe Couvreur. Robust Automatic Speech Recognition in Reverberant Environments by Model Selection. In *Proceedings of the International Workshop on Hands-Free Speech Communication (HSC-2001)*, pages 147–150, Kyoto, Japan, April 2001.

[9] Laurent Couvreur, Christophe Ris, and Christophe Couvreur. Model-based Blind Estimation of Reverberation Time: Application to Robust ASR in Reverberant Environments. In *Proceedings of the European Conference on Speech Communication and Technology (EUROSPEECH-2001)*, volume 1, pages 2631–2634, Aalborg, Denmark, September 2001.

[10] Trevor J. Cox and Francis F. Li nand Paul Darlington. Extracting Room Reverberation Time from Speech Using Artificial Neural Networks. *Journal of The Audio Engineering Society*, 49(4):219–230, April 2001.

[11] Manuel Davy and Simon Godsill. Detection of Abrupt Spectral Changes Using Support Vector Machines. In *Proceedings of the IEEE International Conference on Acoustics, Speech, and Signal Processing (ICASSP 2002)*, Orlando, Florida, USA, May 2002. http://www.irccyn.ec-nantes.fr/˜davy/papers/davy-icassp2002.pdf.

[12] Frédéric Desobry and Manuel Davy. Support Vector-Based Online Detection of Abrupt Changes. In *Proceedings of the IEEE International Conference on Acoustics, Speech, and Signal Processing (ICASSP2003)*, Hong-Kong, China, April 2003. http://www.irccyn.ec-nantes.fr/˜davy/papers/desobry-icassp-03.pdf.

[13] Sasha Devore and Barbara Shinn-Cunningham. Perceptual Consequences of Including Reverberation in Spatial Auditory Displays. In *Proceedings of the International Conference on Auditory Display (ICAD-03)*, Boston, MA, USA, July 2003.

[14] Alain Dufaux, Laurent Besacier, Michael Ansorge, and Fausto Pellandini. Automatic Sound Detection and Recognition for Noisy Environment. In *Proceedings of the European Signal Processing Conference (EUSIPCO 2000)*, Tampere, Finland, September 2000.

[15] Antti Eronen, Juha Tuomi, Anssi Klapuri, Seppo Fagerlund, Timo Sorsa, Gaëtan Lorho, and Jyri Huopaniemi. Audio-based Context Awareness - Acoustic Modeling and Perceptual Evaluation. In *Proceedings of the IEEE International Conference on Acoustics, Speech, and Signal Processing (ICASSP2003)*, Hong-Kong, China, April 2003. http://www.cs.tut.fi/sgn/arg/music/eronen_icassp03.pdf.

[16] Laurent Faiget, Claude Legros, and Robert Ruiz. Optimization of the Impulse Response Length: Application to Noisy and Highly Reverberant Rooms. *Journal of The Audio Engineering Society*, 46(9):741–750, September 1998.

[17] Martin Hansen. A Method for Calculating Reverberation Time from Musical Signals. Technical Report 60, The Acoustics Laboratory, Technical University of Denmark, Building 352, DK-2800 Lynbgy, 1995.

[18] Monson H. Hayes. *Statistical Digital Signal Processing and Modeling*. John Wiley & Sons Ltd, 1996.

[19] Aki Härmä, Julia Jakka, Miikka Tikander, Matti Karjalainen, Tapio Lokki, Jarmo Hiipakka, and Gaëtan Lorho. Augmented Reality Audio for Mobile and Wearable Appliances. *Journal of The Audio Engineering Society*, 52(6):618–639, June 2004.

[20] Aki Härmä, Julia Jakka, Miikka Tikander, Matti Karjalainen, Tapio Lokki, Heli Nironen, and Sampo Vesa. Techniques and Applications of Wearable Augmented Reality Audio. In *Proceedings of the AES 114th International Convention*, Amsterdam, the Netherlands, March 2003.

[21] Tommi Ilmonen. Mustajuuri - An Application and Toolkit for Interactive Audio Processing. In *Proceedings of the The Seventh International Conference on Auditory Display (ICAD 2001)*, Espoo, Finland, July/August 2001.

[22] Jean-Marc Jot, Laurent Cerveau, and Olivier Warusfel. Analysis and Synthesis of Room Reverberation Based on a Statistical Time-Frequency Model. In *Proceedings of the AES 103rd International Convention*, New York, USA, 1997. Preprint 4629.

[23] Matti Karjalainen. Kommunikaatioakustiikka. Technical Report 51, Teknillinen korkeakoulu, Sähkö- ja tietoliikennetekniikan osasto, Akustiikan ja äänenkäsittelytekniikan laboratorio, TKK, Otaniemi, 1999.

[24] Matti Karjalainen, Poju Antsalo, Aki Mäkivirta, Timo Peltonen, and Vesa Välimäki. Estimation of Modal Decay Parameters from Noisy Response Measurements. *Journal of The Audio Engineering Society*, 50(11):867–878, November 2002.

[25] Matti Karjalainen and Hanna Järveläinen. More About This Reverberation Science: Perceptually Good Late Reverberation. In *Proceedings of the AES 111th International Convention*, New York, USA, September 2001. Convention Paper 5415.

[26] Erwin Kreyszig. *Advanced Engineering Mathematics*. John Wiley & Sons Ltd, 7th edition, 1993.

[27] Pauli Kuosmanen and Jaakko Astola. *Fundamentals of Nonlinear Digital Filtering*. CRC Press Inc., 1998.

[28] Tapio Lahti. Akustinen mittaustekniikka. Technical Report 38, Teknillinen korkeakoulu, sähkötekniikan osasto, akustiikan ja äänenkäsittelytekniikan laboratorio, TKK, Otaniemi, 1995. Toinen korjattu painos 1997.

[29] Hélène Laurent and Christian Doncarli. Abrupt Changes Detection in the Time-Frequency Plane. In *Proceedings of the IEEE-SP International Symposium on Time-Scale Analysis*, pages 285–288, Paris, France, 1996.

[30] Hélène Laurent and Christian Doncarli. Stationarity Index for Abrupt Changes Detection in the Time-Frequency Plane. *IEEE Signal Processing Letters*, 5(2):43–45, 1998.

[31] Hélène Laurent, Eric Hitti, and Marie-Francoise Lucas. Abrupt Changes Detection in the Time-Scale and in the Time-Frequency Planes: a Comparative Study. In *Proceedings of the IEEE-SP International Symposium on Time-Scale Analysis*, pages 501–504, Pittsburgh, Philadelphia, USA, October 1998.

[32] Katia Lebart, Jean-Marc Boucher, and Philippe Denbigh. A New Method Based on Spectral Subtraction for Speech Dereverberation. *Acustica/Acta Acustica*, 87(3):359–366, 2001.

[33] Sébastien Lefèvre, Benjamin Maillard, and Nicole Vincent. A Two Level Classifier Process for Audio Segmentation. In *Proceedings of the IAPR International Conference on Pattern Recognition*, pages 891–894, Quebec City, Canada, August 2002.

[34] Stan Z. Li. Content-Based Audio Classification and Retrieval Using the Nearest Feature Line Method. *IEEE Signal Processing Letters*, 8(5):619–625, September 2000.

[35] Chen Liu, Bruce C. Wheeler, William D. O'Brien Jr., Robert C. Bilger, Charissa R. Lansing, and Albert S. Feng. Localization of Multiple Sound Sources with Two Microphones. *Journal of The Acoustical Society of America*, 108(4):1888–1905, October 2003.

[36] Tapio Lokki, Heli Nironen, Sampo Vesa, Lauri Savioja, Aki Härmä, and Matti Karjalainen. Application Scenarios of Wearable and Mobile Augmented Reality Audio. In *Proceedings of the AES 116th International Convention*, Berlin, Germany, May 2004.

[37] Lie Lu, Hao Jiang, and Hong Zhang. A robust audio classification and segmentation method. In *Proceedings of the 9th ACM International Conference on Multimedia*, pages 203–211. ACM Press, 2001.

[38] Anders Lundeby, Tor Erik Vigran, Heinrich Bietz, and Michael Vorländer. Uncertainties of Measurements in Room Acoustics. *Acustica*, 81:344–355, 1995. Dedicated to Prof. Dr. Heinrich Kuttruff on the occasion of his 65th birthday.

[39] Janet S. Milton and Jesse C. Arnold. *Introduction to Probability and Statistics*. McGraw-Hill, 2nd edition, 1990.

[40] Sanjit K. Mitra. *Digital Signal Processing - A Computer-Based Approach*. McGraw-Hill, 2nd edition, 2001.

[41] Dennis R. Morgan. A Parametric Error Analysis of the Backward Integration Method for Reverberation Time Estimation. *Journal of The Acoustical Society of America*, 101(5):2686–2693, 1997.

[42] Swen Müller and Paulo Massarani. Transfer-Function Measurement with Sweeps. *Journal of The Audio Engineering Society*, 49(6):443–471, June 2001.

[43] Theodoros I. Niaounakis and William J. Davies. Perception of Reverberation Time in Small Listening Rooms. *Journal of The Audio Engineering Society*, 50(5):343–350, May 2002.

[44] Naoki Nitanda, Miki Haseyama, and Hideo Kitajima. An Audio Signal Segmentation and Classification Using Fuzzy c-means Clustering. In *Proceedings of the 2nd International Conference on Information Technology for Application (ICITA 2004)*, Harbin, China, January 2004.

[45] Timo Peltonen. A Multichannel Measurement System for Room Acoustics Analysis. Master's thesis, Helsinki University of Technology, 2000. http://www.acoustics.hut.fi/publications/files/theses/peltonen_mst.pdf.

[46] Allan D. Pierce. *Acoustics - An Introduction to Its Physical Principles and Applications*. The Acoustical Society of America, 2nd edition, 1991.

[47] Lawrence R. Rabiner. A Tutorial on Hidden Markov Models and Selected Applications in Speech Recognition. *Proceedings of the IEEE*, 77(2):257–286, 1989.

[48] Rama Ratnam, Douglas L. Jones, and William D. O'Brien Jr. Fast Algorithms for Blind Estimation of Reverberation Time. *IEEE Signal Processing Letters*, 11(6):537–540, 2004.

[49] Rama Ratnam, Douglas L. Jones, Bruce C. Wheeler, William D. O'Brien Jr., Charissa R. Lansing, and Albert S. Feng. Blind Estimation of Reverberation Time. *Journal of The Acoustical Society of America*, 114(5):2877–2892, November 2003.

[50] Thomas D. Rossing. *The Science of Sound*. Addison Wesley, 2nd edition, 1990.

[51] Lauri Savioja. *Modeling Techniques for Virtual Acoustics*. PhD thesis, Helsinki University of Technology, Telecommunications Software and Multimedia Laboratory, Espoo, Finland, 1999. http://www.tml.hut.fi/˜las/publications/thesis/.

[52] Manfred R. Schroeder. A New Method of Measuring Reverberation Time. *Journal of The Acoustical Society of America*, 37:490–412, 1965.

[53] Manfred R. Schroeder. Integrated-Impulse Method Measuring Sound Decay Without Using Impulses. *Journal of The Acoustical Society of America*, 66(2):497–500, 1979.

[54] Barbara Shinn-Cunningham. Learning Reverberation: Considerations for Spatial Auditory Displays. In *Proceedings of the International Conference on Auditory Display (ICAD-00)*, Atlanta, GA, USA, April 2000.

[55] Janusz M. Smulko. Abrupt Changes Detection of Broad-Band Signals. In *Proceedings of the IEEE Instrumentation and Measurement Technology Conference*, Budapest, Hungary, May 2001.

[56] Jongseo Sohn, Nam Soo Kim, and Wonyong Sung. A Statistical Model-Based Voice Activity Detection. *IEEE Signal Processing Letters*, 6(1):1–3, 1999.

[57] Andrew S. Tanenbaum. *Modern Operating Systems*. Prentice-Hall, 2nd edition, 2001.

[58] Miikka Tikander, Aki Härmä, and Matti Karjalainen. Binaural Positioning System for Wearable Augmented Reality Audio. In *Proceedings of the IEEE Workshop on Applications of Signal Processing to Audio and Acoustics (WASPAA'03)*, New Paltz, New York, USA, October 2003.

[59] Michel Vacher. Smart audio sensor for telemedicine. In *Smart Objects Conference 2003*, pages 222–225, Grenoble, France, May 2003.

[60] Michel Vacher, Dan Istrate, Laurent Besacier, Jean-Francois Serignat, and Eric Castelli. Life Sounds Extraction and Classification in Noisy Environment. In *Proceedings of the 5th IASTED International Conference on Signal and Image Processing 2003*, Honolulu, Hawaii, USA, August 2003.

[61] José Vieira. Automatic Estimation of Reverberation Time. In *Proceedings of the AES 116th International Convention*, Berlin, Germany, May 2004.

[62] Mark Allen Weiss. *Data Structures and Algorithm Analysis in Java*. Addison Wesley Longman, Inc., 1999.

[63] Thomas Wittkopp. *Two-Channel Noise Reduction Algorithms Motivated by Models of Binaural Interaction*. PhD thesis, Carl von Ossietzky University Oldenburg, March 2001. http://docserver.bis.uni-oldenburg.de/publikationen/dissertation/2001/wittwo01/pdf/wittwo01.pdf.

[64] Erling Wold, Thom Blum, Douglas Keislar, and James Wheaton. Content-Based Classification, Search, and Retrieval of Audio. *IEEE MultiMedia*, 3(3):27–36, 1996.

[65] Ning Xiang. Evaluation of Reverberation Times Using a Nonlinear Regression Approach. *Journal of The Acoustical Society of America*, 98(4):2112–2121, 1995.

Appendix A

Algorithm configurations used in evaluation

These figures show the control panel of the algorithm with all parameters set as they were in different parts of the evaluation.

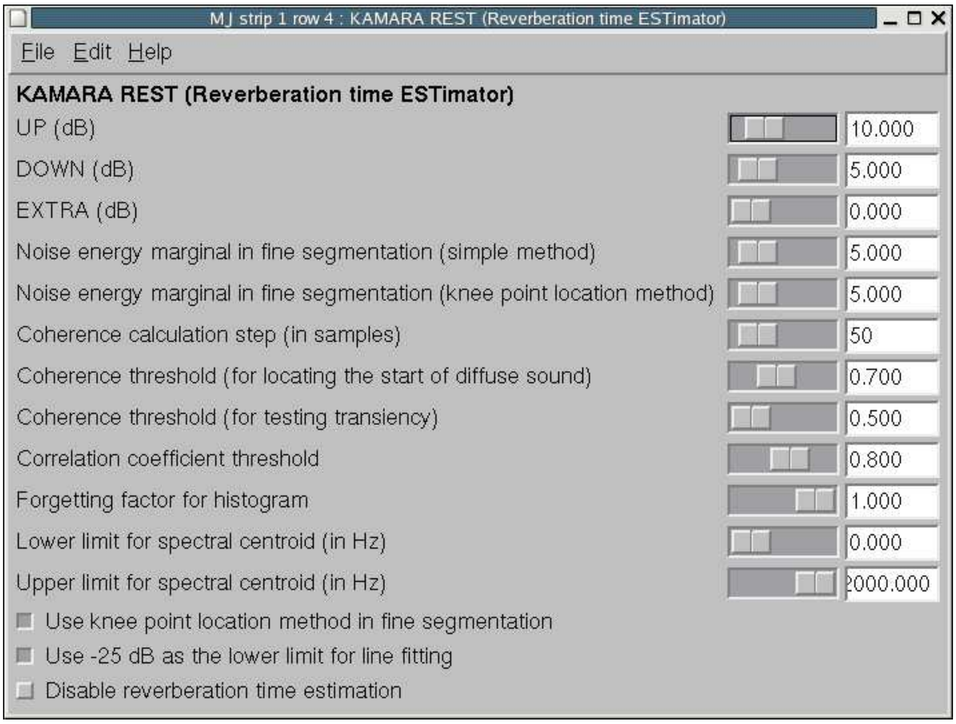

MJ strip 1 row 4 : KAMARA REST (Reverberation time ESTimator)
File
Edit
Help

KAMARA REST (Reverberation time ESTimator)

UP (dB)	10.000
DOWN (dB)	5.000
EXTRA (dB)	0.000
Noise energy marginal in fine segmentation (simple method)	5.000
Noise energy marginal in fine segmentation (knee point location method)	5.000
Coherence calculation step (in samples)	50
Coherence threshold (for locating the start of diffuse sound)	0.700
Coherence threshold (for testing transiency)	0.500
Correlation coefficient threshold	0.800
Forgetting factor for histogram	1.000
Lower limit for spectral centroid (in Hz)	0.000
Upper limit for spectral centroid (in Hz)	2000.000

☑ Use knee point location method in fine segmentation

☑ Use -25 dB as the lower limit for line fitting

□ Disable reverberation time estimation

Figure A.1: Algorithm configuration for Sections 4.2 and 4.3.

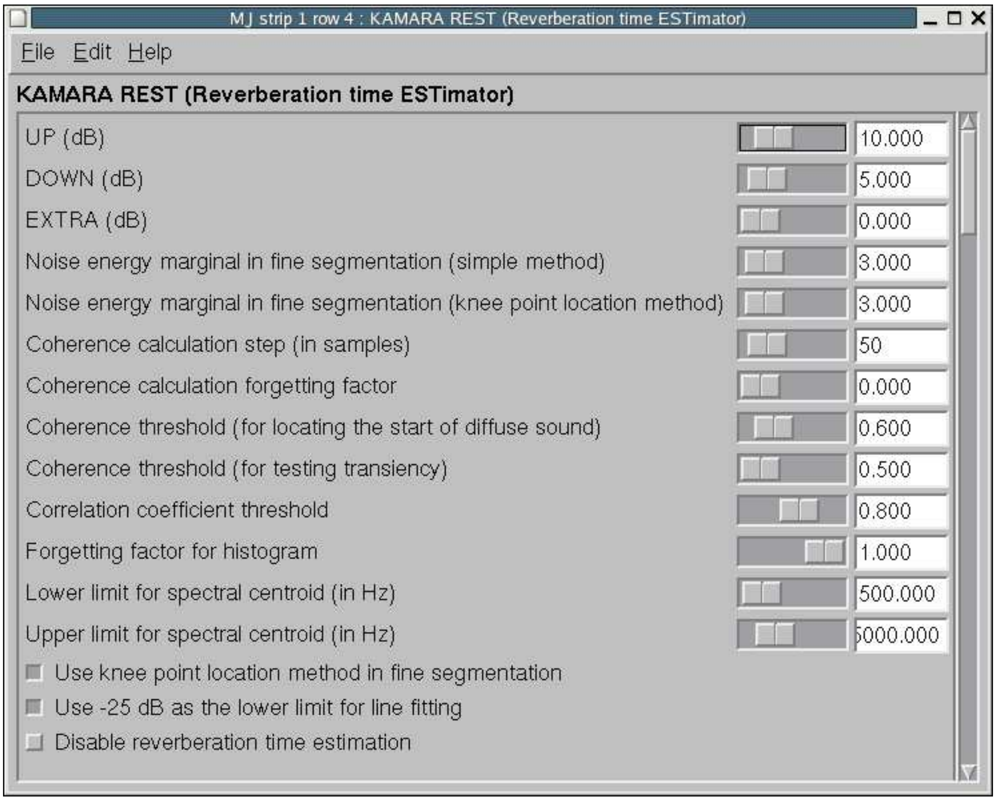

MJ strip 1 row 4 : KAMARA REST (Reverberation time ESTimator)

KAMARA REST (Reverberation time ESTimator)

UP (dB) 10.000

DOWN (dB) 5.000

EXTRA (dB) 0.000

Noise energy marginal in fine segmentation (simple method) 3.000

Noise energy marginal in fine segmentation (knee point location method) 3.000

Coherence calculation step (in samples) 50

Coherence calculation forgetting factor 0.000

Coherence threshold (for locating the start of diffuse sound) 0.600

Coherence threshold (for testing transiency) 0.500

Correlation coefficient threshold 0.800

Forgetting factor for histogram 1.000

Lower limit for spectral centroid (in Hz) 500.000

Upper limit for spectral centroid (in Hz) 5000.000

□ Use knee point location method in fine segmentation

□ Use -25 dB as the lower limit for line fitting

□ Disable reverberation time estimation

Figure A.2: Algorithm configuration for Section 4.4.

Appendix B

Energy-time curves of signals used in evaluation

These plots present energy-time curves of the signals used in Section 4.3. The curves are calculated by taking the mean between channels, squaring and converting to decibels.

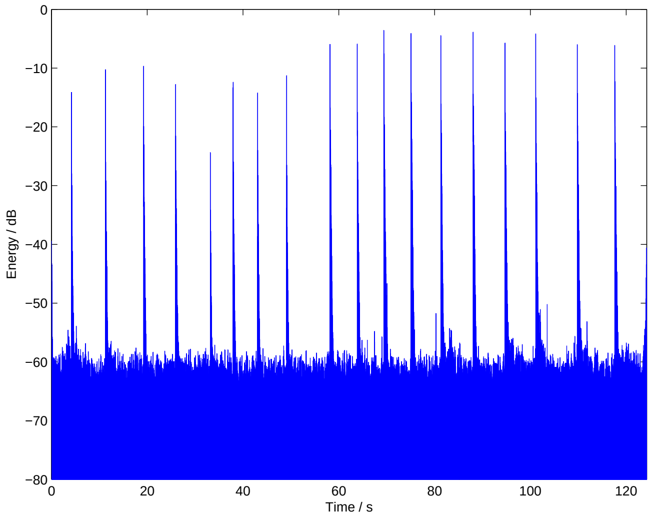

Figure B.1: Snaps and claps convolved with BRIR of room A152.

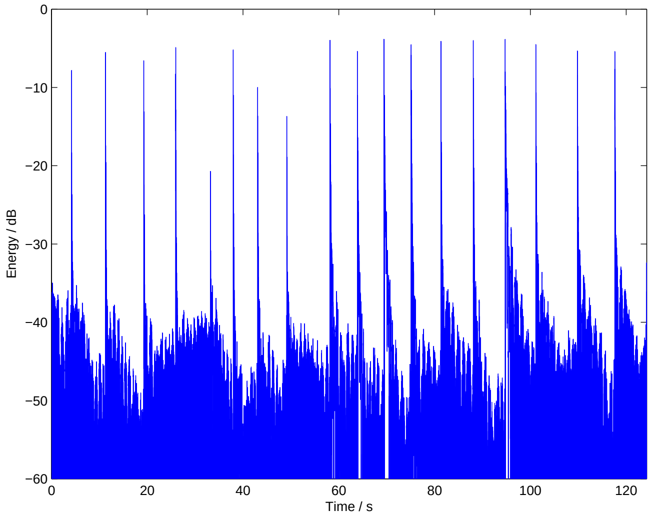

Figure B.2: Snaps and claps convolved with BRIR of room T3.

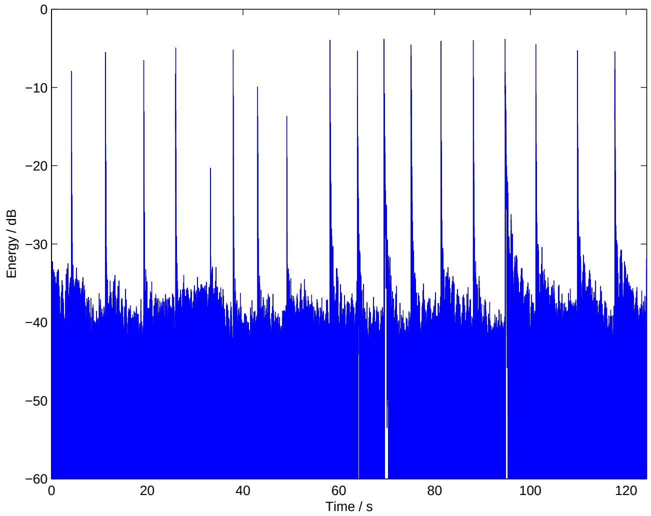

Figure B.3: Snaps and claps convolved with BRIR of room T3 (pink noise added).

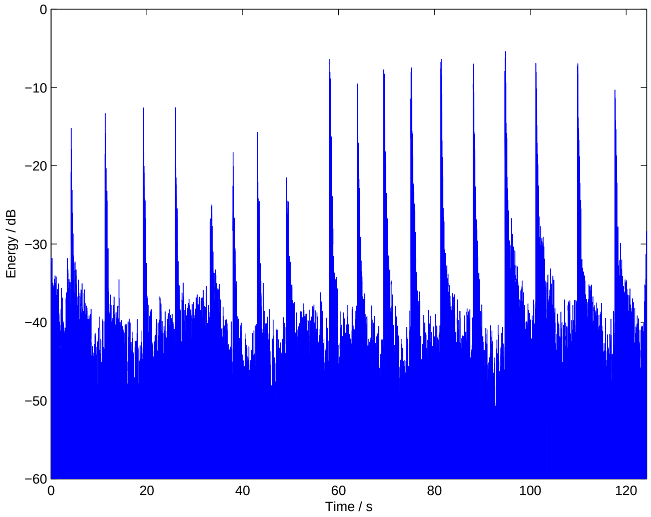

Figure B.4: Snaps and claps convolved with BRIR of room Pergola.

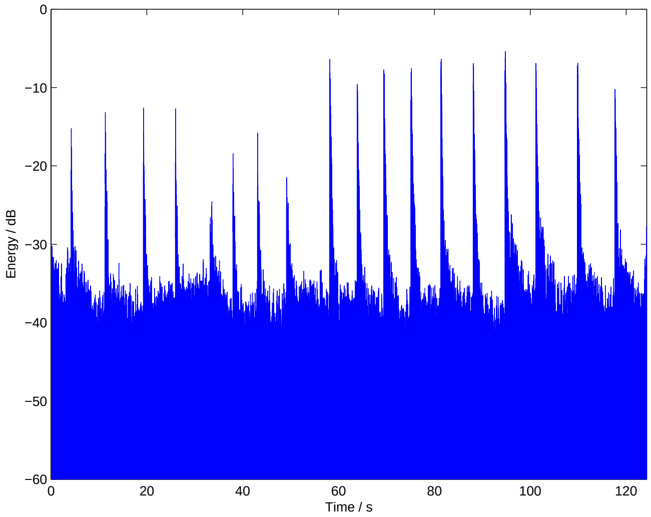

Figure B.5: Snaps and claps convolved with BRIR of room Pergola (pink noise added).